**The Blood-Brain Barrier as a Therapeutic Target for Alzheimer's Disease and Related Disorders**

by

Sweilem Baseem Al-Rihani

A dissertation submitted to the Graduate Faculty of
Auburn University
in partial fulfillment of the
requirements for the Degree of
Doctor of Philosophy

Auburn, Alabama
May 6, 2019

Keywords: Blood-brain barrier; Alzheimer's disease; Granisetron; Oleocanthal-rich extra virgin olive oil; High throughput screening



Approved by

Amal Kaddoumi, Chair, Professor of Pharmaceutics
Robert D. Arnold, Professor of Pharmaceutics
Miranda Reed, Associate Professor of Pharmacology
Rajesh Amin, Associate Professor of Pharmacology

## Abstract

The blood-brain barrier (BBB) is a highly selective and protective membrane that preserves brain homeostasis and prevents the free entry of chemicals, toxins and drugs to the brain. The BBB barrier function is primarily provided by the endothelial cells lining the brain capillaries, which create a physical barrier separating the brain from blood. In aging and in numerous neurological diseases, including Alzheimer's disease (AD), the BBB integrity is affected, as supported by several studies reported leaky BBB in the brains of aged and AD mice models, and brains of AD patients. These findings point toward the BBB as a potential therapeutic target to prevent or halt AD progression by restoring its integrity and function. In the first project, we utilized our recently developed high-throughput screening (HTS) assay to find and evaluate agents that improve BBB integrity from toxic amyloid. In this assay, an *in-vitro* BBB model composed of mouse brain endothelial cells (bEnd3) grown on 96-well plate inserts was used. Lucifer Yellow as a paracellular permeability marker was used to assess the effect of screened compounds on the intactness of the *in-vitro* BBB model with and without amyloid-β (Aβ). Using this model, we screened more than 3000 compounds from 3 different libraries namely, Sigma LOPAC1280 library (1280 compounds), NIH Clinical Collection (716 compounds) and NINDS Custom Collection (1040 compounds) to identify enhancers of the *in-vitro* BBB model intactness. Identified hits were FDA approved drugs, investigational compounds, and natural product compounds. Among the FDA approved drugs, granisetron emerged as a promising candidate selected for further evaluation. In my second project, I evaluated the ability of granisetron to enhance the integrity of

the BBB *in-vivo* using aged and AD mouse models. Granisetron was tested in C57Bl/6J young and aged wild-type mice and in a transgenic mouse model of AD namely TgSwDI. Findings demonstrated granisetron enhanced the BBB integrity in both aged and AD mice. This effect was accompanied by an overall reduction in Aβ load and neuroinflammation in TgSwDI mice brains. Supported by proteomics analysis of mice brains, the effect of granisetron to reduce Aβ-induced calcium influx significantly *in-vitro* and modulate calcium dyshomeostasis could be mediated by inducing calmodulin-dependent protein kinase II (CaMKII)/cAMP-response element binding protein (CREB) pathway in the TgSwDI mice brains. These results suggest granisetron repurposing as a potential drug to withhold, slow and/or treat AD. Besides BBB dysfunction, AD is characterized by the accumulation of extracellular Aβ plaques and neurofibrillary tangles, neuroinflammation and impaired autophagy. Thus, novel strategies that target multiple disease pathways would be indispensable to prevent, halt and/or treat the disease. Growing body of evidence including our studies supported a protective effect of oleocanthal (OC) and extra-virgin olive oil (EVOO), a major component of the Mediterranean diet, at early AD stages before the pathology onset starts, however, the mechanism(s) by which OC and EVOO exert such effect, and whether this effect extends to a later stage of AD remain unknown. Thus, in my third project, I sought to evaluate the effect of OC-rich EVOO consumption on enhancing the BBB integrity at an advanced stage of AD in TgSwDI mice and on Aβ-related pathology, starting at 6 months of age for 3 months treatment ending at 9 months of age, and then to elucidate the potential mechanism(s) by which OC-rich EVOO exerts the observed beneficial effect. Overall our findings suggest OC-rich EVOO reduced Aβ-related pathology by reducing neuroinflammation through

inhibition of NLRP3 inflammasome and inducing autophagy markers through activation of the AMPK/ULK1 pathway. Thus, diet supplementation with OC-rich EVOO could have the potential to slow and/or hold the progression of AD.

## Dedication

I dedicate my dissertation work to the soul of my father, Baseem Sweilem Al Rihani, whose words of encouragement and push for tenacity ring in my ears every day and who would have been very happy and proud to see me getting my PhD. I also dedicate it to my amazing mother, my sisters and my brother for their constant, unconditional love and support.

**Acknowledgments**

I would like to express my deep appreciation and gratitude to my advisor, Prof. Amal Kaddoumi, for the patient guidance and mentorship she provided to me, all the way from when I was first considering applying to the Ph.D. in the pharmacy program, through to completion of this degree. Prof. Kaddoumi intellectual heft is matched only by her genuinely good nature and down-to-earth humility, and I am truly fortunate to have had the opportunity to work with her.

I would also like to thank my committee members, Drs. Miranda Reed, Rajesh Amin, and Robert Arnold for the friendly guidance thought-provoking suggestions, and the general collegiality that each of them offered to me over the years. In a similar vein, I'd like to recognize my previous mentees Dr. Rasha Abu Blan, Dr. Lama Al Nazer and Dr. Khalid ElSayed for the contributions that each of them made to my intellectual growth during my years of work, study and research at King Hussein Cancer Center and at the University of Louisiana at Monroe. Also, I would like to thank my seniors, Dr. Loqman Mohamed, Dr. Yazan Batarseh, Dr. Khaled Hamad and Dr. Andrew Duong. I am also grateful for my current lab mates Lucy, Ihab and Kamal, for providing a positive and supportive work environment.

Finally, I'd be remiss if I didn't acknowledge the innumerable sacrifices made by my wife, Lucy in shouldering far more than her fair share of the parenting and household burdens while we both are pursuing our Ph.D. degrees and to my number one cheerleader, my soul, my beloved son Lucas.

## Table of contents

## List of Tables

## List of Figures

## List of Schemes

## List of Abbreviations

AD Alzheimer's disease

APP Amyloid Precursor Protein

sAPPα Soluble amyloid precursor protein alfa

sAPPβ Soluble amyloid precursor protein beta

Aβ Amyloid-β

BBB Blood-brain barrier

CAA Cerebral amyloid angiopathy

CaMKII $Ca^{2+}$/calmodulin-dependent protein kinase II

CNS Central nervous system

CREB cAMP response element-binding protein

IP3R Inositol trisphosphate receptor

CSF Cerebrospinal fluid

EC Endothelial Cells

ELISA Enzyme-linked immunosorbent assay

EVOO Extra virgin olive oil

HPLC High-performance liquid chromatography

IL-1β Interleukin-1β

ISF Brain interstitial fluid

MCI Mild cognitive impairment

MWM The Morris water maze

NLRP3 Nucleotide-binding domain, leucine-rich-containing family, pyrin domain-containing-3

NVU Neurovascular unit

PD Parkinson’s disease

ROS Reactive oxygen species

SOD Super oxide dismutase

VaD Vascular dementia

# Chapter 1

## Introduction

### The Blood-Brain Barrier

The human body contains several biological barriers that separate the blood from the interstitial fluid surrounding tissues. Of these barriers, the blood-brain barrier (BBB) is recognized as one of the most selective and precisely controlled barriers (van de Haar *et al.*, 2016).

The human brain represents only 2% of total body mass and consumes around 20% of the body's glucose and oxygen (Iadecola, 2013). The brain is rich with blood vessels to provide oxygen, nutrients, and energy to the brain cells, and to eliminate carbon dioxide and other metabolic wastes to the blood (Goadsby *et al.*, 2016; Bowman *et al.*, 2018). In brain capillaries, endothelial cells (ECs) lining the inside lumen and attached to the basement membrane are considered the main cellular component of the BBB to function as a barrier. The BBB-endothelium is connected by tight and adherent junction proteins that produce high transendothelial electrical resistance (TEER) to limit paracellular access of unwanted molecules to the brain (Goadsby *et al.*, 2016). Besides the ECs, the BBB constitutes pericytes, vascular smooth muscle cells, basement membrane, and astrocytes, that with the neurons form what is known by the neurovascular unit (NVU) (Nelson *et al.*, 2016). These cells provide vital support for the endothelium of the BBB to maintain its barrier function (Yamazaki and Kanekiyo, 2017).

In addition, molecular barrier systems through specialized receptors and/or transporters expressed in the endothelial cells play an important role in controlling the influx and efflux of a variety of molecules to and from the brain across the BBB (Yamazaki and Kanekiyo, 2017).

Barrier characteristics of brain ECs are supported by tight and adherent junction (AJ) proteins that connect the ECs to control penetrations, receptors, efflux transporters, and degradative enzymes (van de Haar *et al.*, 2016). The BBB transporters provide important support in maintaining a functional central nervous system (CNS) by controlling in and out brain access of certain molecules. (van de Haar *et al.*, 2016).

A healthy and intact BBB, thus, is essential for healthy brain and functional neurons (Montagne *et al.*, 2017). Therefore, the disruption of the BBB function has gained much attention as a key player in neurological diseases, including late-onset AD (Ujiie *et al.*, 2003; Erickson and Banks, 2013). BBB dysfunction could be attributed to a) BBB disruption, which results in a leaky barrier allowing access of blood circulating neurotoxins to the brain; b) dysfunctional transport proteins essential for brain nutrients supply and waste products removal; and c) alteration in the expression of proteins and secretions by brain cells that can damage the endothelial cells of the BBB (Erickson and Banks, 2013), which collectively could result in a chronic neuroinflammation, mitochondrial and neuronal damage, and oxidative stress (Erickson and Banks, 2013).

**Blood-Brain Barrier and Aging**

Aging is considered a major risk factor for neurodegenerative diseases. In the US alone, almost 50% of those aged 80 years or above have been diagnosed with different forms of dementia including AD and vascular dementia (Elahy *et al.*, 2015). Several studies have reported that with aging significant changes in the function of BBB associated with increased barrier permeability to occur (Elahy *et al.*, 2015). In preclinical rodent studies, increased BBB permeability with aging has been linked to reduced levels of tight junction proteins (Popescu *et al.*, 2009; Elahy *et al.*, 2015; Montagne *et al.*, 2016a). In addition, several *in-vitro* and *in-vivo* studies have shown that

pro-inflammatory cytokines such as interleukin-1beta (IL-1β) and tumor necrosis factor-alpha (TNF-α) could play a key role in regulating tight junction (TJ) proteins expression in the endothelium of the BBB (Elahy *et al.*, 2015). With aging, increased entry of blood-derived neuroinflammatory and neurotoxic molecules to the brain could also contribute to BBB breakdown (Elahy *et al.*, 2015). While the exact mechanism(s) for the aging-associated effects on BBB function are not understood fully (Elahy *et al.*, 2015), healthy aging has been linked with morphological changes in the brain including; a) a reduction in brain microvascular density (Liu *et al.*, 2015); b) endothelial necrosis, which results in a significant decrease in the number of ECs and the density of endothelial mitochondria (Marques *et al.*, 2013); c) thickening of the vascular basement membrane leading to brain hypoperfusion (Marques *et al.*, 2013); and d) an increase the size of mitochondrial pericytes, leading to pericytes degeneration (Montagne *et al.*, 2015).

Functional and morphological changes in the brain with aging is a research topic of interest by several groups. However, the vibrant role of the BBB breakdown in the pathology of age-related neurodegeneration has just recently gained much attention (Erdö *et al.*, 2017). Understanding and recognizing key factors leading to neurodegeneration at the level of the BBB could help in identifying and developing new therapeutic strategies to treat neurodegenerative disorders (Erdö *et al.*, 2017). Neurodegenerative disorders are characterized by neuronal death associated with several motor and/or cognitive impairment symptoms, which could significantly alter life quality (Gorlé *et al.*, 2016; Erdö *et al.*, 2017).

BBB breakdown has recently shown to be a major contributor to cognitive impairment (Nation *et al.*, 2019). Several *in-vivo* studies in animals demonstrated signaling disruption between ECs, pericytes, and astrocytes, and nuclear DNA damage with aging lead to compromised BBB

due to infiltration of blood circulating neurotoxins to the brain leading to neuronal loss (Erdö *et al.,* 2017; Sweeney *et al.,* 2019).

**Blood-Brain Barrier Breakdown in Alzheimer's Disease**

Alzheimer's disease (AD) is the most common form of dementia accounting for more than 60-80% of all cases worldwide (Alzheimer's Association, 2018). Based on the 2018 world Alzheimer's report, someone develops dementia every 3 seconds with about 50 million people living with AD, a number that is expected to increase to 132 million by 2050 (Alzheimer's Disease International, 2018a).

One of the major hallmarks of AD pathology is the deposition of extracellular Aβ in the form of senile plaques in brain parenchyma and vessels (Querfurth and LaFerla, 2010). Another major hallmark of AD is tau phosphorylation and formation of neurofibrillary tangles (Yin *et al.,* 2016; Kinney *et al.,* 2018). Besides these two main pathological hallmarks in AD brains, other pathologies have been observed including the BBB disruption. For example, in recently published neuroimaging studies in subjects with mild cognitive impairment (MCI) and early AD, authors reported BBB breakdown in a number of brain regions including the hippocampus and several gray and white matter regions before brain atrophy or dementia (Liu *et al.,* 2015; Montagne *et al.,* 2016a; van de Haar *et al.,* 2016). Furthermore, magnetic resonance imaging (MRI) studies revealed loss of BBB integrity as shown by increased levels of microbleeds in 25% of MCI subjects, and 45–78% of early AD subjects (Liu *et al.,* 2015; Montagne *et al.,* 2016a). Although the precise mechanism leading to BBB dysfunction is yet to be explained, in AD, the accumulation of Aβ could, directly or indirectly, disrupts TJ proteins by disturbing calcium homeostasis, that could lead to BBB dysfunction (Mattson *et al.,* 1992; Kook *et al.,* 2012). Of the most widely accepted methods to measure and evaluate BBB breakdown is the determination of endogenous plasma-

derived molecules in the brain parenchyma (Kassner and Merali, 2015). Example of those molecules is the extravasation of plasma proteins like albumin and immunoglobulin G (IgG), which were detected in AD brains, specifically surrounding microvessel segments located in close proximity to senile plaques (Yamazaki and Kanekiyo, 2017).

**Blood-Brain Barrier and Neuroinflammation**

Besides being a physical barrier, the BBB is considered a center for communication and a regulatory interface connecting the brain and immune system (Erickson *et al.*, 2012). The BBB is connected at many levels with the CNS and both affects and affected by the body's immune system (Erickson and Banks, 2019). The CNS and the immune system interact in several ways. One of these ways, for example, is mediated by the BBB that is involved in the trafficking of immune cells and transport of cytokines between the blood and brain (Erickson and Banks, 2019). The immune system contributes and determines BBB function, and modulates the brain function in health and disease (Sweeney *et al.*, 2019), suggesting a dynamic and cross-talk between the CNS, the BBB and the immune system in both disease and healthy states (Sweeney *et al.*, 2018a).

Several studies have shown that gram-negative endotoxin is associated with BBB disruption (Eckman *et al.*, 1958; Allen, 1965; Banks *et al.*, 2015). Endotoxin, specifically the lipopolysaccharide (LPS) derived from the cell wall of gram-negative bacteria, is known to potentiate a significant increase in cytokines levels in blood and brain leading to BBB breakdown (Banks *et al.*, 2015). Cytokines can affect the brain ECs significantly leading to breakdown or modification of the restrictive features of the BBB by modulating actin cytoskeleton and tight junction expressions (Banks *et al.*, 2015). Another important mediator of neuroinflammation associated with increased brain levels of cytokines is reactive oxygen species (ROS). ROS

significantly alters proteins function and enhance the production of several inflammatory cytokines including interleukin-1 (IL-1), interleukin-6 (IL-6), interleukin-18 (IL-18), TNF-α and transforming growth factor beta (TGF-β), which subsequently induce additional inflammation and leukocyte permeation across the BBB (De Giusti *et al.*, 2013). Therefore, inflammation plays a significant role in inducing BBB permeability, stimulating leukocyte and neurotoxins extravasation into the brain, thus creating a state of chronic neuroinflammation (Elahy *et al.*, 2015; Bowman *et al.*, 2018).

**Blood-Brain Barrier and Calcium dyshomeostasis**

Calcium ($Ca^{2+}$) dysregulation role in the development of AD was first reported in 1994 by Disterhoft et al (Disterhoft *et al.*, 1994). Calcium hypothesis was further studied by Khachaturian who stated the prolonged disturbances in $Ca^{2+}$ homeostasis as a major cause of neurodegeneration in AD (Khachaturian, 2006). $Ca^{2+}$ is a key modulator of several processes in the neurons and synaptic plasticity (Popugaeva *et al.*, 2018). Available evidence demonstrated the contribution of $Ca^{2+}$ dysregulation to AD progression by increasing Aβ oligomers (Aβo) production and *vice-versa*, which creates a vicious cycle between Aβ production and neuronal $Ca^{2+}$ increase leading to neurodegeneration accompanied by chronic brain inflammation, cognitive impairment and memory loss (Popugaeva *et al.*, 2018).

The endoplasmic reticulum (ER) is one of the major organelles responsible for regulating $Ca^{2+}$ levels in the cell, therefore the dysregulation of intracellular calcium induced by ER stress or dysfunction is significantly associated with AD (Stutzmann, 2005). The role of $Ca^{2+}$ dyshomeostasis is also evident in the brains of familial AD (LaFerla, 2002). Thus, rectifying intracellular calcium levels could provide a potential therapeutic opportunity to treat AD. For example, memantine, an NMDA receptor antagonist and one of the food and drug administration

(FDA) approved medications for moderate-to-severe AD patients, works by inhibiting the sustained and prolonged $Ca^{2+}$ influx, which leads to intracellular $Ca^{2+}$ ($Ca^{2+}_i$) maintenance (Popugaeva *et al.*, 2018). Several studies reported that the dysregulation of $Ca^{2+}_i$ homeostasis, especially that caused by calcium atypical release from the ER through the inositol 1,4,5-trisphosphate receptor ($IP_3R$), is associated and contributes significantly to AD pathology and memory dysfunction (Egorova and Bezprozvanny, 2018). Decades of research have shown the elevated resting $Ca^{2+}$ environment due to increased $Ca^{2+}$ influx and/or excessive release from the ER through IP3R (Stutzmann, 2005) and ryanodine receptor (RYR) (Oulès *et al.*, 2013) as key players in the pathology of AD that can be directly linked to the altered processing of amyloid precursor protein (APP), tau phosphorylation and synaptic dysfunction, which are defining features of AD, and thus further production of Aβ (Pierrot *et al.*, 2006). Studies have also described that disruption of neuronal $Ca^{2+}$ homeostasis could promote mechanisms of negative plasticity through increase in calcineurin (CaN) expression and activity, which activates a downstream signaling pathway leading to induction of the long-term depolarization (LTD) that disrupt memory function (Mulkey *et al.*, 1994). Although $Ca^{2+}$ dysregulations have been known for several years, targeting $Ca^{2+}$ dysregulation have not been translated clinically, therefore, targeting disrupted $Ca^{2+}$ signaling pathways, specifically preventing ER-$Ca^{2+}$ leak offers the opportunity for the development of AD therapeutic agents.

In addition to the aforementioned effects of $Ca^{2+}$ dyshomeostasis, at the BBB level and specifically the ECs lining the BBB microvessels, ECs maintain their gate characteristics *via* cell-cell connections though AJs and TJs that depends on $Ca^{2+}$ regulation to maintain their proper function (Yarlagadda *et al.*, 2007). In addition to its key function in several signal transduction cascades that maintains the BBB integrity and function, $Ca^{2+}$ seems to directly interact with AJs

and TJs and therefore, maintaining $Ca^{2+}$ homeostasis is very important for maintaining BBB integrity and Function (Yarlagadda *et al.*, 2007). In this regard, recent studies found that the sustained increase in $Ca^{2+}i$ post stroke initiated several signaling pathways that altered AJs and TJs proteins expression in the endothelial cells of the BBB (Brown and Davis, 2002). $Ca^{+2}$ regulates activation of calmodulin-dependent kinase (CaMK) through its binding to calmodulin, a ubiquitous $Ca^{2+}$ receptor, which then activate transcription factors among which is cAMP response element binding protein (CREB) (Marambaud *et al.*, 2009). $Ca^{+2}$ also regulates extracellular signal-regulated kinase 1 (ERK1), ERK2 and PKC (Marambaud *et al.*, 2009). Collectively, strong evidence exists to support the importance of $Ca^{2+}$ signaling and its major role in the pathology and prognosis of AD. While some of the $Ca^{2+}$ signaling changes observed in AD are vital to maintaining healthy neurons, some pathways could be activated in response to stimuli (Supnet and Bezprozvanny, 2010). Therefore, mechanistic studies are indeed essential to clarify the role of $Ca^{2+}$ dyshomeostasis in aging and AD.

**Blood-Brain Barrier and Autophagy**

Autophagy, from the Greek origin, means "self-eating", is a survival mechanism by which cells degrade misfolded proteins, eliminate toxic molecules and damaged cellular components through lysosomal degradation to maintain cellular homeostasis (Yang *et al.*, 2019), and cellular proper function through its roles as anti-inflammatory and anti-necrotic for tissue protection (Deretic and Levine, 2018).

Autophagy is classified into three major classes depending on the mechanism through which intracellular components are engulfed into the lysosome for degradation. Microautophagy where cytoplasmic material is engulfed through the lysosomal membrane for degradation (Uddin

*et al.*, 2018). Chaperone-mediated autophagy where the cytoplasmic material is attached to a chaperon that direct it to the lysosome for degradation (Uddin *et al.*, 2018). Macroautophagy where cytoplasmic degraded components are engulfed inside autophagosomes that act as cargos to transport waste products to the lysosomes for degradation (Uddin *et al.*, 2018).

In addition, autophagy plays an important role in the fight against pathogens and starvation (Seglen and Bohley, 1992). Autophagy activity can be induced by physiological processes and in response to stress factors such as starvation, inflammation or hypoxia (Boland *et al.*, 2008). Besides, autophagy is also important for cells adaptation to changing conditions, determines the life-span of several organisms, and might have a potent anti-aging role (Rubinsztein *et al.*, 2011). Conversely, reduced autophagy has been linked to accelerated aging and neurodegeneration (Boland *et al.*, 2008; Rubinsztein *et al.*, 2011).

Recently, Yang et al. showed that autophagy induction by serum starvation protected and enhanced the BBB integrity by maintaining functional claudin-5, and removal of cytoplasmic aggregated claudin-5 and ROS (Yang *et al.*, 2019). On the other hand, in the same study, autophagy downregulation impaired the endothelial barrier function as determined by reduced the expression of claudin-1 and zona occludin-1 (ZO-1) that was associated with increased paracellular permeability and reduced TEER (Yang *et al.*, 2019). Therefore, autophagy is considered a viable target for drug development and therapeutic intervention for neurodegenerative disorders including AD.

**Drug Development Alzheimer's Disease**

Unfortunately, to date, no single drug is available for AD treatment. Thus, there is an urgent need for novel targets and innovative approaches that can treat the underlining mechanism(s) of the disease. Currently, only two classes of pharmacologic therapy are approved by the FDA for

AD treatment (Weller and Budson, 2018). Tacrine is the first approved acetylcholinesterase inhibitor (AChEI) used for mild to moderate AD. Later on, rivastigmine, galantamine, and donepezil were introduced as newer AChEIs and are used for AD and Parkinson's disease. These drugs work by improving the concentration and duration of the action of the neurotransmitter acetylcholine (Korabecny *et al.*, 2015; Dong *et al.*, 2019). Rivastigmine and galantamine are proved to have a beneficial effect in treating mild to moderate forms of AD, while donepezil is used for mild to severe cases of AD (Korabecny *et al.*, 2015). AChEIs are used to enhance the cognition and behavior of AD patients, but are not capable of slowing down the progression or reversing the disease; in addition, several adverse effects such as nausea, vomiting, diarrhea, headaches, and dizziness are usually associated with using AChEIs (Korabecny *et al.*, 2015; Dong *et al.*, 2019).

Memantine is another clinically used treatment and is FDA approved for use in patients with moderate-to-severe AD. Memantine mechanism of action is by blocking the glutamate receptor N-methyl-D-aspartate (NMDA) receptor (Weller and Budson, 2018). In AD brains, NMDA receptors are continuously active because of the excessive release of glutamate by neurons, causing a chronic and sustained rise in $Ca^{2+}$ influx and neuronal cell death. Memantine displays some beneficial effects on the symptoms in moderate-to-severe AD, whereas it displays limited effectiveness in mild AD (Alzheimer's Association, 2018; Dong *et al.*, 2019).

In the absence of disease-modifying treatments for AD, there is a crucial need to develop new medications. Over the past 20 years, a significant focus on developing a disease-modifying treatment that mainly focuses on the two major hallmarks of AD, amyloid and Tau misfolded proteins, that unfortunately failed. As a major hallmark of AD pathology, Aβ peptide misfolding is one of the most studied targets for drug development. Several studies and drugs were developed

for the prevention of Aβ production and aggregation, as well as anti-Aβ vaccines for immunotherapies (Uzuki *et al.*, 2017). Drugs targeting Aβ is one of the most studied areas in AD. The main strategies for drug development include the reduction in the overall Aβ load either through targeting Aβ production or through enhancing Aβ clearance. β- and γ-secretase modulators were tested to reduce Aβ production by regulating APP processing. In addition, active or passive immunotherapeutic is another strategy that was heavily evaluated to remove accumulated Aβ (Wisniewski and Goñi, 2015). With all these efforts, unfortunately, until now, there is no successful disease-modifying treatment for AD. Thus, a paradigm shift in AD therapies so to prevent the disease instead of treatment could be the right approach to reduce AD risk (Uzuki *et al.*, 2017). For example, studies showed a link between cardiovascular diseases and AD (Zhu *et al.*, 2004), thus controlling cardiovascular risk factors could maintain a healthy brain and reduce the risk of AD and other neurodegenerative diseases (Zhu *et al.*, 2004). In addition, several studies have linked exercise and active lifestyle (Cass, 2017), and Mediterranean diet, which consists mainly of vegetables, extra-virgin olive oil (EVOO), whole-grains and seafood, with a lower risk of AD (Gardener and Caunca, 2018).

One of the major challenges to developing treatments for AD is the lack of surrogate biomarkers that are important for disease diagnosis. Finding such biomarkers for AD would significantly improve the accuracy of AD diagnosis for drugs development (Weller and Budson, 2018).

**TgSwDI as a mouse model for Aβ-related pathology and BBB disruption**

Since 1995, several transgenic mouse models have been developed to better understand the pathology of AD, and to test and identify potential drugs for AD (Kamba and Lamb, 2018). One of the earliest mouse models of AD is the PDAPP transgenic model. This model was designed to

overexpress human APP with the V717F mutation (Indiana mutation), which is associated with extensive brain accumulation of Aβ and exhibits cognitive dysfunction at 4 months of age (Games *et al.,* 1995). In addition to PDAPP mice, several other transgenic mouse models with mutations in APP were developed including Tg2576 (with Swedish mutation; KM670/671NL), APP23 (with Swedish mutation; KM670/671NL), J20 (with Swedish KM670/671NL and Indiana V717F mutations) and TgCRND8 (with Swedish KM670/671NL, and Indiana V717F mutations) (Hsiao *et al.,* 1996; Sturchler-Pierrat *et al.,* 1997; Mucke *et al.,* 2000; Chishti *et al.,* 2001). These models proved useful and have been extensively used for the analysis of Aβ production and deposition in brain parenchyma, Aβ associated neuroinflammation, development of drugs that target Aβ production and clearance, and for behavioral studies (Hsiao *et al.,* 1996; Sturchler-Pierrat *et al.,* 1997; Mucke *et al.,* 2000; Chishti *et al.,* 2001). On the other hand, these models have several drawbacks. One of the major disadvantages is that these models mimics the familial cases of AD but not the sporadic that represent more than 95% of AD cases. In addition, these mice models have limited representation of the aged human and AD brain where other chronic diseases could simultaneously exist, which makes the findings interpretation from these models challenging. Other disadvantages include the lack of perfect negative control mice, overexpression of related artifacts, sudden death, absence of NFT formation and cognitive impairment that precedes Aβ accumulation and pathology (Sasaguri *et al.,* 2017). Few years later, mice containing multiple genes with mutations were developed; example of these models are the double transgenic APP/PS1 (mutations in APP and presenilin 1 proteins) (Radde *et al.,* 2006), 5XFAD (3 mutations in APP and 2 mutations in presenilin 1 proteins) models (Jawhar *et al.,* 2012), and the triple transgenic 3xTg-AD (mutations in APP, MAPT (tau) and presenilin 1 proteins) mouse model (Oddo *et al.,* 2003). While these models, similar to the above mentioned models, are associated with the familial

form of AD, these mice showed faster Aβ accumulation in brain parenchyma at age of 2 months compared to the single gene mutation, such as the PDAPP mouse model, where Aβ starts to accumulate at the age of 6 months (Games *et al.*, 1995).

Several other mouse models to study Aβ-related AD pathology are available, however, for the purpose of my work, which focusses on the BBB, the use of a mouse model that possesses a disrupted BBB is essential to assess drugs/interventions ability to ameliorate BBB integrity and reduce Aβ deposit. Thus, in my studies I used TgSwDI mice, a mouse model that is characterized by cerebrovascular Aβ deposition, i.e. Aβ accumulation on brains microvessels, associated with disrupted BBB as the disease progresses. TgSwDI mice express human APP gene with 3 mutations namely the Swedish, Dutch and Iowa mutations (Davis *et al.*, 2004). In humans, the Swedish mutations in APP increase the production and deposition of Aβ (Mullan *et al.*, 1992), while the Dutch and Iowa APP mutations result in significant accumulation of Aβ in the cerebrovasculature of patients causing vascular fragility with cerebral hemorrhages and dementia (Levy *et al.*, 1990; Grabowski *et al.*, 2001). Similarly, TgSwDI mice develop fibrillar Aβ plaques mainly in brain microvessels, in addition to brain parenchyma (beginning at three months of age) (Davis *et al.*, 2004). TgSwDI mice also develop astrogliosis at early age with a significant increase in the number of GFAP-positive astrocytes and activated microglia as they age (Davis *et al.*, 2004). At three months of age, TgSwDI mice show a significant increase in the accumulation of insoluble $A\beta_{40}$ and $A\beta_{42}$ peptides in brain parenchyma and microvessels (Davis *et al.*, 2004). Aβ deposition on brain microvessels was associated with microhemorrhage (Davis *et al.*, 2004), and vascular degeneration (Miao *et al.*, 2005a). Collectively, these characteristics made TgSwDI mouse model suitable for ours studies.

**Hypothesis and Aims**

To date, drug discovery and development in AD has been largely unsuccessful in finding any disease-modifying treatment. Currently approved medications for AD only address its symptoms once they have reached the stage of clinical dementia (Weller and Budson, 2018). Thus, there is an urgent need to develop a disease-modifying treatment that will stop, halt the onset and/or slow the progression of AD.

BBB breakdown enables the entry of several blood-derived neurotoxins and pathogens, which is expected to cause a state of chronic neuroinflammation and oxidative stress to name some, leading to neurodegeneration and specifically AD (Sweeney *et al.*, 2019). Current evidence suggests that aging, Aβ and tau accumulation, and cerebrovascular dysfunction could damage the BBB by altering and disrupting the neurovascular unit (Sweeney *et al.*, 2019).

Based on available evidence supporting compromised BBB by aging and in AD, in this work, we hypothesized that improving the BBB function could be a novel therapeutic approach to reduce Aβ-related pathology.

To evaluate our hypothesis, the following specific aims were established:

1. To utilize our developed HTS *in-vitro* BBB model to screen and identify hit compounds that improve the intactness of the BBB model (Chapter 2)
2. To investigate the hit compound granisetron in wild-type and TgSwDI AD mouse models to confirm its potential effect on the BBB integrity and Aβ clearance, and to evaluate the potential mechanism by which granisetron exerts its potential effect (Chapter 3)

3. To evaluate the effect of diet supplementation with oleocanthal-rich extra-virgin olive oil the integrity of the BBB, Aβ clearance, neuroinflammation, and autophagy in TgSwDI mice (Chapter 4)

## Chapter 2

Utilizing and application of high-throughput screening cell-based model to identify blood-brain barrier enhancers


### Abstract

The endothelial cells of the blood-brain barrier (BBB) have vital role in protecting the brain from circulating neurotoxins access to the brain. In addition, these endothelial cells play a key role in the removal of waste products from the brain. In neurological diseases, including Alzheimer's disease (AD), the intactness and function of the endothelial cells (ECs) of the BBB is compromised, which could contribute to the pathology and progression of these diseases. Recently, our laboratory developed and validated a high-throughput screening (HTS) assay to find hit compounds, which are able to improve an *in-vitro* ECs based BBB model. For application, the *in-vitro* model was used to screen compounds for enhancers. Screened libraries were Sigma LOPAC®1280 library and 716 compounds of the NIH Clinical Collection® and 1040 compounds of the NINDS® Custom Collection. Library screening identified 337 compounds that were able to enhance the integrity of the endothelial cells of the *in-vitro* ECs based BBB model. Of the identified hits, 7 drugs were evaluated further against amyloid-β (Aβ) toxicity in mouse and human endothelial cells namely bEnd3 and hCMEC/D3 cells with 20 drugs are still undergoing further evaluation. From the tested drugs, granisetron was able to improve the *in-vitro* ECs based BBB model intactness in both mouse and human cells and thus was selected for further evaluation.

## Introduction

The BBB, a complex barrier, consists of multiple cellular components including pericytes, perivascular mural cells and astrocytes end-feet (Montagne *et al.*, 2016a), however, the barrier or gate function of the BBB is provided primarily by the ECs lining the brain capillaries (Bowman *et al.*, 2018). These ECs are attached to a basement membrane and EC cell-EC cell attachment is maintained and controlled by tight and adherents junctions (Keaney and Campbell, 2015). Several lines of evidence implicate that disruption of the BBB may precede, accelerate, or contribute to neuronal dysfunction (Elahy *et al.*, 2015). Moreover, the compromised BBB is associated with several neurodegenerative diseases (e.g., AD and amyotrophic lateral sclerosis) (Marques *et al.*, 2013; Yamazaki and Kanekiyo, 2017) cerebrovascular diseases (e.g., stroke) (Nelson *et al.*, 2016) and inflammatory disorders (e.g., multiple sclerosis) (Erdö *et al.*, 2017). In addition to pathological conditions, many chemicals circulating in the blood could affect BBB integrity. Some of these chemicals are capable of increasing the BBB permeability while others have the opposite effect, i.e. improving tightness and function of the BBB (Qosa *et al.*, 2016).

In AD, BBB breakdown is associated with enhanced BBB permeability, disrupted transport of molecules, brain hypoperfusion and inflammation (Yamazaki and Kanekiyo, 2017). Several studies have attributed the pathological changes in the BBB to multiple factors among which is the accumulation of Aβ in the brain of AD patients. Increased levels of soluble Aβ have been shown to affect BBB-ECs integrity by altering TJ proteins levels (Elahy *et al.*, 2015).

We have developed an *in-vitro* endothelial cells (ECs) based BBB model for high-throughput screening (HTS), which was previously characterized and validated for its robustness and applicability (Qosa *et al.*, 2016). In this project, we utilized this developed assay to screen and find compounds that are able to enhance the ECs-based BBB model intactness in the absence or

presence of amyloid toxicity to mimic AD pathology. For this, we screened Sigma LOPAC®1280 library (Sigma-Aldrich, St. Louis, MO), 716 compounds of the NIH Clinical Collection® (ICCB-Longwood Screening Facility, Boston, MA), and 1040 compounds of the NINDS® Custom Collection (ICCB-Longwood Screening Facility). Findings from the HTS identified 337 compounds that enhanced the monolayer intactness and decreased the *in-vitro* ECs based BBB model permeability (See appendix 1). In addition, among the identified integrity enhancers, several FDA-approved drugs were recognized, a finding which is significant for their repurposing potential to treat or prevent the BBB breakdown caused by Aβ in AD. Repurposing of FDA-approved drugs for AD treatment is an innovative approach because these drugs are well studied and evaluated, and thus could be taken forward to clinical trials.

## Materials and Methods

### Materials

Fibronectin, Lucifer Yellow, 96-well plates HTS with polycarbonate membrane transwell (3 μm) and 24-well plates polyester membrane transwell (0.45 μm) were purchased from Corning (Corning, NY). Sterile PBS, DMEM medium and penicillin/streptomycin antibiotics were obtained from Gibco (Grand Island, NY). 14C-inulin ([carboxyl-14C]-inulin, M.W.: 5000 Da) was purchased from American Radiolabeled Chemicals (St. Louis, MO). The MTT assay was obtained from Trevigen (Gaithersburg, MD). All other reagents and materials were purchased from VWR (West Chester, PA) or Sigma-Aldrich (St. Louis, MO).

### Cell culture

Cell culture conditions were similar to our previous report (Qosa *et al.*, 2016). In brief, the mouse brain endothelial cell line, bEnd3, was purchased from ATCC (Manassas, VA), and were

used at passage 25-35. Cells were cultured in DMEM medium supplemented with 10% fetal bovine serum (FBS), penicillin G (100 IU/ml), streptomycin (100 µg/ml). Cultures were maintained in a humidified atmosphere (5% $CO_2$/ 95% air) at 37° C. The human brain endothelial cell line hCMEC/D3 (kindly donated by Dr. Couraud, Institute Cochin, Paris, France), passage 25-30, were cultured in EBM-2 medium containing 1 ng/ml human basic fibroblast growth factor (Sigma-Aldrich, MO), chemically defined lipid concentrate (1%; Gibco, NY), ascorbic acid (5 µg/ml), hydrocortisone (1.4 µM), HEPES (10 mM), penicillin-streptomycin (1% ) and heat-inactivated FBS "gold" (5%). Cultures were maintained in a humidified atmosphere (5% $CO_2$/ 95% air) at 37°C (Qosa *et al.*, 2014a).

**Application of the BBB endothelium model for HTS**

To identify hit compounds, we utilized our HTS model that was developed and validated by my lab colleagues (Qosa *et al.*, 2016). In this model, bEnd3 cells were seeded at a density of 50,000 cells/$cm^2$ on polycarbonate membrane inserts in 96-well HTS transwell plate (3 µm pores size, and 4.26 mm diameter). Prior to seeding the cells, the inserts were coated with 50 µl of 30 µg/ml fibronectin from bovine plasma diluted in sterile PBS added to the apical side of each transwell filter as described previously (Qosa *et al.*, 2016). Cells were incubated at 37°C, 5% $CO_2$/95% air for 5 days. On day 5, library compounds were added to the apical side of the transwells after dilution in DMEM to a final concentration of 10 µM and the barrier intactness was evaluated by measuring LY permeability as reported previously (Qosa *et al.*, 2016), and described below. The model performance for HTS of compounds, Z′ factor (a measure for assay quality), signal-to-noise (S/N) and signal-to-background (S/B) ratios, which measure the system ability to distinguish between positive and negative controls, were determined and published (Qosa *et al.*,

2016). As described previously (Qosa *et al.*, 2016), hydrocortisone (10 µM) was utilized as a positive control for compounds that improve integrity and barrier intactness of bEnd3 monolayer; hydrocortisone is a well-established molecule to enhance tightness of endothelial monolayer by increasing expression of TJs proteins (Kashiwamura *et al.*, 2011).

**Permeability assay**

The permeability assay using Lucifer Yellow (LY) was achieved as published (Qosa *et al.*, 2016). On the experiment day, the endothelial monolayer integrity was measured by assessing LY permeability across the endothelial cells. LY is a small molecule, which pass across the bEnd3 monolayer by paracellular route (i.e. between cells), thus, alteration in the tightness of bEnd3 monolayer will alter LY permeability across the monolayer. To initiate the transport experiment, 50 µl of transport buffer (141 mM NaCl, 4 mM KCl, 2.8 mM $CaCl_2$, 1 mM $MgSO_4$, 10 mM HEPES, and 10 mM D-glucose, pH 7.4) containing 100 µM LY was added to the apical side of each transwell filter. Two hundred microliters of fresh and pre-warmed transport buffer were added to the basolateral side of each transwell filter. The transwell plate was then placed in a 37°C, 5% $CO_2$/95% air incubator for 1 h. LY fluorescence intensities in apical and basolateral compartments were determined at excitation wavelength of 485 nm and emission wavelengths of 529 nm (Synergy 2 microplate reader; Biotek, VT). Fluorescence intestines were converted to concentrations by running standards with known concentrations to determine LY concentration in apical and basolateral sides. Data acquisition was accomplished using Gene5 software (Biotek, VT). The following equation was used to calculate the apparent permeation coefficient (Pc):

$$Pc\ (cm/sec) = \frac{V_b \times C_b}{C_a \times A \times T} \qquad \text{Equation 1}$$

where $V_b$ is the volume of basolateral side (200 µl), $C_b$ is the concentration of LY (µM) in the basolateral side, $C_a$ is the concentration of LY (µM) in the apical side, A is the membrane area (0.143 $cm^2$), and T is the time of transport (3600 sec). In addition, permeability measurements from 1 to 7 days of seeding were analyzed to determine the day on which bEnd3 cells forms the tightest monolayer measured as lowest LY permeation (i.e. day of maximum barrier integrity).

**Compounds screening**

Sigma LOPAC®1280 library, 716 compounds of the NIH Clinical Collection® and 1040 compounds of the NINDS® containing pharmacologically active compounds with known mechanisms, were used for compounds screening. These compounds were screened for their effects on the barrier integrity of bEnd3 monolayer using the LY permeation assay described above (Qosa *et al.*, 2016). Compounds were added to the apical side of the transwells on day 5 of seeding after dilution in DMEM to a final concentration of 10 µM (containing 0.1% DMSO, v/v). The concentration of 10 µM was selected for screening based on available studies (Wu *et al.*, 2003). Preliminary studies describe by Qosa et al. (2016), showed that DMSO used at 0.1% had no effect the monolayer intactness as compared to the medium.

Each compound was tested in 6 replicates. Plates were incubated with drugs for 24-h at 37ºC, 5%CO2/95% air. LY permeation assay was performed on day 6 post seeding, and the Pc was calculated as described above. For each compound, the average Pc of the 6 replicates. Hits were selected based on Pc that is +/- 3 SD of HTZ as a positive control (Qosa *et al.*, 2016).

**Immunostaining of the tight junction claudin-5**

Immunostaining of claudin-5 was accomplished as previously reported (Qosa *et al.*, 2016). Briefly, on day 6, cells grown on inserts were pre-fixed with 1:1 ratio of ice-cold PBS and 4% formaldehyde for 5 min. Next, cells were fixed with a mixture of 4% formaldehyde in PBS for 10 min, permeabilized with 0.2%TritonX-100 for 10 min, and then blocked for 1 h and washed with PBS. The primary antibody claudin-5 (H-52, 1:200 dilution; Santa Cruz Biotechnology Inc. Dallas, Texas) was added, then donkey anti-rabbit IgG-CFL594 (dilution 1:400, Santa Cruz) was added for detection. Images were captured at 20X magnification using Nikon Eclipse Ti-S inverted fluorescence microscope (Melville, NY), Nikon-standard series filter cubes for DAPI, FITC, TRITC were used.

**Statistical analysis**

Data were expressed as mean ± SD. Results were statistically analyzed for significant difference by one-way analysis of variance (ANOVA) with *Dunnett* post hoc test. Values of $P<.05$ were considered statistically significant.

## Results

A schematic presentation of the model and its application is demonstrated in Scheme 1.

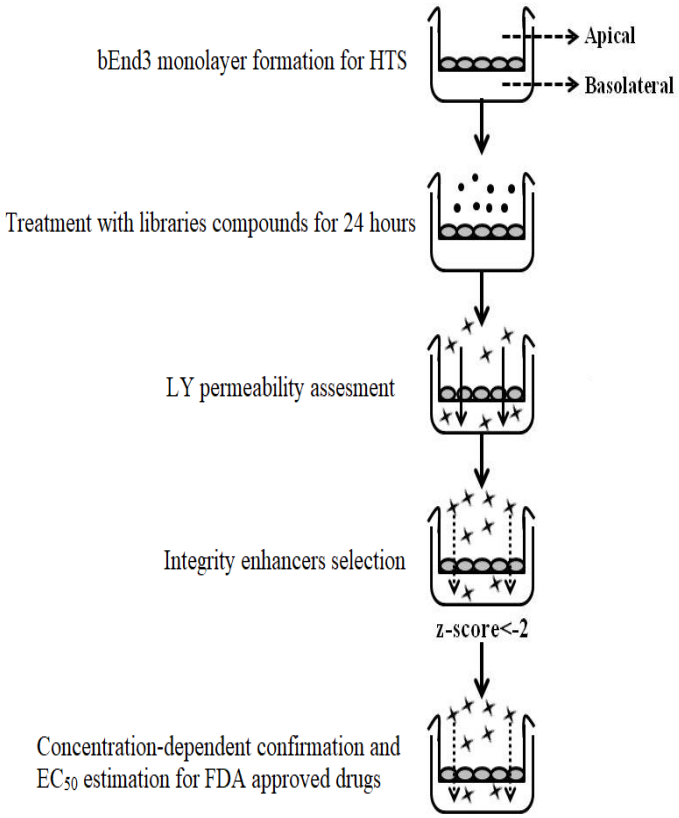


**Scheme 1** Schematic presentation of bEnd3 cells-based BBB model optimization and application. Modified from our published figure (Qosa *et al.*, 2016).

### Screening of the 3036 compounds

The model was then used to screen Sigma LOPAC®, NIH Clinical Collection® and the NINDS® compound libraries comprising of 1280, 716 and 1040 compounds, respectively, for enhancers of the *in-vitro* ECs based BBB endothelium model tightness. All compounds were tested at single concentration of 10 μM in 6 replicates. Hits were selected based on Pc that is +/- 3 SD of

HTZ as a positive control as described above. Using the aforementioned cut-off criteria for integrity enhancers, 337 compounds were identified based on their ability to increase the monolayer integrity (Appendix 1).

Out of the 337 compounds that were able to enhance bEnd3 monolayer integrity, several FDA approved drugs were identified. Seven of these FDA approved drugs were advanced for secondary screen (Qosa *et al.*, 2016). The 7 drugs showed a sigmoidal concentration-response decrease in LY permeability with EC50 values ranged from 0.76-4.56 μM (Qosa *et al.*, 2016). Another 20 FDA drugs are currently undergoing further evaluation.

**Effect of hit FDA-approved drugs on the claudin-5 expression**

Hit FDA drugs were further investigated for their effect on tight junction proteins mainly claudin-5 by immunocytochemistry. Claudin-5 was specifically evaluated as previous studies (Kashiwamura *et al.*, 2011), have shown hydrocortisone (the positive control used in the current study) to enhance BBB tightness via up-regulation of claudin-5 expression. The expression and localization of claudin-5 in bEnd3 monolayer using immunocytochemistry analysis demonstrated oxaprozin, etodolac, beclomethasone and candesartan to significantly induce claudin-5 expression by 1.6- to 2.1-fold ($p<.05$, Figure 1).

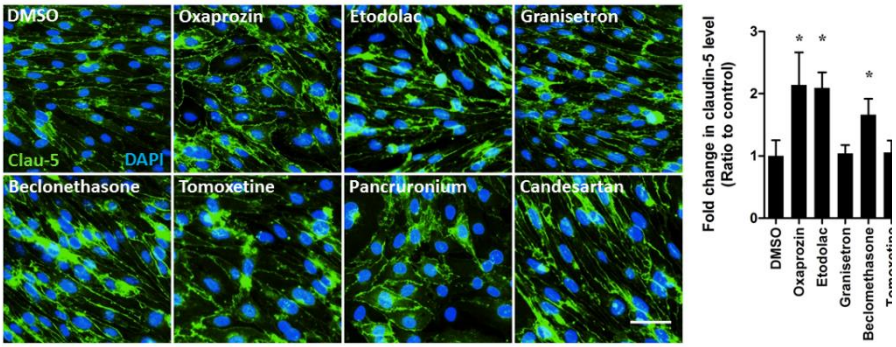


Figure 1. Representative image of claudin-5 in bEnd3 cells monolayer grown on the top of the transwell membrane showing claudin-5 localization in the membrane of bEnd3 cells (scale bar = 50 µm). Data represented as mean±SD from 3 independent experiments. * $P<.05$. Statistical analysis was determined by one-way analysis of variance (ANOVA) with *Dunnett* post hoc test. This figure is published (Qosa *et al.*, 2016).

**Protective effect of hit FDA drugs against Aβ vascular toxicity in bEnd3 cells**

We evaluated the potential of the hit FDA drugs to reduce the disruptive effect of Aβ mixture. This study was performed based on our previous report (Qosa *et al.*, 2016). As shown in Figure 2, the addition of Aβ mixture (100 nM $A\beta_{40}$ monomers and 200 nM $A\beta_{42}$ oligomers) to the basolateral side for 24 h caused a significant increase in LY permeation by 45% compared to control treated cells ($p<.05$). Simultaneous treatment with the hit FDA drugs demonstrated that all drugs, except tomoxetine and pancuronium, to reduce the disruptive effect of Aβ mixture to levels comparable to those of control ($p<.05$, Figure 2). Pancuronium showed a trend toward reduction, however, the effect was not statistically significant from that of Aβ mixture only treated cells ($p>.05$).

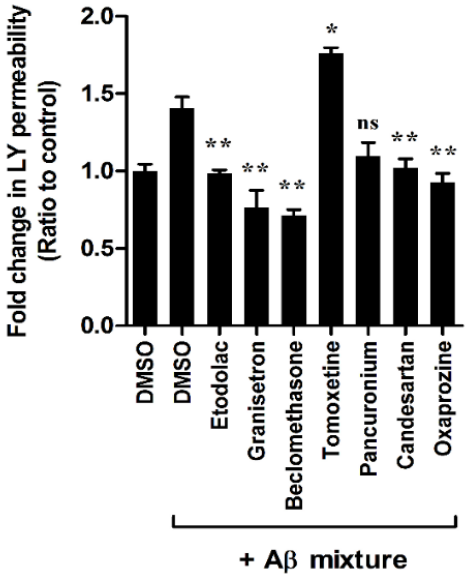


Figure 2. Effect of the hit FDA drugs on improving the attenuated integrity on bEnd3 cells-based BBB model by Aβ mixture (composed of 100 nM $A\beta_{40}$ monomers and 200 nM $A\beta_{42}$ oligomers). Data represented as mean±SD for 6 replicates from 2 independent experiments. * $P$<.05, ** $P$<.01 values compared to filter. Statistical analysis was determined by one-way ANOVA with Dunnett post hoc test. This figure is published (Qosa *et al.*, 2016).

**Hit FDA drugs have a deferential effect against amyloid vascular toxicity in hCMEC/D3 cells**

To evaluate whether the protective effect of hit FDA drugs observed in bEnd3 could be extended to humans, these hits were tested for their potential to reverse the toxic effect of Aβ mixture (50 nM $A\beta_{40}$ monomers and 100 nM $A\beta_{42}$ oligomers) in hCMEC/D3. As shown in Figure 3, 24 h treatment with the hit FDA drugs demonstrated that only granisetron, etodolac, and beclomethasone to significantly reduce Aβ mixture disruptive effect on the ECs based BBB model integrity.

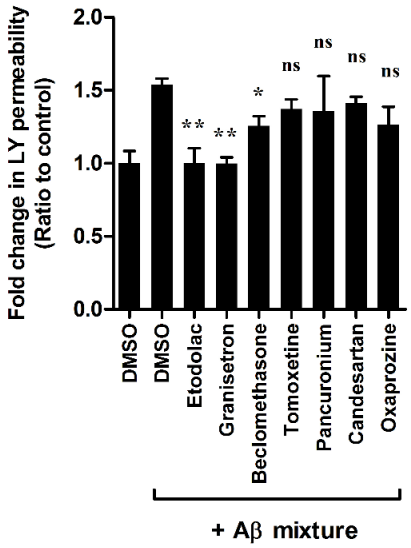


Figure 3. Effect of the hit FDA drugs on improving the attenuated integrity on the human hCMEC/D3 cells-based BBB model by Aβ mixture 50 nM Aβ40 monomers and 100 nM Aβ42 oligomers with hCMEC/D3 cells). Data represented as mean±SD for 6 replicates from 2 independent experiments. * $P$<.05, ** $P$<.01 values compared to filter. Statistical analysis was determined by one-way ANOVA with Dunnett post hoc test. This figure is published (Qosa *et al.*, 2016).

**Discussion**

Recently, our lab has developed an *in-vitro* ECs based BBB model for HTS purposes, that was recently characterized and validated for its robustness as reported by Qosa et al (Qosa *et al.*, 2016). In brief, the model was developed by optimizing the following parameters: number of cells,

the concentration of fibronectin as a basement membrane, changes in transepithelial electrical resistance (TEER) readings over time, and permeability markers (LY vs $^{14}$C-Inulin). Based on the optimization, the following conditions were established, number of cells of 50,000 cells/cm$^2$ seeded on fibronectin-coated inserts (30 µg/ml) for 5 days (TEER value of ~35Ω.cm$^2$). LY was selected as the permeability marker over $^{14}$C-Inulin (Qosa *et al.*, 2016).

This optimized model was then used to screen 3 different libraries that include 3036 compounds for their potential to enhance the *in-vitro* ECs based BBB model integrity compared to hydrocortisone (used as a positive control for enhancers) and mannitol (as a negative control for disruptors). The screen libraries were: a) Sigma LOPAC®1280 containing a collection of 1,280 pharmacologically active compounds that contains the latest, drug-like molecules in the fields of cell signaling and neuroscience. b) NIH Clinical Collection® from ICCB-Longwood Screening Facility (716 compounds); this library contains molecules that have a history of use in human clinical trials. c) NINDS® Custom Collection from ICCB-Longwood Screening Facility (1040 compounds); more than 75% of the compounds in this collection are FDA-approved drugs.

The 3 libraries of compounds were first screened for their ability to enhance the BBB integrity in the absence of Aβ mixture as monolayer disruptor (primary screen). The screen identified 337 compounds, with several FDA approved drugs (Appendix 1). While studies are still ongoing with most of the identified hit compounds, in this work, we focused on seven FDA approved drugs for potential repurposing. Previous reports suggested the repurposing of FDA approved drugs as an efficient drug discovery strategy to identify drugs that could be used in the treatment of neurological diseases including AD (Appleby *et al.*, 2013; Corbett *et al.*, 2013). This strategy offers an alternative and cost-effective drug development approach with the potential to identify new treatments in a fraction of the time required to develop a treatment from scratch

(Appleby and Cummings, 2013). Concentration-response studies demonstrated the 7 drugs are effective in enhancing the intactness of bEnd3 monolayer with EC50 values in the range of 0.76 to 4.56 μM (Qosa *et al.*, 2016).

Findings from AD patients and preclinical studies using AD mice models suggested that increased brain Aβ levels has a disruptive effect on the integrity and function of the BBB (Bowman *et al.*, 2018). These observed alterations in the BBB observed in AD suggest the BBB as a target for therapeutic interventions to improve the BBB normal activity (Montagne *et al.*, 2016a). Thus, in this work, we tested the selected drugs for their protective effect against Aβ toxicity. When tested in the bEnd3 ECs based BBB model, the FDA drugs granisetron, candesartan, beclomethasone, etodolac, and oxaprozin demonstrated a significant potential to ameliorate the integrity of the BBB model exposed to Aβ mixture. Interestingly, however, when these hits tested for their translational potential to humans in hCMEC/D3-based BBB model, only granisetron, etodolac and beclomethasone demonstrated a significant reduction in LY permeation when compared to Aβ mixture treated cells ($p<.05$), suggesting that these drugs were able to reduce the toxic effect of Aβ. Collectively, the above findings propose differences between mouse and human cell lines; while 5 out of the 7 drugs demonstrated a positive effect in bEnd3 cells-based BBB model, only 3 drugs were able to reduce the disruptive effect of Aβ mixture in hCMEC/D3-BBB model. This difference, however, is not surprising. In a recent study, our lab reported differences between bEnd3 and hCMEC/D3 cells where the former cell line is metabolically more active than the latter and clear Aβ species (by degradation) at a higher rate (Qosa *et al.*, 2014b). Besides, granisetron and etodolac belong to drug classes that have demonstrated beneficial effects against AD (Fakhfouri *et al.*, 2015; Callahan *et al.*, 2017). Similarly, when administered to scopolamine-induced memory-impaired mice, granisetron improved fear memory and spatial recognition

memory (Javadi-Paydar *et al.*, 2012). Thus, for the efficient translation of the current findings, drugs demonstrated to ameliorate and/or protect the mouse and human ECs-based BBB models will be further evaluated *in-vivo* in AD mouse models.

In conclusion, utilizing our developed *in-vitro* ECs based BBB model we were able to identify hit compounds that could enhance the integrity (a list of enhancers are described in Appendix 1 and in Qosa et al., 2016) & (Figures 2 & 3) of the endothelial monolayer when Aβ was added as a disruptor of the ECs based BBB model (Figures 2 & 3; Qosa et al 2016), and protect from amyloid toxicity in both mouse and human-derived endothelial cell lines. From these drugs, granisetron was selected for further *in-vivo* evaluation for its ability to improve the BBB function in aged and AD mouse model. It worth mentioning, however, while the developed model was able to identify hit compounds, it has some limitations. For example, the *in-vitro* model is very simple and based only on the endothelial cells, thus doesn't accurately represent the BBB that is composed of multiple cellular components such as astrocytes and pericytes.

**Acknowledgments**

This chapter is part of our published article entitled "High-Throughput Screening for Identification of Blood-Brain Barrier Integrity Enhancers: A Drug Repurposing Opportunity to Rectify Vascular Amyloid Toxicity", for the authors: Qosa, H., Mohamed, L. A., Al Rihani, S. B., Batarseh, Y. S., Duong, Q. V., Keller, J. N., & Kaddoumi, A. (2016). This article is published in the Journal of Alzheimer's Disease, 53(4), 1499–1516, doi.org/10.3233/JAD-151179. I would like to acknowledge all co-authors and below is the detailed description of each author contribution.

Qosa H: developed, optimized and upgraded the *in-vitro* ECs based BBB model, screened the Sigma LOPAC® 1280 library, analyzed and interpreted data and wrote the manuscript. Mohamed LA: screened Sigma LOPAC® 1280 compounds, analyzed and interpreted data. Al Rihani SB: secondary screening of identified hits from Sigma LOPAC® 1280, and primary screened NIH Clinical Collection® and NINDS® library, performed experiments described in this chapter, analyzed and interpreted data and wrote the manuscript. Batarseh Y: screened Sigma LOPAC® 1280 compounds. Duong Q: screened Sigma LOPAC®1280 compounds. Keller J: designed the study and reviewed the manuscript. Kaddoumi A: designed the study and experiments, analyzed and interpreted the data and wrote the manuscript.

## Chapter 3

Granisetron ameliorate the blood-brain barrier function in TgSwDI mice as an Alzheimer's disease model


### Abstract

Alzheimer's disease (AD) is characterized by two pathological hallmarks namely amyloid-β plaques and neurofibrillary tangles. In addition, calcium dyshomeostasis and compromised blood-brain barrier (BBB), are observed in the brains of AD patients. Enhancing the BBB integrity and normalizing $Ca^{+2}$ homeostasis could be an effective strategy to treat AD. We have, recently, developed an HTS method to screen for compounds that enhance an *in-vitro* BBB model intactness, which identified multiple hits among which is granisetron, an FDA approved drug. Here, we evaluated the therapeutic potential of granisetron against AD. Granisetron was tested in C57Bl/6J young and aged wild-type mice and in a transgenic mouse model of AD namely TgSwDI. Findings demonstrated granisetron enhanced the BBB integrity in both aged and AD mice. This effect was associated with an overall reduction in amyloid-β load and neuroinflammation in TgSwDI mice brains. Supported by proteomics analysis of mice brains, granisetron significantly reduced amyloid-β induced calcium influx *in- vitro,* and modulated calcium dyshomeostasis by restoring calmodulin-dependent protein kinase II (CaMKII)/cAMP-response element binding protein (CREB) pathway in TgSwDI mice brain.

## Introduction

Several neuropathological hallmarks of AD have been recognized since Alois Alzheimer's reporting of the disease over a century ago. While the major cause remains unknown, AD is described clinically by the gradual deterioration in cognitive function and memory loss, leading to slow and progressive behavioral changes (Uzuki *et al.*, 2017). The pathological characteristics of the disease include the accumulation of extracellular amyloid-β (Aβ) in brain parenchyma in the forms of senile plaques and in brain vessels as cerebral amyloid angiopathy (CAA), intracellular neurofibrillary tangles (NFTs) composed of deposited hyper-phosphorylated tau protein, and brain atrophy due to extensive loss of the neuronal cells (Nelson *et al.*, 2016). In addition, AD is characterized by chronic brain inflammation, elevated intracellular calcium ($Ca^{+2}$), and a disrupted blood-brain barrier (BBB) (Disterhoft *et al.*, 1994; Brown and Davis, 2002; Yarlagadda *et al.*, 2007; Gibson *et al.*, 2017).

To date, drug discovery and development in AD has been largely unsuccessful in finding any disease-modifying treatment. Currently approved medications for AD only address its symptoms once they have reached the stage of clinical dementia. Two classes of medications are available, the cholinesterase inhibitors and N- methyl-D-aspartate (NMDA) antagonists. Besides, numerous AD clinical trials have failed for several reasons including the lack of extent in molecular targets of new treatments, which have predominantly focused on amyloid to provoke disease modification (Uzuki *et al.*, 2017). Thus, there is an urgent need to find disease-modifying therapies necessary to prevent, delay the onset and/or slow AD progression.

One important therapeutic target is the BBB. Current evidence suggests that aging, cerebrovascular impairment, and/or the accumulation of Aβ or tau can induce BBB dysfunction by affecting the cellular components of the neurovascular unit ( Kang *et al.*, 2016; Montagne *et*

*al.,* 2016; Nelson *et al.,* 2016). BBB disruption results in compromised Aβ clearance, which in turn results in further disruption of the BBB and Aβ accumulation, ultimately leading to BBB dysfunction and neuronal damage as the disease progress (Wisniewski *et al.,* 1997; Shibata *et al.,* 2000). Therefore, targeting the BBB as a therapeutic approach could provide a novel strategy to prevent or treat AD. Recently, we have developed an *in-vitro* BBB model that possesses CAA features to high-throughput screen (HTS) thousands of compounds to identify drugs that enhance the integrity of the *in-vitro* BBB model and improve its function against Aβ toxicity (Qosa *et al.,* 2016). Among the hit compounds tested in Chapter 2, granisetron emerged as a potential drug to protect the BBB model against Aβ toxicity. Granisetron, a 5-hydroxytryptamine-3 (5-HT3) receptor antagonist, is widely used to treat chemotherapy-induced nausea and vomiting (Yarker and McTavish, 1994). The 5-HT3 receptor is a ligand-gated ion channel, which increases the intracellular levels of multiple cations including calcium ($Ca^{+2}$). Stimulation of 5-HT3 receptor enhances rapid and transient depolarization and excitation of neurons due to elevation in intracellular $Ca^{+2}$ levels, an effect that could be blocked by 5-HT3 receptor antagonists, such as granisetron (Nayak *et al.,* 1999).

Granisetron is an FDA approved drug and thus its disposition and safety profiles are well established. Several studies, human and non-human, investigated granisetron pharmacokinetic (PK) following intravenous (IV) (Chein-Tsai *et al.,* 1999; Spartinou *et al.,* 2017) , subcutaneous (SC) (Spartinou *et al.,* 2017), and transdermal (TD) administration (Chaturvedula *et al.,* 2005; Chen *et al.,* 2019). In healthy human subjects, plasma concentration profiles of granisetron following IV administration displayed a rapid initial decline, which implied granisetron has an extensive tissue uptake (Spartinou *et al.,* 2017), and a relatively large apparent volume of distribution (2.4-3.5L/Kg). Its clearance is mainly by non-renal (37-50 L/h), with about 12% of

the administered dose is eliminated unchanged in the urine. Granisetron half- life is 5 h in average (Spartinou *et al.*, 2017). In addition to the IV route and in order to increase patient compliance to granisetron and to provide controlled effect with a lesser maximum plasma concentration, a sustained delivery using granisetron transdermal system (GTS) has been developed (Howell *et al.*, 2009). GTS is composed of a 52 $cm^2$ patch containing 34.3 mg of granisetron delivered at a rate of 3.1 mg per 24 h for up to 7 days (Howell *et al.*, 2009). From this patch, granisetron reaches its maximum concentration in 48-56 h. Moreover, granisetron is available in extended release product pre-filled in a syringe containing 10 mg granisetron for SC injection (Spartinou *et al.*, 2017). The PK parameters for SC injections were described previously (Gurpide *et al.*, 2007); after the subcutaneous injection of 3 mg dose, gransiteron maximum concentration was reached after 30 min with 100% bioavailability when compared to the IV administration (Gurpide *et al.*, 2007).

In addition, in rats, Tsai et al. studied granisetron PK in plasma and brain using simultaneous microdialysis consists of flexible and rigid microdialysis probes to sample granisetron in rat blood and brain, respectively. (Chein-Tsai *et al.*, 1999).

According to Tsai et al. findings, following IV administration, granisetron was detected in plasma and brain dialysates demonstrating granisetron crosses the BBB with unbound brain to plasma ratio of 0.13 (Chein-Tsai *et al.*, 1999). These findings that granisetron crosses the BBB were further supported by others (Bachy *et al.*, 1993; Bufton *et al.*, 1993).

Intraperitoneal injections of granisetron in rodents are available (Fakhfouri *et al.*, 2010; Javadi-Paydar *et al.*, 2012), however, these studies focused on granisetron therapeutic effect but not disposition. For example, Fakhfouri et al. evaluated the effect of IP injection of 2 mg/kg granisetron as a potential therapeutic drug for inflammatory bowel disease in rats and reported that granisetron successfully ameliorated acetic acid-induced colitis (Fakhfouri *et al.*, 2010). In

addition, Javadi-Paydar et al., demonstrated that the IP administration of 10 mg/kg granisetron significantly rectified scopolamine induced short-term and fear memory impairment in amnesic mice (Javadi-Paydar *et al.*, 2012). Furthermore, the effect of granisetron following SC injections was also tested. For example, Honda et al., evaluated the effect of granisetron administered SC on fluvoxamine induced-antinociceptive effect, and reported that granisetron was able to antagonize such effect (Honda *et al.*, 2006). Collectively, these findings suggest that following IP and SC administrations, granisetron was able to have an effect on the brain function.

The overall objective of this work is to evaluate the effect of granisetron on BBB integrity and Aβ related pathology. To investigate this objective, *in-vitro* and *in-vivo* studies in young and aged wild-type mice as well as in AD mouse model were performed. Proteomics analysis of young and aged mice brains was also performed to examine the proteomic response to granisetron. In these studies, granisetron was administered SC via Alzet pump to the wild-type mice, and IP to an AD mouse model. While it would be useful to evaluate granisetron PK following IP and SC administration, these studies were not performed based on the available evidence showing granisetron continues to exhibit its therapeutic effect following IP and SC administrations (Honda *et al.*, 2006; Fakhfouri *et al.*, 2010; Javadi-Paydar *et al.*, 2012).

## Materials and methods

### Materials

Granisetron HCl was purchased from TCI America (Portland, OR). Texas red-Dextran 10 KDa and FITC-Dextran 40 KDa, bovine serum albumin (BSA) and Thioflavin-S (Thio-S) were purchased from Sigma-Aldrich (St. Louis, MO). Fetal bovine serum (FBS) was purchased from Atlanta Biological (Flowery Branch, GA). Dulbecco's modified Eagle's medium (DMEM) was

purchased from Gibco (Grand Island, NY), Fluo-4 Direct™ Calcium Assay Kit was purchased form ThermoFisher Scientific Inc. (Waltham, MA). Total protein analysis kit was obtained from Pierce (Rockford, IL). Choline/Acetylcholine assay kit was purchased from Abcam (Cambridge, MA). All other chemicals and reagents were readily available from commercial sources.

**Antibodies**

Antibodies against light chain LRP1 and BACE1 were obtained from Abcam, P-glycoprotein (P-gp) monoclonal antibody (C219) and human-specific anti-Aβ antibody namely 6E10 labeled with Alexa-fluor 488 were purchased from BioLegend (San Diego, CA). Zona-occludin-1 (ZO-1), claudin-5, occludin, and BDNF were purchased from ThermoFisher. Junctional adhesion molecule-1 (JAM-1), actin, tubulin, glial fibrillary acidic protein (GFAP), insulin degrading enzyme (IDE), MMP-9, RAGE, neprilysin (NEP) and Fluorescein-conjugated donkey anti-IgG were purchased from Santa Cruz Biotechnology Inc (Santa Cruz, CA). HRP-labeled secondary anti-rabbit and anti-mouse antibodies were purchased from Invitrogen (Carlsbad, CA), HRP-labeled secondary anti-goat antibody was purchased from R&D systems (Minneapolis, MN). Nicastrin, cAMP-dependent protein kinase (PKAc), IP3 receptor, phospho-IP3 receptor (Ser1756), CREB, phospho-CREB (Ser133), caspase-3, Bcl-2, αCaMKII, phospho-CaMKII (Thr286) and calbindin D28K were purchased from Cell Signaling Technology, Inc. (Danvers, MA). Anti-collagen-IV antibody was purchased from Millipore (Burlington, MA). Specific antibodies against soluble APPα (sAPPα) and APPβ (sAPPβ) were purchased from Immuno-Biological Laboratories (Minneapolis, MN). Synaptic markers, PSD-95, and SNAP-25 antibodies were purchased form GeneTex, Inc. (Irvin, CA) and Synapsin-1 antibody was purchase from Cell Signaling Technology, Inc. (Danvers, MA). For collagen-IV detection, secondary

antibodies used were CFL594-conjugated donkey anti-rabbit IgG (Santa Cruz Biotechnology) or goat anti-rabbit IgG (H+L) F(ab′)2 fragment, CF™350 from Sigma-Aldrich.

**Cell culture**

The mouse brain ECs (bEnd3; ATCC, Manassas, VA), passage 27–33, were cultured in DMEM growth medium with 10% FBS, and penicillin G (100 units/ml)/streptomycin (100 g/ml). Cells were grown to confluence in 75 $cm^2$ cell culture flasks for one to two days in a humidified atmosphere (5%$CO_2$/95% air) at 37°C. Neuronal cultures were prepared from SH-SY5Y cell line transfected with APP695 (hereafter SH-SY5Y-APP). Neuronal cells were grown in DMEM media containing 10% FBS. Geneticin (400 µg/ml; Gibco) was added to SH-SY5Y-APP cells. Cultures were maintained in a humidified atmosphere (5% CO2/95% air) at 37°C and the media were changed every other day.

**Calcium flux measurement**

Cells were plated at 100,000 cells/$cm^2$ in 96-well black-walled clear bottom microplates (Costar® 3603; ThermoFisher). Twenty-four hours later, cells were treated with 50 µl media (control) or 50 µl media containing granisetron in a final concentration of 5 and 10 µM for 24 h. To determine the effect on $Ca^{+2}$ flux, the fluorescent $Ca^{+2}$ sensor Fluo-4 Direct was added to the cells for 30 min at 37 °C, 5% $CO_2$ (following the manufacturer instructions), and then allowed to equilibrate to room temperature for another 30 min. Fluorescence intensity was measured at excitation and emission wavelengths of 490 and 520 nm, respectively, for baseline (10 reads at 32-s intervals) followed by another 10 reads after $A\beta_{42}$ addition (final concentration of 2 µM) as described preciously (Gunn *et al.*, 2016). Cytation™ 5 cell imaging multi-mode reader (BioTek

Instruments, Inc., Winooski, VT) was used. $Ca^{+2}$ flux values ($\Delta F/F_0$) were expressed as the difference between the mean baseline and immediately following Aβ application as reported previously (Bussiere *et al.*, 2017).

**Animals**

All animal experiments and procedures were approved by The University of Louisiana at Monroe Animal Care and Use Committee and according to the National Institutes of Health guidelines Principles of laboratory animal care (NIH publication No. 86-23, revised 1996). Wild type C57Bl/6 male mice at age of 4 months, representing the young group, and 18 months, representing the aged group, and TgSwDI transgenic mice at age of 4 months (a CAA/AD mouse model) were purchased from Jackson Laboratories (Bar Harbor, ME). TgSwDI mice express human APP under control of Thy 1.2 neuronal promoter with double Swedish mutations and the Dutch and Iowa vasculotropic Aβ mutations, which lead to extensive deposition of Aβ associated with astrogliosis and memory decline (Davis *et al.*, 2004). In the brain of TgSwDI mice, Aβ accumulation starts at age 2 to 3 months leading to extensive deposition at the age of 12 months (Davis *et al.*, 2004). All mice were housed in plastic cages under standard conditions, 12-h light/dark cycle, 22°C, 35% relative humidity, and *ad libitum* access to water and food.

**Animals' treatment**

To evaluate the effect of granisetron on the BBB integrity, young (4 months) and aged (18 months) wild type C57BL/6J mice. The rationale for selecting these age groups was based on the definition of young and aged described Jackson laboratory (www.jax.org/research-and-faculty/research-labs/the-harrison-lab/gerontology/life-span-as-a-biomarker). According to the

website, for C57BL/6J mice, young mice (mature adult) are aged between 3–6 months and are considered past development but not affected yet by senescence; at this age, mice are compared to human adults aged between 20-30 years. While aged (old) mice are aged between 18–24 months and are referred as old age because these mice are in the period where senescent changes can be detected in almost all biomarkers; at this age, mice are compared to adults aged between 56-69 years (www.jax.org/research-and-faculty/research-labs/the-harrison-lab/gerontology/life-span-as-a-biomarker).

For each age group, mice were divided into 2 groups each, vehicle and treatment groups (n=7 mice/group). Treatment groups of young and aged mice received a dose of 3 mg/day/kg (i.e. 0.09 mg/day/30g mouse body weight) that was delivered via ALZET® (DURECT Corporation, Cupertino, CA) osmotic minipumps (model 1004). Each pump contained 3.4 mg of granisetron dissolved in 100 µl sterile water pumped at 0.11 µl per hour (enough for 37.8 days consumption). The control groups received sterile water as a vehicle. Sterile water was used as the vehicle of choice because granisetron is a water-soluble molecule. Although saline is preferred to be used, it has been reported that distilled water also could be used as a vehicle (Shimizu, 2004; Rigalli alfredo and Veronica, 2009) and thus it was used in our studies at low volumes (about 2.6 µl per day for 28 days via Alzet pump, and 100 µl per day by IP for 28 days). Available concerns with the use of sterile water (hypotonic solution) is causing pain at the site of injection, and could lead to hemolysis if given by IV administration (Shimizu, 2004; Rigalli alfredo and Veronica, 2009).

An additional groups of young and aged mice to act as sham controls without the Alzet pump implantation could be necessary to exclude the potential effect of Alzet pump installation surgery and to neutralize any possible biases, however, in this study, they were not performed based on our laboratory previous experience with Alzet pumps (Mohamed *et al.*, 2015, 2016).

Treatments continued for 28 days and mice were killed by an overdose of anesthesia at the age of 5 months. Granisetron dose was selected based on previous reports using granisetron in the range of 0.1-10 mg/kg/day to test its effect against several diseases/conditions other than nausea and vomiting (Fakhfouri *et al.*, 2010; Javadi-Paydar *et al.*, 2012; Aithal *et al.*, 2014). Thus, in this study and for proof-of-concept, granisetron at 3 mg/kg/day dose was used to evaluate its effect on the BBB integrity. Granisetron disposition in mice and rats has been previously described (Bufton *et al.*, 1993; Chein-Tsai *et al.*, 1999; Chaturvedula *et al.*, 2005). For example, Chein-Tsai et al., reported that when administered to rats, granisetron was able to cross the BBB (Chein-Tsai *et al.*, 1999).

Alzet pumps were implanted subcutaneously by making a small cut on the mouse back specifically in the midscapulary region; the region was used as advised by the micro-osmotic pump model 1004 datasheet for subcutaneous implantation (http://www.alzet.com/downloads/1004specs.pdf) and based on our previous publications (Mohamed *et al.*, 2015, 2016). After pump insertion, the wound was closed with clips as previously described (Mohamed *et al.*, 2016). Pumps delivered 100 µl of solution at a rate of 0.11 µl/h for 28 days.

Granisetron stability in water was previously reported and proved stable up to 90 days in water (Quercia *et al.*, 1997; Nahata *et al.*, 1998). In addition, before initiating the experiments, I performed a relative stability study to confirm granisetron stability in water for one month by measuring relative changes in granisetron peak area. Results suggested granisetron is stable in water for at least one month (98.8%; Figure 4). HPLC analysis was performed by an isocratic Prominence Shimadzu HPLC system (Columbia, MD). The system consisted of a SIL 20-AHTautosampler, fluorescence detector (Shimadzu, RF10A XL), PDA detector and a LC-20AB

pump connected to a Dgu-20A3 degasser. Data acquisition was achieved by LC Solution software version 1.22 SP1.

The chromatographic conditions consisted of a Luna 5 µm C18 column (250 × 4.6 mm i.d.; Phenomenex, Torrance, CA); a mobile phase consisting of a mixture of 25% phosphate buffer (5 mM, pH 3.0), methanol (HPLC grade) and acetonitrile (40:35 v/v). Delivered at a 1.0 ml/min flow rate, and wavelength of 210 nm.

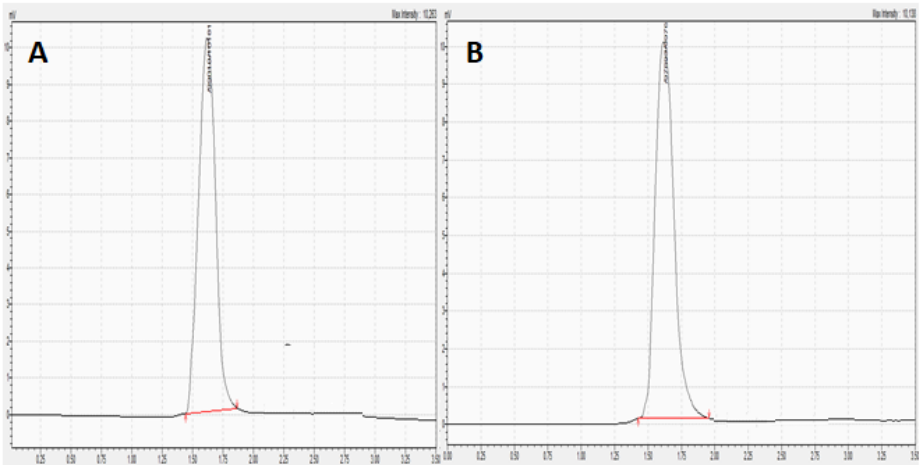


C

| | Day 0 | Day 30 |
|---|---|---|
| conc. µM | 5 | 4.76 |
| Peak area | 99010 | 97893 |
| RT (min) | 1.6 | 1.6 |
| Peak height | 10389 | 10093 |

Figure 4. Representative chromatograms from HPLC analysis for granisetron relative stability. (A) Granisetron dissolved in distilled water at Day 0 (B) Sample of Granisetron after 1 month. (C) Table showing the concentration (µM), peak area, retention time (RT), and peak height for granisetron on day 0 and Day 30, lot #: EZEOM-6N. No other lots were analyzed for stability.

For TgSwDI mice experiments, mice were divided into two groups (n=5 mice/group); control group received sterile water as a vehicle administered intraperitoneally (IP), and treatment group that received IP granisetron at 3 mg/kg/day (0.09 mg/day/30g mouse body weight dissolved in 100 µl sterile water). Granisetron was administered by IP route for practicality reasons due to the frequency of once daily (QID) and the number of injections (#30) in this study, making other routes like tail vein injections not practical (Javadi-Paydar *et al.*, 2012). As a limitation in this work, granisetron levels in mice plasma and brain following the IP and SC by Alzet pump were not determined; doing that would allow us to determine and compare the drug levels following both routes. As we didn't do these measurements, it would be difficult to compare granisetron effect on the BBB and Aβ-related pathology between IP and SC via Alzet pump routes, which could impact the drug bioavailability, brain levels and thus efficacy.

Treatments continued for 28 days. Within the 3-months of treatment, animals were monitored weekly for changes in body weights, the average mouse weight was 27±3 g and 28±2 for the wild type aged control and granisetron treated groups, respectively. For young wild type mice, the average weight was 24±2 g and 23±3 g for control and granisetron treated groups, respectively. In addition, the average body weights of TgSwDI mice during the treatment period were 24±2g for control group compared to 25±2 g for granisetron group. Health status and normal behavior were monitored every day; mice didn't show any signs of side effects.

**Florescent tagged-Dextran to monitor BBB permeability in wild type young and aged mice**

At the end of the treatment period, vehicle and granisetron treated mice were intravenously (IV) injected with 100 µl solution of two different molecular sizes florescent tagged dextran; 10 kDa Texas-red dextran and 40 kDa FITC-dextran (20 mg/ml of each dextran dissolved in 0.9%

saline) through the mice tail vein as previously reported (Egawa *et al.*, 2013). Four hours after the injection, mice were anesthetized with ketamine 100 mg/kg with xylazine 12.5 mg/kg cocktail IP. Mice were transcardially perfused with heparinized-PBS (20 units/ml final concentration) using a peristaltic pump (Harvard Apparatus, Holliston, MA) for 4-5 min until the PBS starts to run clear from the right atrium cut as described previously (Gage *et al.*, 2012). Brains were then collected for immunochemical and biochemical analysis.

**Brain microvessels extraction**

Brain microvessels were prepared by their isolation the brains of young and aged wild type mice, and TgSwDI mice as described previously (Batarseh *et al.*, 2017). In brief, brain hemispheres were collected and directly homogenized in ice-cold DPBS (2.7 mM KCl, 1.46 mM KH2PO4, 136.9 mM NaCl, 8.1 mM Na2HPO4, 0.9 mM CaCl2, and 0.5 mM MgCl2 supplemented with 5 mM D-glucose, 1 mM sodium pyruvate, pH 7.4). Brain homogenate samples were added to 30% ficoll in 1:1 volume, thoroughly mixed and then centrifuged at 5800×*g* for 15 min at 4°C. The supernatant was removed to obtain pellet-containing microvessels, which was gently re-suspended in ice-cold DPBS containing 1% BSA. Microvessels were collected by separation over glass beads packed in a glass column. After separation, the glass beads were gently shaken and centrifuged to collect adhered microvessels. Collected microvessels were lysed in radioimmunoprecipitation assay (RIPA) buffer containing 1% protease inhibitor and were used for Western blot analysis.

**Western Blot analysis**

Western blotting was performed as we reported previously (Mohamed *et al.*, 2016). In brief, protein samples (25 µg) were loaded and resolved using 10% SDS-polyacrylamide gel at

140V for 1 h and transferred electrophoretically to PVDF membrane (Millipore) at 300 mA for 3 h at 4°C. Nonspecific binding was blocked by pre-incubation of the PVDF membrane in PBS solution containing 1% skimmed milk with rocking for 1 h at room temperature followed by overnight incubation at 4°C with primary antibodies. Primary antibodies used to immunoblot bEnd3 cells lysate and isolated microvessels proteins are P-gp (C-219), LRP1 (light chain), ZO-1, claudin-5, occludin, JAM-1, and β-actin. For brain homogenate samples, primary antibodies used are sAPPα, sAPPβ, PSD-95, SNAP-25, Synapsin-1, Iba-1, GFAP, IDE, neprilysin, MMP-9, RAGE, BACE-1, IP3 receptor-1, phospho-IP3 receptor (Ser1756), CREB, phospho-CREB (Ser133), PKA-c, Nicastrin, caspase-3, Bcl-2, αCaMKII, phospho-CaMKII (Thr286), calbindin D28K, BDNF, β-actin, and β-Tubulin. Secondary antibodies used were: HRP-conjugated anti-mouse IgG secondary antibodies (1:1000 dilutions) for P-gp, PSD-95, sAPPα, claudin-5, β-actin, IDE, Bcl-2 and β-tubulin; HRP-conjugated anti-rabbit IgG secondary antibodies (1:1000 dilutions) for LRP1, SNAP-25, GFAP, neprilysin, IP3 receptor, phospho-IP3 receptor (Ser1756), CREB, phospho-CREB (Ser133), caspase-3, αCaMKII, phospho-CaMKII (Thr286), calbindin D28K, BDNF, sAPPβ, ZO-1, occludin and JAM-1. Proteins' blots were developed using a chemiluminescence detection kit (SuperSignal West Femto substrate; ThermoFisher). Bands were visualized using ChemiDoc™ MP Imaging System (Bio-Rad Hercules, CA, USA) and quantified by densitometric analysis of each protein normalized to the housekeeping protein used (Actin-β or Tubulin) using Image Lab™ Software V.6.0 (Bio-Rad).

**Immunohistochemical analysis**

Immunohistochemical analysis was accomplished as we previously reported (Batarseh *et al.*, 2017) Brain sections (16 μm-thick) were prepared using Leica CM3050S Research Cryostat

(Buffalo Grove, IL, USA); mice hemispheres were snap-frozen in dry-ice cold liquid 2-methyl butane (Sigma-Aldrich) and stored at -80°C. Subsequently, sections were fixed by incubation in methanol or 10 min at -20°C. Sections were washed 5 times in PBS and blocked in PBS containing 10% donkey serum for 1 h at room temperature. Immunostaining was performed for brains hippocampi of the wild-type young and aged mice, and TgSwDI. The entire hippocampus region was included in the analysis. IgG extravasation from brain microvessels was assessed by double staining for collagen IV to stain microvessels and mouse IgG to stain IgG extravasation using rabbit anti-collagen IV and fluorescein-conjugated donkey anti-IgG (both at 1:200 dilution), respectively (Batarseh *et al.*, 2017). CFL594-conjugated donkey anti-rabbit IgG was used as the secondary antibody for collagen IV (Batarseh *et al.*, 2017). For dextran extravasation, brain sections from young and aged wild-type mice were fixed and blocked, as described above, incubated with the rabbit anti-collagen-IV at 1:200 dilution, then probed with CF™ 350 goat anti-rabbit IgG (H+L) secondary antibody for collagen-IV. To detect brain Aβ, sections were immunostained with 6E10 antibody at 1:200 dilution. To detect Aβ-plaque load in the hippocampus, the brain sections were stained with a freshly prepared 0.02 % (w/v) Thio-S powder dissolved in 70 % ethanol for 30 min followed by incubation in 70% ethanol, as described previously (Kruyer *et al.*, 2015). For reactive astrocytes, TgSwDI sections were probed with rabbit anti-GFAP polyclonal IgG at 1:100 dilution followed by anti-rabbit IgG-CFL594 secondary antibody. Image acquisition was performed in 10 sections (separated by 150 μm) containing the hippocampus (total of 40 sections/mouse). Total Aβ load and Thio-S were captured and quantified at a total magnification of 4X, GFAP, IgG and dextran extravasation images were captured at 20X. Total images captures were 40 per mouse, and fluorescence intensity quantification was performed using ImageJ® version 1.6.0 software (Research Services Branch, National Institute of Mental

Health/National Institutes of Health, Bethesda, MD) after adjusting for threshold. Images were visualized by Nikon Eclipse Ti-S inverted fluorescence microscope (Melville, NY), Nikon-standard series filter cubes for DAPI, FITC, TRITC were used.

**Human $A\beta_{40}$ and $A\beta_{42}$ determination by ELISA**

To quantitatively extract soluble Aβ from TgSwDI mice brains, mouse brain tissue was homogenized in diethylamine buffer (0.2%), with complete mammalian protease inhibitor (Sigma-Aldrich). Then, it was centrifuged at 21,000g for 45 min at 4°C to collect supernatant (Qosa *et al.*, 2015b). Collected supernatants were used to analyze $A\beta_{40}$ and $A\beta_{42}$ brain levels using commercially available ELISA kits following the manufacturer protocols (ThermoFisher). All samples were run in triplicates, and obtained data was corrected to protein content using BCA assay.

**Analysis of brain acetylcholine levels**

Acetylcholinesterase (AChE) activity in TgSwDI mice brains' homogenates was determined indirectly by assessing acetylcholine (ACh) levels. The choline/acetylcholine assay kit from Abcam following the manufacturer instructions was used. The fluorescence detection of choline was measured at excitation/emission of 535/590 nm. This assay measures, besides free choline, total choline (i.e. free choline and ACh). ACh level was calculated by subtracting free choline from total choline.

**Sample preparation for tandem mass tagging labeling and proteomic analysis**

Proteomics analysis was performed and analyzed by the Proteomics core of the University of Arkansas for Medical Sciences (UAMS). Three of each granisetron-treated mice and control mice were used for proteomic experiment in both age groups. Proteins in tissue lysate were reduced, alkylated, and digested using filter-aided sample preparation (FASP) based on previous method with a minor modification (Coleman *et al.*, 2016). Tissues were lysed and solubilized in lysis buffer containing 0.1% (w/v) SDS, 150mM NaCl, 25 mM Tris-HCl pH 7.6, 1% (w/v) NP-40,1% (w/v) sodium deoxycholate. Protein extracts were alkylated using FASP in 50mM iodoacetamide in 8M urea, 100 mM Tris-HCl pH 8.5. Proteins were then digested with sequencing grade porcine trypsin (Promega, Madison, WI). Digested peptides were cleaned by 50 mg Sep-Pak SPE (Waters Milford, MA). Resuspended tryptic peptides were then labeled using a tandem mass tag 6-plex isobaric label reagent set (Thermo, Rockford, IL) following the manufacturer's instructions. Aged and young mice were grouped into two different TMT experiments. The combined samples of each TMT experiment were cleaned by 50 mg Sep-Pak SPE immediately before offline high pH fractionation.

The offline high pH fractionation was achieved as previously reported (Kore *et al.*, 2018). Briefly, labeled peptides were separated into 13 fractions on a 100x1.0 mm Acquity BEH C18 column (Waters, Milford, MA) using an UltiMate 3000 UHPLC system (Thermo) with a 40 min gradient from 99:1 to 60:40 buffer A:B ratio under basic pH conditions, and then consolidated into 13 super-fractions. Buffer A = 0.1% formic acid, 0.5% acetonitrile; buffer B = 0.1% formic acid, 99.9% acetonitrile. Both buffers adjusted to pH 10 with ammonium hydroxide for offline separation. Each super-fraction was then further separated by reverse phase Jupiter Proteo resin (Phenomenex, Torrance, CA) on an in-line 200 x 0.075 mm column using a nanoAcquity UPLC system (Waters Corporation, Milford, MA) as reported previously (Zybailov *et al.*, 2019).

Peptides were eluted by gradient separation followed by electrospray ionization (2.15 kV). The mass spectrometric analysis was achieved on an Orbitrap Fusion Tribrid mass spectrometer (Thermo) using multi-notch MS3 parameters (Zybailov *et al.*, 2019). MS/MS data were acquired over a range of 400-2000 m/z using the ion trap analyzer (Zybailov *et al.*, 2019).

**Protein identification and quantification**

Proteins were identified and reporter ions were quantified using MaxQuant (Max Planck Institute of Biochemistry, Martinsried, Germany; version 1.5.8.3) with a parent ion tolerance of 3 ppm, a fragment ion tolerance of 0.5 Da, and a reporter ion tolerance of 0.01 Da. Scaffold Q+S (Proteome Software Inc., Portland, OR; version 4.8.5) was used to verify MS/MS based peptide and protein identifications as well as to quantitate TMT Label Based Quantitation and data analysis.

**Ingenuity pathway analysis and bioinformatics analysis**

Ingenuity pathway analysis (IPA) was done by the Proteomics core of the University of Arkansas for Medical Sciences (UAMS). To understand the biological events in relation to the treatment, the entire complement of proteins that were statistically significantly different (FDR<0.05) between treatment and control groups containing 2-fold up- or down-regulated proteins were analyzed by Ingenuity Pathway Analysis version 42012434 (Ingenuity® Systems, www.ingenuity.com, Mountain View, CA). Right-tailed Fisher's exact test was used to calculate the P value in the canonical pathway. Calcium pathways-related protein networks analysis with differently expressed proteins were evaluated.

**Statistical analysis**

Data were expressed as mean ± SEM (to compare and test the difference between the data means which depends on the data size) for n=7 mice/group for wild type mice and n=5 mice/group for TgSwDI mice. The experimental results were statistically analyzed for significant difference using Student's t-test for two groups and one-way ANOVA for more than two-group analysis with *Bonferroni* post-hoc test. Data analyses were performed using GraphPad Prism, version 6.0. In the figures, the fold change for control groups was calculated by dividing each control value on the average of all control mice values for a specific protein. Treatment values were then normalized to control (1.0).

**Results**

**Effect of granisetron on endogenous IgG and exogenous dextran extravasations across the BBB and on the expression of BBB tight junction proteins**

Effect of granisetron on BBB leakiness was evaluated by immunostaining. Results showed that with age, there was an increase in dextran 10 KDa extravasation, dextran 40 KDa extravasation, and IgG extraversion that were significantly decreased by treatment only in the aged group (age*treatment: P=.0337, F= 4.705; P=.0006, F= 12.88; P=.0048, F= 9.455 interaction, respectively). However, it did not restore the levels to that of young controls.

As shown in Figure 5A-F, the extravasation of 10 KDa Texas-red dextran and 40 kDa FITC-dextran was significantly increased with aging (Figure 5C, E,F). In young mice, however, dextran extravasation was very low for the low molecular weight dextran (10 kDa) and was not observed with 40 kDa dextran (Figure 5A,B E,F). In aged mice, compared to vehicle treatment, granisetron significantly reduced extravasation of the florescence-tagged 10 and 40 kDa dextran

by 40 and 60%, respectively (Figure 5C-E). On the other hand, granisetron has no significant effect on dextran extravasation in young mice (Figure 5A, B and E). Florescence-tagged dextrans are biologically inert due to the poly-(α-D-1,6-glucose) linkages, which are resistant to cleavage by endogenous cellular glycosidases; in addition, dextran has low immunogenicity according to the manufacture data sheet (Sigma-Aldrich, https://www.sigmaaldrich.com/catalog/product/sigma/fd40s). Florescence-tagged dextran has been used extensively as exogenous traces for BBB permeability (Northrop, 2018). To evaluate granisetron effect on an endogenous and higher molecular weight BBB permeability marker, IgG extravasation was tested (Figure 5G-K). IgG is an established extravasation marker, where in healthy BBB, IgG is not detected in the brain; however with BBB breakdown, IgG extravasates by paracellular route into the brain parenchyma (Bowman *et al.*, 2007). Similar findings to those observed with dextran extravasation, IgG extravasation significantly increased with aging (Figure 5I), which was significantly reduced by granisetron (Figure 4, I, J and K), and such effect was not observed in the young mice (Figure 5G, H, and K).

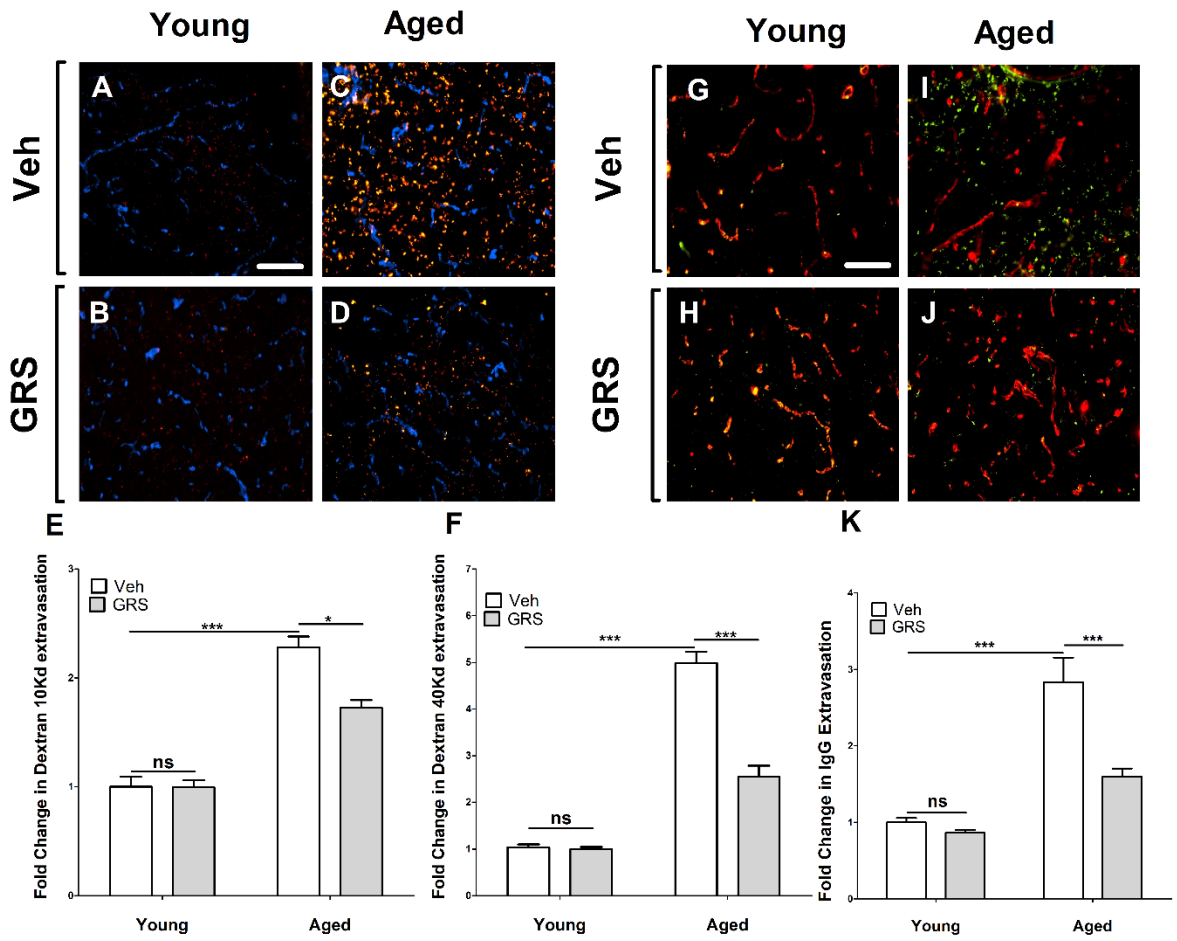


Figure 5**.** Granisetron enhanced BBB tightness in wild-type mice brains. Mice were treated with granisetron (3 mg/day) for 28 days**.** (A-D) Representative brain sections measured using two different molecular weight fluorescents tagged dextran 10KD (red) 40 KD (green) as exogenous markers for BBB permeability and anti-Collagen IV antibody (Blue) to detect microvessels where (A) young control group, (B) young granisetron group, (C) aged control group, and (D) aged granisetron group. (E,F) Optical density semi-quantification of dextran 10 KD and 40 KD extravasation respectively. (G-J) Representative brain sections immunostained with mouse IgG (green) and collagen (red) antibodies in wild type mice brains and IgG levels quantification where (G) young control group, (H) young granisetron group, (I) aged control group, (J) aged granisetron

group, (K) optical density semi-quantification of IgG extravasation. All values in E, F and J were normalized to Young-Veh that has a value of 1.0. In addition, GRS treatment values in E,F and J were compared to each group corresponding Veh. Veh is for vehicle-treated mice, GRS for granisetron, ns = not significant, **P<.01 and ***P<.001 by 2-way with Bonferroni post-test; n= 5-7 mice. Scale bar, 200 μm.

This increase in BBB tightness was associated with increased expression of tight junction proteins as determined by Western blot. Granisetron increased the tight junction proteins expression significantly in the isolated microvessels from both young and aged mice (Figure 6). In young mice, granisetron increased ZO-1, occludin, claudin-5, and JAM-1 by 2.0-, 1.4-, 1.7- and 1.3-fold (Figure 6A), and in aged mice by 2.5-, 1.4-, 2.1- and 1.6-fold, respectively (Figure 6B).

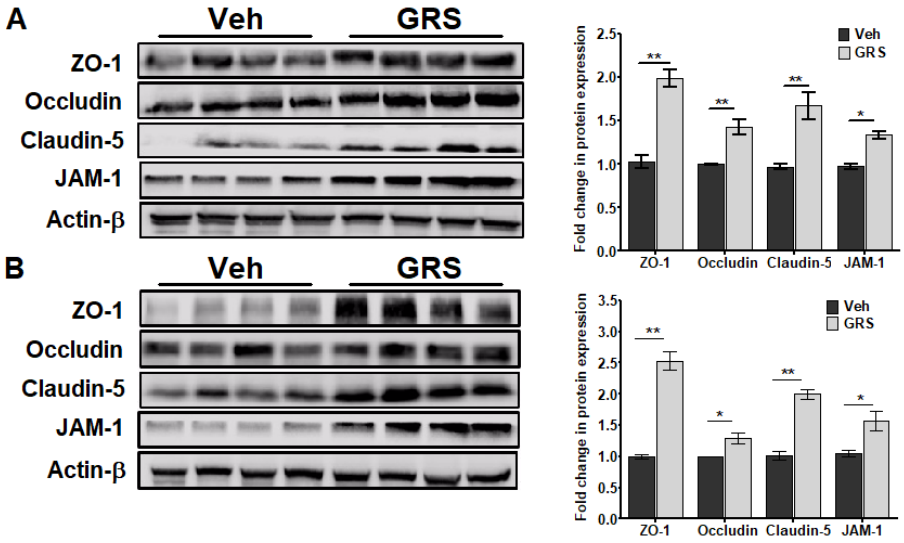


Figure 6**.** Granisetron (GRS) increased tight junction proteins expression in isolated microvessels from mice brains compared to vehicle-treated mice (Veh, control group). Representative western blots and densitometry analysis of the BBB tight junction proteins ZO-1, occludin, claudin-5 and JAM-1 in brain microvessels isolated from young (A), aged (B) wild type mice. Statistical analysis was determined by Student's t-test (n=5-7 mice). All values were normalized to Veh (1.0). *P<.05,

and **P<.01. Student's t-test for two groups was used for analysis.

Next, the effect of granisetron on BBB integrity was evaluated in TgSwDI mouse model for AD, and consistent with the wild-type aged mice results, granisetron significantly reduced IgG extravasation by 80% in the brains of TgSwDI mice (Figure 7A-C). This reduction was accompanied with significant increase in ZO-1, occludin, claudin-5 and JAM-1 by 2.8-, 3.1, 2.9- and 1.5-fold, respectively in TgSwDI mice (Figure 7 D, E).

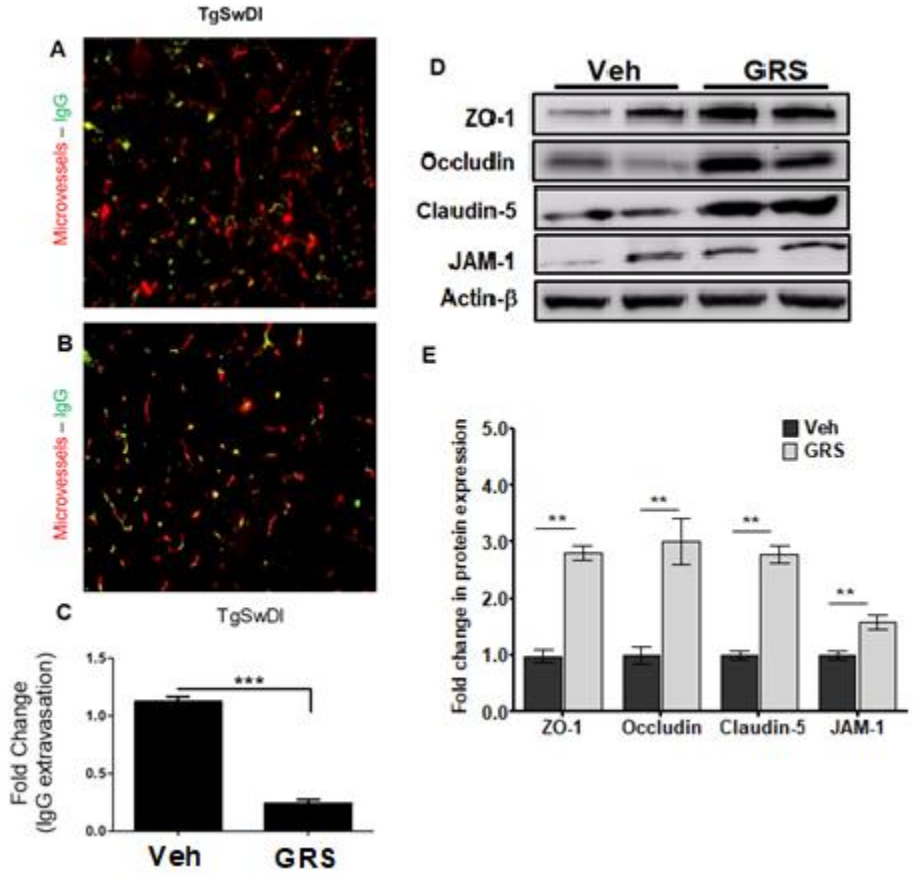


Figure 7. Granisetron (GRS) enhanced BBB tightness in TgSwDI mice brains compared to vehicle-treated mice (Veh). (A-B) Representative sections immunostained with mouse IgG (green) and collagen (red) antibodies in TgSwDI mice brains and IgG levels quantification where (A) Vehicle-treated TgSwDI, (B) GRS-treated TgSwDI mice, (C) optical density semi-quantification

of IgG extravasation. (D-E) Representative western blots and densitometry analysis of the BBB tight junction proteins ZO-1, occludin, claudin-5 and JAM-1 in brain microvessels isolated from TgSwDI mice. Statistical analysis was determined by Student's t-test (n=5-7 mice). All values were normalized to Veh (1.0). *P<.05, and **P<.01. Student's t-test for two groups was used for analysis.

### *In-vitro* studies on the effect of granisetron on bEnd3 cells tightness and calcium intracellular levels in bEnd3 and SH-SY5Y-APP695 cells

Mouse brain endothelial cells (bEnd3) treatment with 10 μM granisetron for 72 h increased expression of tight junction proteins significantly (Figure 8). Granisetron increased ZO-1, occludin, claudin-5, and JAM-1 by 3.5, 1.3, 3.4 and 1.3-fold respectively.

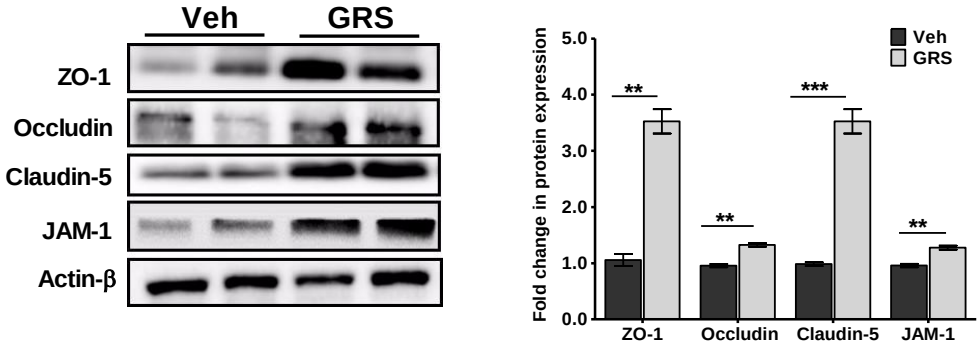


Figure 8. Granisetron (GRS) increased tight junction proteins in bEnd3 cells. Granisetron (10 μM) treatment for 72 h upregulated tight and adherent junction proteins levels in bEnd3 cells as shown in the representative blots and their densitometry analysis. All values were normalized to Veh (1.0). Statistical analysis was determined by Student's t-test, **P<.01, and ***P<.001 versus

vehicle-treated cells (Veh; n=3 dishes/experiment, with 3 independent experiments per treatment). Student's t-test for two groups was used for analysis.

The effect of granisetron on intracellular $Ca^{+2}$ levels was evaluated by testing the inhibitory effect of granisetron on calcium flux. For this, bEnd3 cells and SH-SY5Y-APP-transfected cells were treated with either granisetron (10 and 20 µM) or media for 24 h. The media was removed and replaced with HBSS buffer ($Ca^{+2}$/$Mg^{+2}$ free) and incubated with the exact volume of the sensitive $Ca^{+2}$ fluorescence indicator Fluo-4 direct as described in the methods section. As shown in (Figure 9A and B), intracellular $Ca^{+2}$ was significantly reduced in both bEnd3 and SH-SY5Y-APP cells. In another separate experiment, granisetron effect on neuronal $Ca^{+2}$ flux induced by $A\beta_{42}$ (2 µM) acute exposure was also evaluated. Granisetron significantly reduced $A\beta_{42}$-induced $Ca^{+2}$ flux by ~40% (Figure 9C).

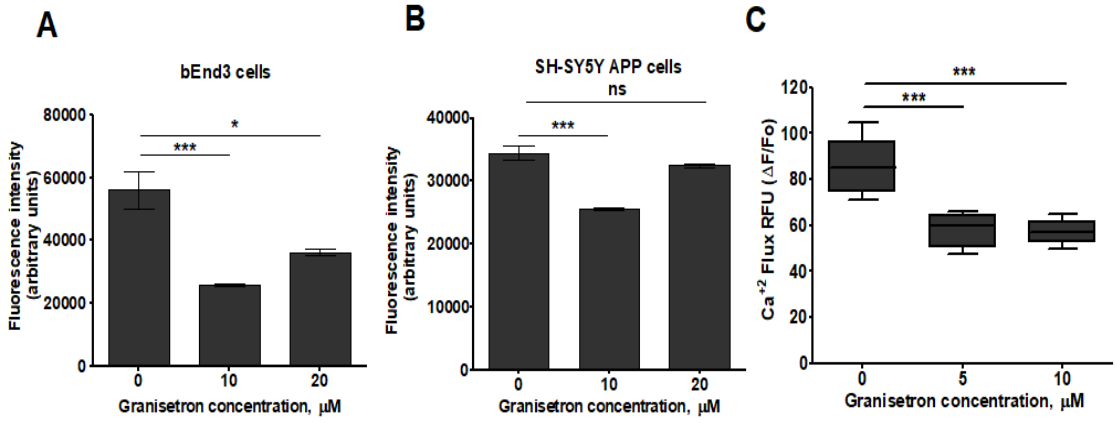


Figure 9. Granisetron (GRS) reduced intracellular calcium levels *in-vitro*. Comparison of the effect of granisetron on intracellular $Ca^{+2}$ level measured using the Fluo-4 $Ca^{+2}$senor in (A) bEnd3 cells, and (B) SH-SY5Y-APP cells after 24 h treatment with 10 and 20 µM. (C) SH-SY5Y-APP cells were additionally pre-treated with granisetron 5 and 10 µM for 24 h and were then acutely exposed

to freshly prepared $A\beta_{42}$ (2 μM) to measure $Ca^{+2}$ flux kinetics using Fluo-4 $Ca^{+2}$ senor. $Ca^{+2}$ flux assays were accomplished in HBSS buffer free of $Ca^{+2}$ and $Mg^{+2}$ to clarify $Ca^{+2}$ source in the cytosol. Each treatment was evaluated at least in eight replicate wells/assay, and each assay was repeated at least three times. Statistical analysis was done using one-way ANOVA with Dunnett post-hoc test. *P<.05 and ***P<.001 versus vehicle-treated cells (Veh).

**Effect of granisetron treatment on total brain Aβ in TgSwDI mice**

Compared to vehicle-treated mice, granisetron significantly reduced total Aβ immunostaining by 75% (Figure 10A-C). In addition, granisetron reduced Thio-S staining of Aβ plaques significantly by 80% compared to control group (Figure 10D-F).

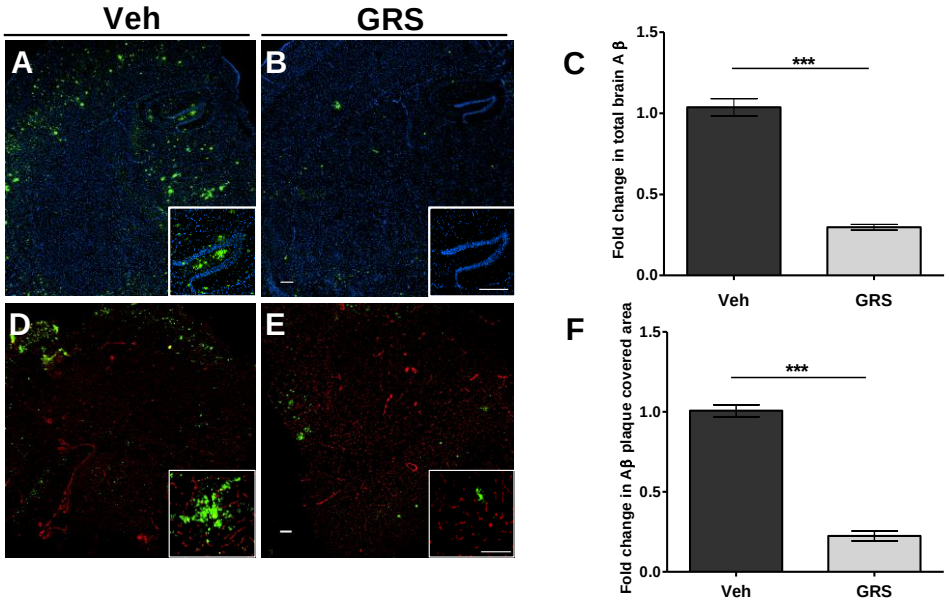


Figure 10. Granisetron (GRS) reduced Aβ burden in the brain and hippocampus of TgSwDI mice. (A-C) Representative brain sections stained with 6E10 (green) antibody against Aβ to detect total Aβ load and anti-collagen IV (blue) to stain microvessels. Hippocampus is seen at higher magnification in the closed inserts; (A) vehicle (Veh) group, (B) granisetron group, (C)

Quantification of total Aβ deposition. Values were normalized to Veh (1.0). (D-F) Representative hippocampus sections stained with Thio-S (green) antibody to detect Aβ plaques load and anti-collagen IV (red) to stain microvessels; (D) Vehicle (Veh) group, (E) granisetron group, (F) quantification of the area covered with Aβ plaques. Values were normalized to Veh (1.0). Statistical analysis was determined by Student's t-test (n=5 mice per group). ***P<.001 versus vehicle group. Scale bar, 200 μm.

ELISA quantification of soluble $A\beta_{40}$ and $A\beta_{42}$ peptides in mice brain homogenates confirmed that granisetron significantly reduced the levels of both peptides (Figure 11A, B).

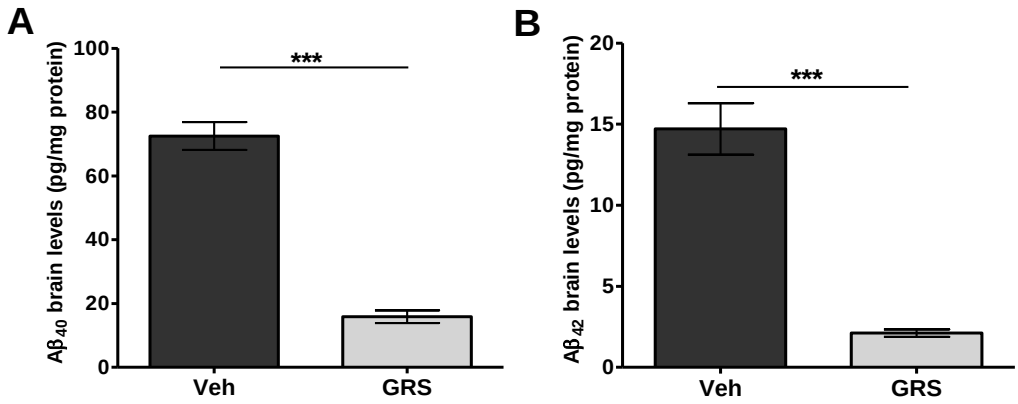


Figure 11**.** Granisetron (GRS) reduced Aβ levels in TgSwDI mice brains. Brain levels of both soluble human Aβ40 (A) and soluble human Aβ42 (B) levels were determined by ELISA. Statistical analysis was determined by Student's t-test (n=5 mice per group). ***P<.001 versus vehicle (Veh) group. Scale bar, 200 μm.

To explain Aβ reduction, the effect of granisetron on Aβ production and clearance proteins was evaluated by western blot. For Aβ production proteins, granisetron treatment reduced soluble APPβ (sAPPβ) and increased soluble APPα (sAPPα) expressions without altering BACE1 and

nicastrin, a subunit of the γ-secretase enzyme (Figure 12A,B). In addition to reduced Aβ production, granisetron enhanced Aβ clearance by inducing Aβ major transport protein P-gp without altering LRP-1 expression and reduced the receptor for advanced glycation end products (RAGE) at the BBB as determined in isolated brain microvessels (Figure 12C,D). Furthermore, granisetron increased significantly the expression of Aβ degrading enzymes IDE and NEP in mice brains homogenate when compared to control group (Figure 12E,F). P-gp and LRP-1 are key transport proteins expressed at the endothelial cells of the BBB that play role in Aβ clearance across the BBB (Mohamed *et al.*, 2016). Thus, their increased expression is expected to increase Aβ transport from brain to the blood. In addition, increased levels of P-gp and decreased levels of RAGE (located at the apical side of the endothelial cells and play role in Aβ transport from the blood to brain) are expected to reduce Aβ access from the blood to the brain across the BBB.

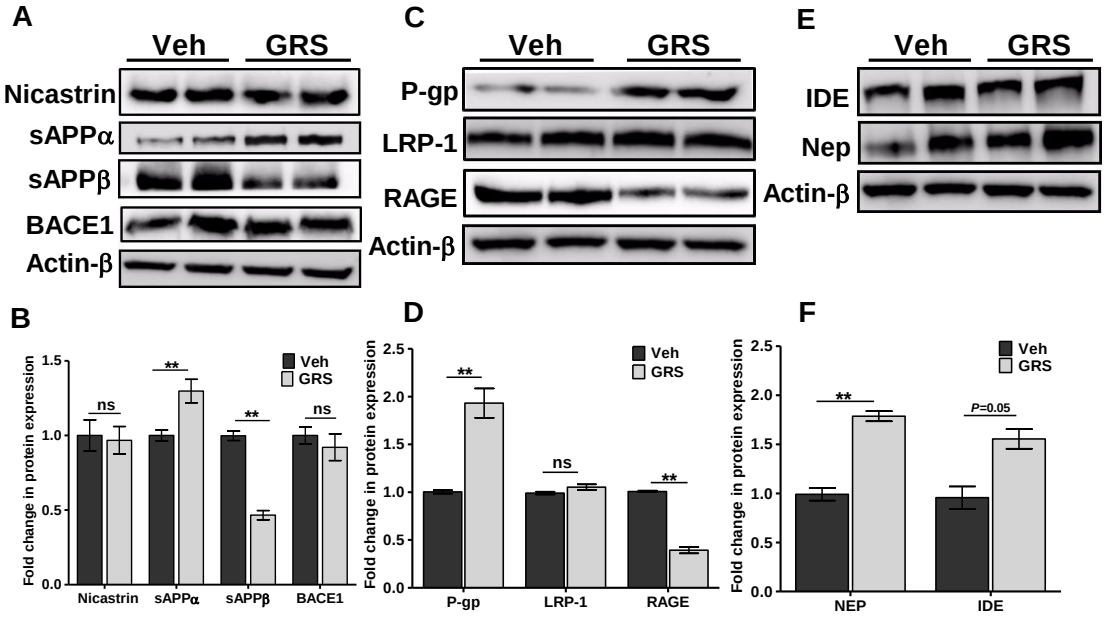


Figure 12**.** Granisetron (GRS) reduced Aβ brain load by reducing Aβ production and increasing Aβ clearance in TgSwDI mice brains. (A) Representative blots and (B) densitometry analysis showed a significant increase in sAPPα and reduction in sAPPβ levels in granisetron treated group,

with no significant effect on either BACE-1 enzyme or the nicastrin subunit of the γ-secretase enzyme in mice brains homogenates of TgSwDI mice. (C) Representative blots and (D) densitometry analysis showed granisetron treatment significantly increased P-gp expression, a major Aβ clearance protein across the BBB, and reduced RAGE responsible for Aβ transport from blood to brain but has no effect on LRP1. (E) Representative blots, and (F) densitometry analysis of major Aβ degrading enzymes IDE and neprilysin (NEP). Statistical analysis was determined by Student's t-test (n=5 mice per group). Values were normalized to Veh (1.0). ns=not significant, *P<.05, and **P<.01 versus vehicle (Veh) group.

**Effect of granisetron on brain inflammatory markers in TgSwDI mice brains**

The anti-inflammatory effect of granisetron against chronic inflammatory diseases in animal models has been reported previously (Fakhfouri *et al.*, 2010; Maleki-Dizaji *et al.*, 2010), however, its anti-inflammatory effect on Aβ-induced brain inflammation is not known. As a marker for Astrocytes activation (astrogliosis) is characterized by GFAP increased levels with an elongated shape and thick branches.

Our results demonstrated granisetron to reduce astrocytes activation (change in astrocytes shape and GAFP intensity) and ameliorated the astrocytes shape when compared to the control group (Figure 13A). Moreover, granisetron treatment reduced brain levels significantly of both the microglial marker Iba-1 by 30% and metalloproteinase-9 (MMP-9) enzyme by 47% (Figure 13 B,C).

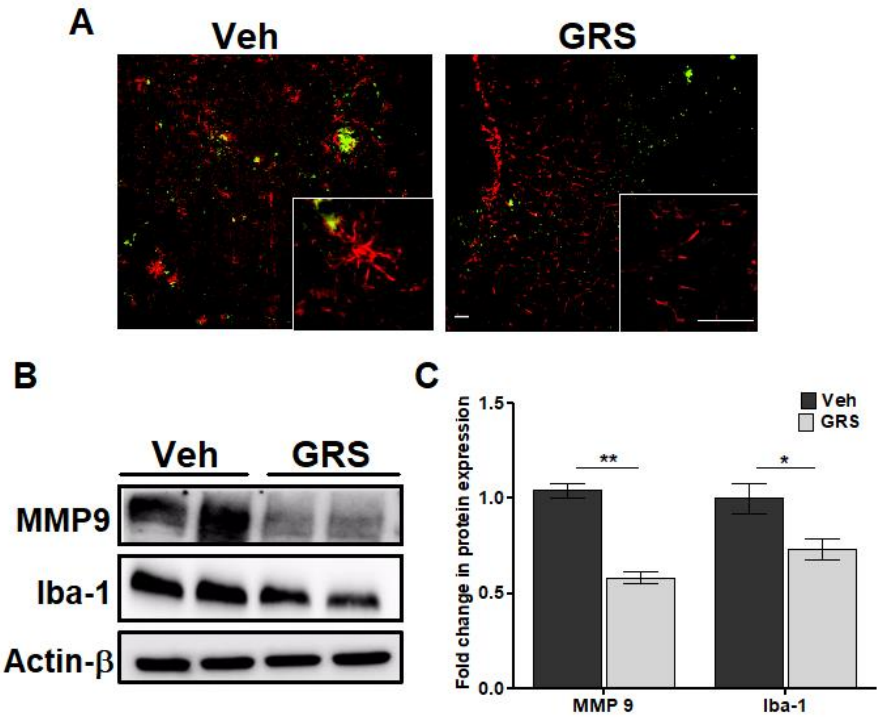


Figure 13**.** Granisetron (GRS) treatment reduced neuroinflammation. Neuroinflammation was assessed by measuring GFAP as a measure for astrocytes activation and by monitoring astrocytes morphology, MMP-9 and the microglial marker Iba-1 expressions where granisetron treatment significantly reduced their levels. (A) Representative brain sections double stained with GFAP (red) to detect activated astrocytes, and 6E10 (green) to detect Aβ in vehicle (Veh) and granisetron (GRS) groups (seen at higher magnification in the closed inserts). Scale bar, 200 μm. **(**B) Representative blots, and (C) densitometry analysis of MMP-9 and Iba-1 in TgSwDI mice brains homogenates. Values were normalized to Veh (1.0). Statistical analysis was determined by Student's t-test (n=5 mice per group). *P<.05, ** P <.01, and ***P<.001 versus vehicle treated (Veh) group.

**Effect of granisetron on the expression of synaptic markers and acetylcholine brain levels**

Granisetron increased brain acetylcholine levels significantly by 35% compared to the vehicle-treated group (Figure 14A). In addition, three synaptic markers were evaluated, the pre-synaptic marker SNAP-25, the post-synaptic marker PSD-95, and Synapsin-1. As shown in Figure 14B,C, granisetron treatment increased expression of the three evaluated synaptic markers significantly, PSD-95, synapsin-1, and SNAP-25 by 1.5-, 1.2- and 1.4-fold, respectively. This increase was associated with a significant reduction in levels of the apoptotic marker activated caspase-3 by 30% and increase in the anti-apoptotic marker Bcl-2 by 40% (Figure 14E,F). Caspase-3 is a key apoptotic marker, and its increased levels were associated with to neuronal death in AD (Louneva *et al.*, 2008).

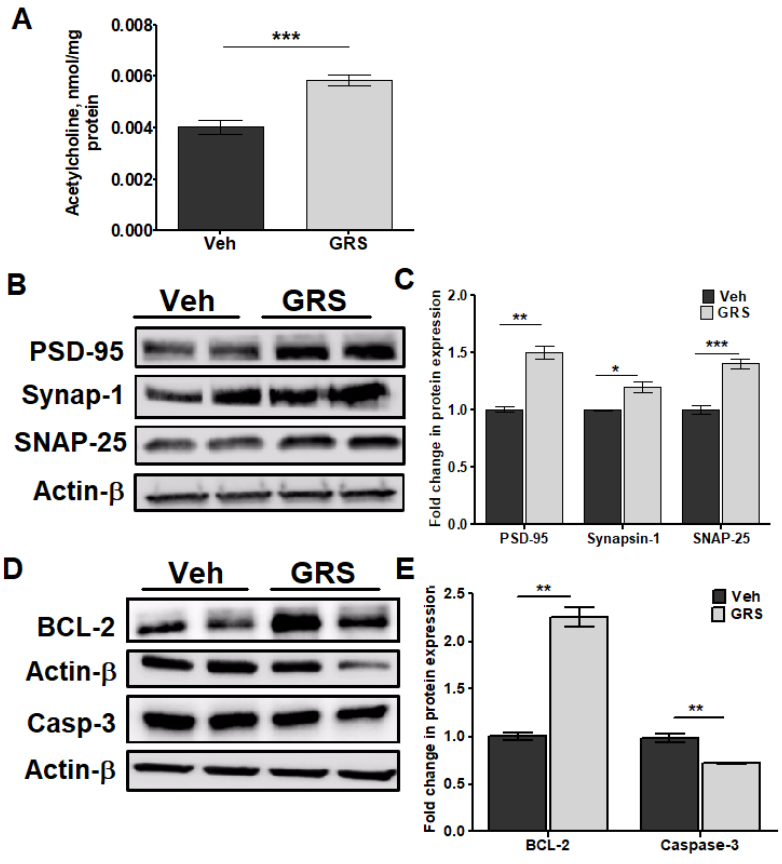

Figure 14. Granisetron (GRS) increased acetylcholine levels, up-regulated neuro-synaptic markers and reduced caspase-3 expression. (A) Acetylcholine level in the brain homogenates of both control and granisetron treated mice was measured using ELISA. (B) Representative blots, and (C) densitometry analysis of the synaptic markers PSD-95, Synapsin-1 and SNAP-25 in mice brains homogenates of TgSwDI mice. (D) Representative blots, and (E) densitometry analysis of the anti-apoptotic marker Bcl-2 and the apoptotic marker caspase-3 in brain homogenates of TgSwDI mice. Values were normalized to Veh (1.0). Statistical analysis was determined by Student's t-test (n=5 mice per group). *P<.05, ** P <.01, and ***P<.001 versus vehicle treated (Veh) group.

**Effect of granisetron on calcium signaling pathway in brains of TgSwDI mice**

To investigate the effect of granisetron on modulating proteins associated with $Ca^{+2}$ pathway, IP3-receptor (responsible for $Ca^{+2}$ efflux from the endoplasmic reticulum (ER) storage), phosphorylated-IP3R (Ser1756), $Ca^{+2}$/calmodulin-dependent protein kinase II (CaMKII) and phosphorylated-CaMKII (α, β, γ) were analyzed by Western blot. As shown in Figure 15, granisetron reduced the expressions of IP3R and phosphorylated-IP3R (Ser1756) significantly by 50% without affecting the ratio suggesting reduced levels of phosphorylated-IP3R is due to reduced total IP3R (Figure 15A,B). In addition, the treatment significantly increased CREB and p-CREB by 2.8 and 1.5-fold, respectively, increased PKA by 50%, and BDNF by 70% (Figure 15A, B). Another important key player in maintaining intracellular $Ca^{+2}$homeostasis is the calcium buffering protein calbindin-D28K, which was also significantly increased by granisetron treatment by 2.3-fold (Figure 15C,D). Besides, granisetron significantly reduced CaMKII expression while increased the three phosphorylated-CaMKII α, β, γ isoforms (Figure 15E-G).

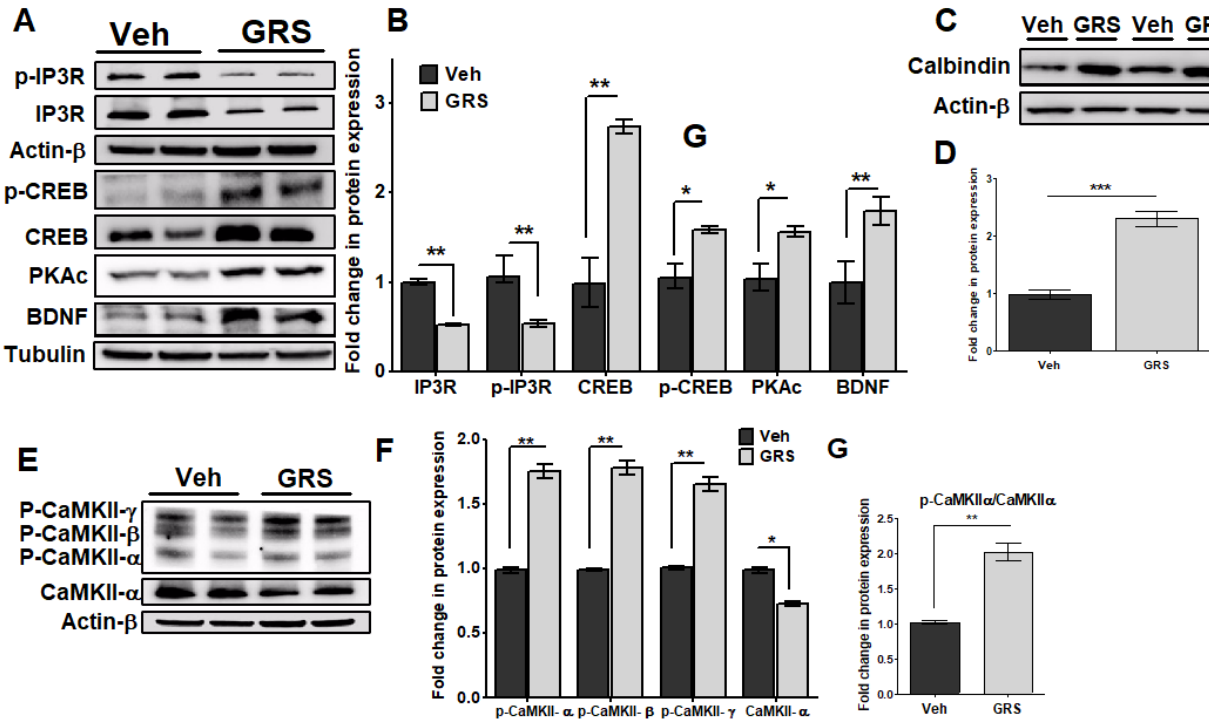


Figure 15**.** Granisetron (GRS) modulated calcium pathway in TgSwDI mice**. (**A) Representative blots and (B) densitometry analysis showed granisetron treatment significantly reduced total IP3R and p-IP3R expressions and increased PKAc, BDNF, CREB, and p-CREB expressions. (C) Representative blots and (D) densitometry analysis showed a significant increase in the expression of the Ca+2 buffering protein calbindin D28K. (E-G) Representative blots and densitometry analysis showed a significant reduction in CaMKII expression with increased levels of phosphorylated-CaMKII α, β, γ isoforms. Values were normalized to Veh (1.0). Statistical analysis was determined by Student's t-test (n=5 mice per group). ns = not significant, *P<.05, **P<.01, and ***P<.001 versus vehicle (Veh) group.

**Identification and quantification of calcium pathway-associated proteins in response to granisetron, and IPA analysis**

TMT-labeled relative quantitative proteomics was used to identify and quantify differentially expressed proteins between granisetron treatment in both young and aged groups and their control groups. Due to effect similarity between young and aged mice, data were pooled. These proteins were further being used in IPA analysis. For combined data set, a total of 434 differentially expressed proteins in response to treatment were identified using Mann-Whitney Test with significance level $P<.05$ corrected by Benjamini-Hochberg.

To better understand the role of granisetron in the brain, differentially expressed proteins were further subjected to IPA core analysis. Among 434 differentially expressed proteins between treatment and control groups, 422 proteins were mapped with IPA (155 down and 267 up) with increased or decreased more than 2-fold change. IPA revealed that 11 proteins (ATP2B1 (PMCA), CACNA2D2 (VGCC), CACNG8, CAMK4, CAMK2G, CAMKK1, GRIA2 (AMPAR), HDAC6 ITPR1 (IP3R), PPP3CA, RAP2B) involved in calcium signaling pathway ($P = 0.002$, Z score = 0.632; Figure 16, Table 1). Also, 15 proteins (CACNA2D2, CACNG8, CAMK4, CAMK2G, GNA13, GNAL, GNB1, GRIA2, GRID2, ITPR1, PLCB3, PLCB4, PRKCA, PRKCD, RPS6KA1) were found in CREB signaling pathway ($P = 1.35E-05$, Z score = -0.632; Figure 16, Table 2).

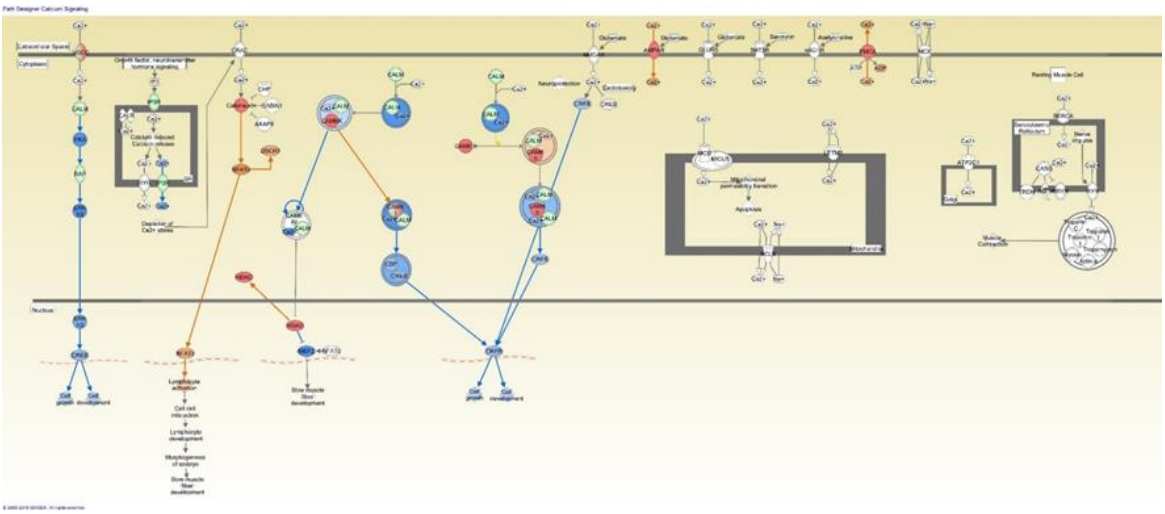

Figure 16. Calcium signaling pathway in response to granisetron treatment with the IPA molecule activity predictor. Red symbols indicate proteins up-regulation, while green symbols indicate down-regulation in granisetron treated mice, respectively. Orange and blue nodes indicate predictions of to be activated or inhibited in granisetron treated mice, respectively. The intensity of the color represents the degree of fold change. Orange edges (arrows) indicates activation of downstream proteins, blue edges indicates inhibition of downstream proteins. Yellow edges indicate inconsistency between observed results with the prediction based on literature findings.

**Table 1:** A selection of significantly changed proteins in calcium pathway (P<.05; fold change > 2) for granisetron effect in C57Bl/6J wild-type mice as determined by IPA analysis.

| Symbol | Entrez Gene Name | Symbol in pathway | Experimental P-value | Experimental Fold Change | Expected | Location | Type |
|---|---|---|---|---|---|---|---|
| CACNA2D2 | calcium voltage-gated channel auxiliary subunit alpha2 delta 2 | CaCn | 0.00009 | -2.46 | | Plasma Membrane | ion channel |
| CACNG8 | calcium voltage-gated channel auxiliary subunit gamma 8 | CaCn | 0.0036 | 2.42 | | Plasma Membrane | ion channel |
| CAMK4 | calcium/calmodulin dependent protein kinase IV | CAMK IV | 0.00012 | -2.23 | Up | Nucleus | kinase |
| CAMK2G | calcium/calmodulin dependent protein kinase II gamma | CAMK II | 0.0009 | 2.22 | Up | Cytoplasm | kinase |
| GNA13 | G protein subunit-α13 | Gα | 0.0022 | -2.16 | | Plasma Membrane | enzyme |
| GNAL | G protein subunit-αL | Gα | 0.0017 | -2.61 | | Cytoplasm | enzyme |
| GNB1 | G protein subunit-β1 | Gβ | 0.00009 | 2.36 | | Plasma Membrane | enzyme |
| GRIA2 | glutamate ionotropic receptor AMPA type subunit 2 | iGLUR | 0.0019 | 2.19 | Up | Plasma Membrane | ion channel |
| GRID2 | glutamate ionotropic receptor δ type subunit 2 | iGLUR | 0.00009 | -5.08 | Up | Plasma Membrane | ion channel |
| ITPR1 | inositol 1,4,5-tris-phosphate receptor type 1 | IP3R | 0.00009 | -2.88 | Up | Cytoplasm | ion channel |
| PLCB3 | phospholipase C β3 | PLC | 0.00028 | -2.42 | Up | Cytoplasm | enzyme |
| PLCB4 | phospholipase C β4 | PLC | 0.00009 | -2.45 | Up | Cytoplasm | enzyme |
| PRKCA | protein kinase C α | PKC | 0.0042 | 2.16 | Up | Cytoplasm | kinase |
| PRKCD | protein kinase C δ | PKC | 0.00011 | 2.25 | Up | Cytoplasm | kinase |
| RPS6KA1 | ribosomal protein S6 kinase A1 | p90RSK | 0.0031 | -2.35 | Up | Cytoplasm | kinase |

**Table 2:** A selection of significantly changed proteins in CREB pathway (P<.05; fold change > 2) for granisetron effect in C57Bl/6J wild-type mice as determined by IPA analysis.

| Symbol | Entrez Gene Name | Symbol in pathway | Experimental P-value | Experimental Fold Change | Expected | Location | Type |
|---|---|---|---|---|---|---|---|
| ATP2B1 | ATPase plasma membrane Ca2+ transporting 1 | PMCA | 0.0016 | 2.17 | Up | Plasma Membrane | transporter |
| CACNA2D2 | calcium voltage-gated channel auxiliary subunit alpha2delta 2 | VGCC | 0.00009 | -2.46 | Up | Plasma Membrane | ion channel |
| CACNG8 | calcium voltage-gated channel auxiliary subunit gamma 8 | VGCC | 0.0036 | 2.42 | Up | Plasma Membrane | ion channel |
| CAMK4 | calcium/calmodulin dependent protein kinase IV | CAMK IV | 0.00012 | -2.23 | Up | Nucleus | kinase |
| CAMK2G | calcium/calmodulin dependent protein kinase II gamma | CAMK II | 0.0009 | 2.22 | Up | Cytoplasm | kinase |
| CAMKK1 | calcium/calmodulin dependent protein kinase 1 | CAMKK | 0.00065 | 2.28 | Up | Cytoplasm | kinase |
| GRIA2 | glutamate ionotropic receptor AMPA type subunit 2 | AMPAR | 0.0019 | 2.19 | Up | Plasma Membrane | ion channel |
| HDAC6 | histone deacetylase 6 | HDAC | 0.0024 | 2.19 | | Nucleus | transcription regulator |
| ITPR1 | inositol 1,4,5-trisphosphate receptor type 1 | IP3R | 0.00009 | -2.88 | Up | Cytoplasm | ion channel |
| PPP3CA | protein phosphatase 3 catalytic subunit α | CALM | 0.0059 | 2.2 | Up | Cytoplasm | phosphatase |
| RAP2B | RAP2B, member of RAS oncogene family | RAP | 0.0032 | -2.18 | Up | Plasma Membrane | enzyme |

The activity of molecules in both pathways were assessed with the molecule activity predictor in IPA. Blue colored molecules are predicted to be inhibited (decreased activity/expression) and orange colored molecules to be activated (increased activity/expression) by granisetron treatment. These predictions are based on Ingenuity Knowledge Base findings (i.e. literature).

Selected proteins from aged mice brain homogenates were analyzed by Western blot for confirmation. These proteins include IP3R, CaMKII, calbindin, and CREB. Results from Western blot revealed consistent pattern with LC/MS analyzed proteins IP3R, calbindin and CaMKII; CREB, on the other hand, was increased that is inconsistent with the pathway prediction (Figure 17). A graphical scheme summarizing the overall proposed effect of granisetron is presented in Scheme 2.

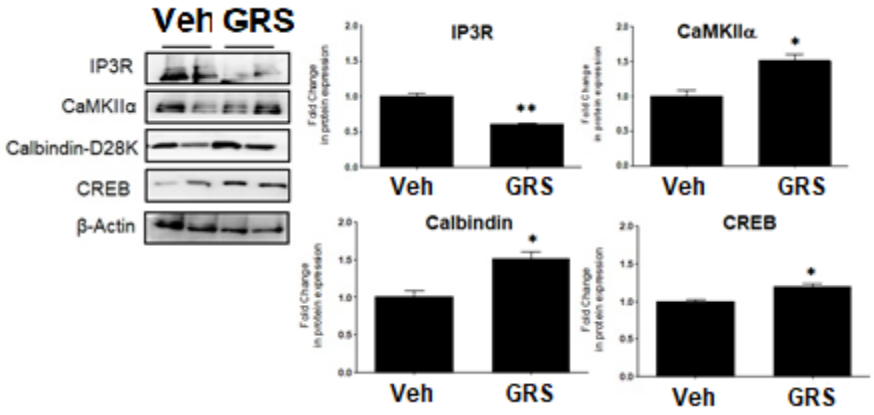


Figure 17. Granisetron modulated CREB pathway in the brains of C57Bl/6J aged mice. Data are presented as mean±SEM of 5 mice in each group. Statistical analysis was determined by Student's t-test. *P<.05 and **P<.01 versus control group.

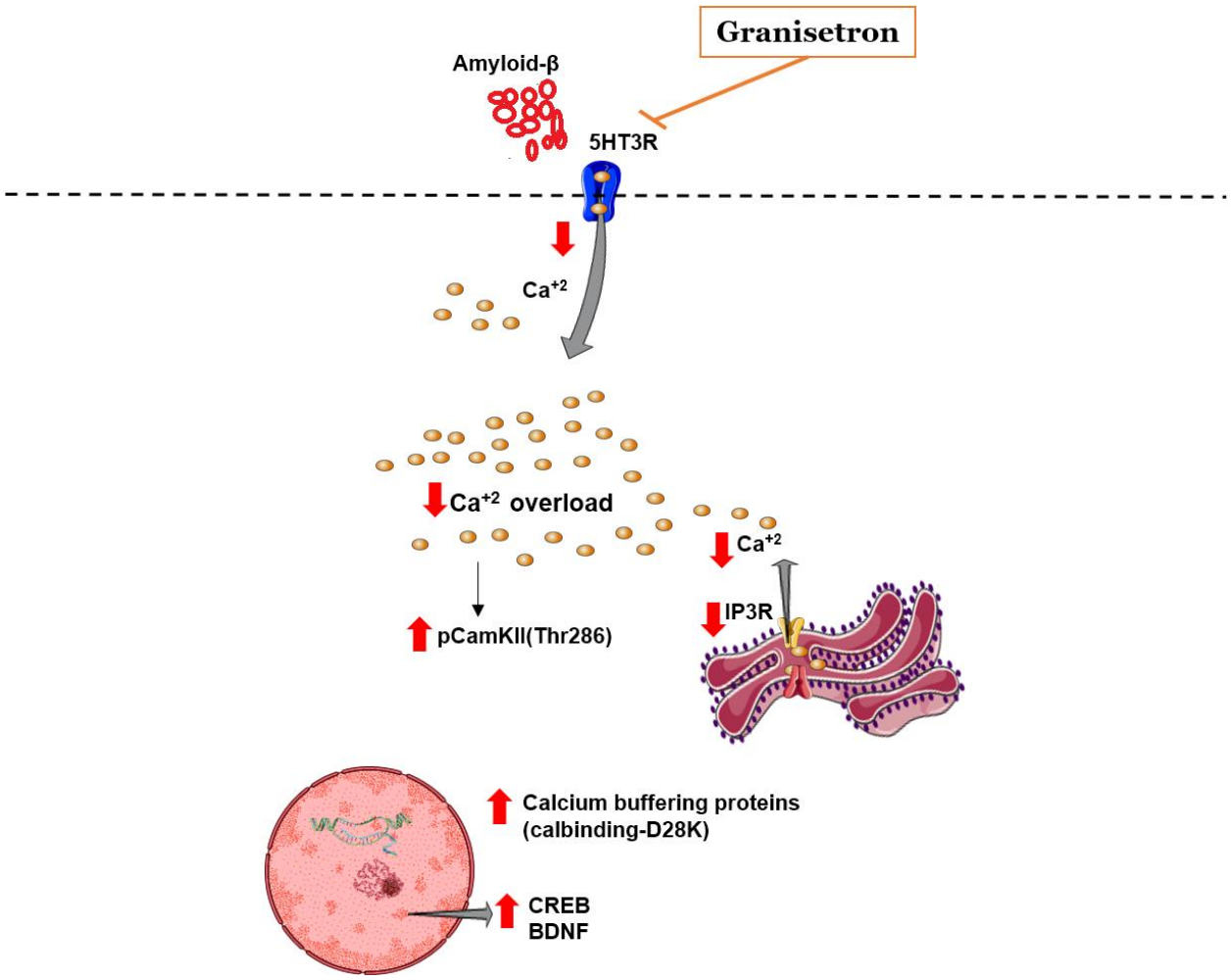


Scheme 2. Schematic summary describing the effect of granisetron on calcium pathway

**Discussion**

Recent studies have reported that 5-HT3 receptor antagonists, including granisetron, have neuroprotective properties in aged mice, and in neurotoxicity- and memory impairment-induced animals (Chugh *et al.*, 1991; Ohno and Watanabe, 1997; Boast *et al.*, 1999; Rahimian *et al.*, 2013) Spilman *et al.*, 2014)). In the current study, our data revealed that granisetron reversed AD pathology in an AD mouse model, suggesting a probable therapeutic role for the 5HT3 receptor in the disease. However, the potential mechanism(s) by which these drugs exert such effects are not fully investigated.

Findings from our HTS assay identified granisetron as a potent drug to reduce Aβ-induced disruption of an *in-vitro* BBB model, an effect that was not observed with other screened 5-HT3 antagonists (Qosa *et al.*, 2016). To confirm these results, in this work, we aimed to evaluate granisetron's effect in wild-type young and aged mice and in a mouse model of AD and investigate the potential mechanism(s) by which granisetron exhibits such effect. Mice were daily administered with granisetron for 28 days via Alzet pump; a treatment period that is longer than other studies evaluated granisetron effect at a single dose up to one-week given every other day (Fakhfouri *et al.*, 2010; Javadi-Paydar *et al.*, 2012; Aithal *et al.*, 2014). The 28 days treatment period was selected in order to test the therapeutic potential of long-term dosed granisetron on BBB integrity and Aβ-related pathology in a mouse model of AD. Our findings demonstrated granisetron ability to enhance the BBB integrity and function, reduce Aβ accumulation and neuroinflammation, decrease sustained calcium flux and synaptic loss in TgSwDI, a mouse model of AD and CAA. In addition, we showed for the first time that granisetron effect was partly associated with changes in the CaMKII/CREB pathway that is perturbed by aging and AD.

Available *in-vitro* studies have demonstrated 5-HT3 receptor antagonists including granisetron to inhibit extracellular calcium influx into cells (Ronde and Nichols, 1997; Homma *et al.*, 2006; Hutchinson *et al.*, 2015). Based on its mechanism, granisetron decrease depolarization and elevation of calcium by blocking the 5-HT3 receptor (Derkach *et al.*, 1989; Maricq *et al.*, 1991). A recent study has reported the treatment of Aβ-challenged cortical neurons isolated from rats brains with 5-HT3 receptor antagonists MDL 72222 and Y 25130 significantly reduced Aβ-caused calcium elevation, caspase-3 activity, and apoptosis, an effect that was mediated by 5-HT3 receptor antagonism (Ban and Seong, 2005). Similarly, our *in-vitro* studies demonstrated treatment of endothelial and neuronal cells with granisetron for 24 h significantly reduced Aβ induced-intracellular calcium levels, suggesting granisetron reduced calcium influx by blocking the 5-HT3 receptor. This effect could explain the positive outcome observed *in-vivo* as blocking 5HT3 receptor by granisetron is expected to reduce intracellular calcium levels, and thus modulate the CaMKII/CREB pathway.

Preliminary results from the proteomics analysis demonstrated granisetron to modulate calcium and CREB pathways associated proteins including IP3R, CaMK proteins, calcium voltage-gated channels and other proteins important to maintain $Ca^{+2}$ homeostasis that are altered in AD (Hardingham *et al.*, 2001; Gu *et al.*, 2009; Yamagata *et al.*, 2009; Teich *et al.*, 2015). Findings from *in vitro* studies using primary mouse neuronal cells, endothelial cells and astrocytes exposed to Aβ demonstrated increased $Ca^{+2}$ influx and disrupted intracellular $Ca^{+2}$ homeostasis caused by calcium abnormal and excessive release from the ER through IP3R (Stutzmann, 2005; Grolla *et al.*, 2013), and ryanodine receptor (RYR) (Thibault *et al.*, 2007; Oulès *et al.*, 2013) have been reported as key players in the pathology of AD that are associated with cognitive dysfunction (Egorova and Bezprozvanny, 2018). To confirm the proteomics data, LC/MS measured, and IPA

predicted proteins were analyzed by Western blotting. For this, a selected number of proteins from the CREB pathway in aged mice brains including IP3R, CaMKII, calbindin, and IPA predicted CREB protein were analyzed. Findings demonstrated a comparable effect between proteomics-measured data and Western blot-analyzed proteins (i.e. reduced IP3R, and increased CaMKII and calbindin) in aged mice. However, the IPA analysis that predicts effect based on the Ingenuity Knowledge Base from literature, predicted two opposing effects on CREB, activation via CaMKII pathway or inactivation via CALM/CaMKIV pathway (Figure 16). Western blot findings in aged and TgSwDI mice brains, however, determined granisetron to up-regulate/activate CREB, which is consistent with the CaMKII/CREB pathway shown in Figure 15.

Similarly, Western blot data from TgSwDI mice brain homogenates confirmed reduced expression of IP3R and p-IP3R with a significant increase in the level of calcium buffering protein calbindin D28K, which plays important role in restricting the amplitude of $Ca^{+2}$ signals (Palop *et al.*, 2003). Our findings also indicated that besides CREB activation through αCaMKII, 5HT3-receptor blocking by granisetron activated PKA/CREB pathway. Both pathways play a major role in memory formation through regulating the long-term potentiation (LTP), which are dysregulated in AD (Vitolo *et al.*, 2002; Yamagata *et al.*, 2009). The nature of αCaMKII dysregulation in AD is complex and not well understood, however, reduced activation of this enzyme was associated with synaptic loss (Gu *et al.*, 2009). Consistent with its effect on CaMKII activation in aged mice brains observed from proteomics data and Western blot, in TgSwDI mice brains, granisetron significantly increased p-CaMKII levels where the treatment was able to activate αCaMKII by phosphorylation at Thr286 site. Phosphorylation of αCaMKII at Thr286 amino acid switches the subunit activity within αCaMKII from a $Ca^{+2}$/CaM-dependent to independent state, which is important for NMDAR-dependent LTP at hippocampal CA1 synapses (Yamagata *et al.*, 2009). In

addition, it has been shown that Aβ inhibits PKA/CREB pathway (Vitolo *et al.*, 2002). The association of the PKA/CREB pathway downregulation with $Ca^{+2}$ dyshomeostasis has been reported (Liang *et al.*, 2007). CREB phosphorylation by CaMKII and PKA is essential for synaptic strengthening (Teich *et al.*, 2015; Rosa and Fahnestock, 2015). Available *in-vivo* studies in AD mouse models showed a significant reduction in CREB activation in the nuclear fraction (Hardingham *et al.*, 2001; Teich *et al.*, 2015), and subsequent BDNF downregulation that was associated with memory impairment (Vitolo *et al.*, 2002; Walton and Dragunow, 2018). CREB is a transcriptional regulator of BDNF that plays an important role in learning and memory processes. BDNF transcription is initiated through the phosphorylation of CREB at Ser133 by CaMKII and PKA activation (Yan *et al.*, 2016; Rosa and Fahnestock, 2015). In our studies, in addition to CaMKII activation, granisetron significantly increased PKAc (the free and active form of PKA) and CREB, which collectively contributed to increased levels of p-CREB (S133) and BDNF. This positive effect on the CREB pathway could be an overall result of the reduced sustained increase in $Ca^{+2}$i levels, which directly and/or indirectly enhanced the BBB integrity and function, reduced Aβ levels and associated neuroinflammation, increased ACh levels and synaptic markers, and reduced neurotoxicity. While these findings support the beneficial effect of granisetron, parallel groups of wild-type mice would help in explaining whether the effect observed is directly related to BBB function improvement or indirectly due to reduced Aβ-related pathology.

The precise mechanism leading to BBB dysfunction remains unclear, however, in AD, Aβ could, directly or indirectly, disrupt tight junction proteins by disrupting calcium homeostasis, leading to an overall BBB dysfunction (Mattson *et al.*, 1992; Kook *et al.*, 2012). Measurements of exogenous and/or endogenous plasma-derived molecules extravasation in brain parenchyma have been widely used as a method to detect BBB disruption (Wisniewski *et al.*, 1997). Findings from

aged mice confirmed granisetron to enhance the BBB tightness as measured by reduced permeability of the endogenous BBB permeability marker IgG (150KDa) and exogenous fluorescent-tagged dextran of 10 and 40 KDa. These results were supported with increased expression of tight junction proteins. When tested in TgSwDI mice, granisetron significantly enhanced BBB integrity and function as measured by reduced IgG extravasation and increased expression of tight junction proteins, which is consistent with our previously reported *in-vitro* finding in chapter 2, in the CAA-cell based BBB model (Qosa *et al.*, 2016), and reduced brain Aβ accumulation. This reduction in Aβ load was concomitant with a significant increase in the expression of P-gp, Aβ major transport protein across the BBB, in isolated microvessels, and Aβ degrading enzymes NEP and IDE in brain homogenates. Reduced levels of P-gp and degrading enzymes with aging and in AD have been previously reported and were related to brain Aβ accumulation (Cirrito *et al.*, 2005; Carty *et al.*, 2013), where their up-regulation reduced brain Aβ levels and related pathology (Qosa *et al.*, 2012; Mohamed *et al.*, 2016). Besides increasing Aβ clearance, granisetron significantly reduced sAPPβ and increased sAPPα levels collectively contributing to reduced Aβ brain load. Several studies reported sAPPα possesses neurotrophic and neuroprotective activities (Mattson *et al.*, 2002a). Interestingly, these findings, possibly through restoring calcium homeostasis, support the ability of granisetron to reduce brain levels of Dutch- and Iowa-mutated Aβ known for their slow brain clearance (Davis *et al.*, 2004), which extends a beneficial effect not only for sporadic but also for familial AD and CAA.

In addition, granisetron successfully reduced neurotoxicity and neuroinflammation as determined by increased expressions of synaptic markers, reduced caspase 3 and increased BCL-2, reduced MMP-9 and glial activation. Mice treated with granisetron exhibited a significant reduction in glial activation markers Iba-1 and GFAP. GFAP-expressing hypertrophic astrocytes

exhibited a widespread pattern in the brain of vehicle-treated TgSwDI mice. These activated astrocytes were readily identified around the senile plaques by their thicker, star-shape and bigger cell bodies. This greater increase in GFAP-positive cells was significantly reduced by granisetron. These findings add to existing reports on the potential anti-inflammatory effect of granisetron (Maleki-Dizaji *et al.*, 2010), and tropisetron (Rahimian *et al.*, 2011a). This anti-inflammatory effect by 5HT3-receptors antagonists could be related to calcineurin inhibition (Rahimian *et al.*, 2011b); calcineurin is a $Ca^{+2}$/CaM-dependent enzyme that upregulates numerous cytokines and pro-inflammatory factors (Medyouf *et al.*, 2007).

In addition, granisetron treatment significantly increased acetylcholine levels in TgSwDI mice brains. The inhibitory role of 5-HT3 receptor agonists on acetylcholine release has been reported. For example, 2-methyl-5-HT, a selective 5-HT3 agonist, inhibited acetylcholine release from the cerebral cortex of freely moving guinea-pigs, an effect that was blocked by ICS205-930, a selective 5-HT3 antagonist (Bianchi *et al.*, 1990). Likewise, granisetron produced a concentration-dependent increase in acetylcholine release in rat entorhinal cortex and striatal slices, an effect that was calcium dependent (Ramirez *et al.*, 1996). Collectively, these findings suggest the granisetron effect on acetylcholine-increased levels is mediated, at least in part, by blocking the 5HT3 receptor. Based on these positive effects, granisetron improved the performance of GRS treated mice as determined by Morris Water Maze test (See appendix 2, Figure 1S).

Several studies linked BBB disruption (Kook *et al.*, 2012), Aβ accumulation (Oulès *et al.*, 2013), neuroinflammation (González-Reyes *et al.*, 2017), and memory impairment to calcium dyshomeostasis. Indeed, further studies are required to answer the question of whether granisetron

observed positive effect on Aβ brain load and other associated pathological hallmarks is through its ability to modulate calcium homeostasis or independent of calcium pathway.

However, data from the *in-vitro* studies and aged mice that do not express Aβ pathology suggest granisetron demonstrated its effect, at least in part, by restoring calcium homeostasis through blocking 5HT3-receptor. Thus, our findings support granisetron repurposing to slow, halt the progression and/or treat AD and related disorders. Furthermore, based on its positive effect to improve the BBB function, in addition to AD, our findings suggest granisetron could be useful for other neurological diseases characterized by disrupted BBB function such as amyotrophic lateral sclerosis, Parkinson disease, multiple sclerosis (Sweeney *et al.*, 2018b).

In conclusion, while further studies are essential to test the effect of long-term administration of granisetron in dose-dependent studies, our findings support the repurposing of granisetron as a therapeutic drug for AD, and possibly other neurological diseases associated with BBB disruption.

# Chapter 4

Oleocanthal-rich extra-virgin olive oil enhance blood-brain barrier integrity and reduce amyloid pathology in Alzheimer's disease model


## Abstract

Alzheimer's disease (AD) is a progressive neurodegenerative disorder characterized not only by extracellular amyloid (Aβ) plaques and neurofibrillary tangles but also by neuroinflammation, dysfunctional blood-brain barrier, and impaired autophagy. Thus, novel strategies that target multiple disease pathways would be essential to prevent, halt and/or treat the disease. Growing body of evidence including our studies supported a protective effect of oleocanthal (OC) and extra-virgin olive oil (EVOO) at early AD stages before the pathology onset starts, however, the potential mechanism(s) by which OC and EVOO exert such effect, and whether this effect extends to a later stage of AD remain unknown. Thus, in the current study, we sought first to evaluate the effect of OC-rich EVOO consumption on AD pathology in TgSwDI, an AD mouse model, starting at 6 months of age for 3 months treatment, and then to elucidate the potential mechanism(s) by which OC-rich EVOO exerts the observed beneficial effect. Overall findings demonstrated OC-rich EVOO showed a significant reduction in Aβ load, reduced neuroinflammation through inhibition of NLRP3 inflammasome and inducing autophagy markers through activation of AMPK/ULK1 pathway. Thus, diet supplementation with OC-rich EVOO could have the potential to slow and/or hold the progression of AD.

## Introduction

Alzheimer's disease (AD) is the most common neurodegenerative disease and form of dementia, which accounts for 60-80% of all cases worldwide (Alzheimer's Disease International, 2018b). Unfortunately, to date, there is no disease-modifying treatment for AD. The pathology of this devastating neurodegenerative disorder is complex. While the cause of AD is not clear, the cardinal features commonly observed in the brain of AD patients are the deposition of amyloid-β (Aβ) plaques, aggregation of hyper-phosphorylated tau protein, abnormal neurites, neuropil threads, synapses and neuronal loss, astrogliosis, microglial activation, cerebral amyloid angiopathy (CAA) , and a disrupted blood-brain barrier (BBB) (Disterhoft *et al.*, 1994; Brown and Davis, 2002; Yarlagadda *et al.*, 2007; Gibson *et al.*, 2017; Uzuki *et al.*, 2017; Lane *et al.*, 2018).

A primary risk factor for most neurodegenerative diseases, especially AD, is advanced age (Guerreiro and Bras, 2015). While aging itself is not a disease (Hayflick, 2000), it is usually accompanied by a low degree of chronic inflammation (Franceschi *et al.*, 2006). Therefore, the term inflamm-aging was introduced, which is a complex systemic process mediated by multiple factors, characterized by several interactions of multiple molecular mediators such as inflammatory markers, for instance increasing circulating levels of C-reactive protein (CRP) and cytokines such as tumor necrosis factor (TNF)-a and interleukin-1β (IL-1β) (Franceschi *et al.*, 2006; Lencel and Magne, 2011). In AD, cerebral neuroinflammation contributes to the pathogenesis of the disease. A growing body of evidence demonstrated increased IL-1β levels, activation of NACHT, LRR and PYD domains-containing protein 3 (NLRP3) inflammasome in microglia and subsequent inflammatory events as a downstream consequence of Aβ deposition (Heneka *et al.*, 2013; Gold and El Khoury, 2015). The continuous presence of stimulus in the AD brain, such as Aβ, has been recently reported to activate NLRP3 and promote the assembly of the

inflammasome complex, which result in caspase-1 activation and production of the pro-inflammatory cytokines including IL-1β and IL-18 (Tan *et al.*, 2013; Li *et al.*, 2018). These findings suggest NLRP3 inflammasome as an important contributor to cerebral neuroinflammation in the AD brain, and its inhibition could provide a therapeutic approach to prevent, stop and/or treat AD. Besides, considerable evidence suggests the dysregulation of autophagy, an essential homeostatic pathway in the brain, occurs in both AD animal models and AD patients (Li *et al.*, 2010; Harris and Rubinsztein, 2011; Hamano *et al.*, 2018). Autophagy plays an important role in the metabolism of Aβ and is considered a major pathway for Aβ clearance (Son *et al.*, 2012), and degradation and clearance of APP and tau(Nixon, 2007; Zhou *et al.*, 2011; Chesser *et al.*, 2013). Thus, autophagy dysregulation could play a key role in AD pathology by accumulating Aβ, APP, and tau. Collectively, there is a substantial interest in the discovery of therapeutic inflammasome and autophagy modulators.

Currently, there is sufficient scientific evidence supporting chronic adherence to the Mediterranean diet (MedD) is associated with a low risk of cognitive impairment and AD (Gardener and Caunca, 2018). Among the key elements of the MedD is the daily consumption of extra-virgin olive oil (EVOO), which possesses an anti-inflammatory and antioxidant effects (Pitozzi *et al.*, 2010), in addition to other health benefits (Keys, 1995; Corona *et al.*, 2009). Data from our group have shown that EVOO added to the diet of AD mouse models at an early age and before the pathology, onset provided a protective effect against Aβ-related pathology (Qosa *et al.*, 2015b; Batarseh and Kaddoumi, 2018a). EVOO consumption for 6 months starting at one months of age significantly reduced total $A\beta_{40}$ and $A\beta_{42}$ brain levels, reduced Aβ production, enhanced Aβ clearance, and decreased parenchymal and vascular deposits of Aβ as well as total tau and phosphorylation in the brains of the AD mouse model TgSwDI (Qosa *et al.*, 2015b). Besides,

available studies have shown that EVOO administration to triple transgenic mice (3xTg) model of AD, ameliorated working memory and spatial learning reduced synaptic pathology, and significantly reduced Aβ deposition by autophagy activation (Lauretti *et al.*, 2017). In addition, EVOO increased brain levels of antioxidants (Pitozzi *et al.*, 2010). Several phenolic compounds were isolated from EVOO and characterized, among which is oleocanthal (OC). The effect of OC on Aβ load and inflammation was described by our lab and others (Abuznait *et al.*, 2013; Qosa *et al.*, 2015a; Batarseh and Kaddoumi, 2018a; Cordero *et al.*, 2018; Hornedo-ortega *et al.*, 2018). These results suggest OC could have largely contributed largely to the observed and reported benefits of EVOO.

The potential beneficial effect of OC and EVOO on AD in disease models, especially at the very early stages, have been studied previously by us and others (Abuznait *et al.*, 2013; Qosa *et al.*, 2015b; Lauretti *et al.*, 2017; Batarseh and Kaddoumi, 2018b), however, the potential mechanism(s) by which OC and EVOO exert this beneficial effect remains unclear; also whether EVOO effectiveness against AD extends to late stages is unknown. Thus, in the current study, we hypothesized that OC-rich EVOO consumption could enhance BBB integrity and reduce Aβ-related pathology in TgSwDI mice.

## Materials and Methods

### Materials

Bovine serum albumin (BSA) and Thioflavin-S (Thio-S) were purchased from Sigma-Aldrich (St. Louis, MO). Total protein measurement kit by the bicinchoninic acid (BCA) assay was purchased from Pierce (Rockford, IL). Mouse IL-1β ELISA kit was purchased from R&D Systems (Minneapolis, MN, USA). Mouse IL-10 ELISA kit was obtained from Mabtech (Nacka Strand, Sweden). Protein carbonyl colorimetric assay kit and super oxide dismutase (SOD)

colorimetric assay kit were purchased from Cayman Chemical Company (Ann Arbor, MI, USA). All other chemicals and reagents were of analytical grade and were readily available from commercial sources.

**Antibodies**

The antibodies used for Western blot and immunostaining are summarized in Table 3.

**Table 3.** List of antibodies used in the EVOO study.

| **Antibody** | **Application** | **Source** |
|---|---|---|
| BACE-1 | WB | Abcam (Cambridge, MA) |
| Alexa-fluor 488-labeled 6E10 | IHC | BioLegend (San Diego, CA) |
| mTOR (7C10) | WB | Cell signaling (Danvers, MA) |
| Phospho-Mtor (Ser2448) (D9C2) | WB | Cell signaling |
| p70 S6 Kinase (49D7) | WB | Cell signaling |
| Phospho-p70 S6 Kinase (Ser371) | WB | Cell signaling |
| 4E-BP1 (53H11) | WB | Cell signaling |
| Phospho-4E-BP1(Ser65) (D9G1Q) | WB | Cell signaling |
| AMPKα (D63G4) | WB | Cell signaling |
| Phospho-AMPKα (Thr172) | WB | Cell signaling |
| ULK1 | WB | Cell signaling |
| Phospho-ULK1 (Ser555) | WB | Cell signaling |
| Beclin-1 | WB | Cell signaling |
| ATG-7 | WB | Cell signaling |
| ATG-5/12 | WB | Cell signaling |
| ATG-3 | WB | Cell signaling |
| SQSTM1/p62 | WB | Cell signaling |
| LC3-I | WB | Cell signaling |
| LC3-II | WB | Cell signaling |
| Synapsin-1 | WB | Cell signaling |
| IKB-α | WB | Cell signaling |

| | | |
|---|---|---|
| Anti-collagen-IV | IHC | EDM-Millipore (Burlington, MA) |
| APP-TOTAL | WB | EDM-Millipore |
| TRPA-1 | WB | EDM-Millipore |
| SNAP-25 | WB | GeneTex (Irvin, CA) |
| PSD-95 | WB | GeneTex |
| S-APP α | WB | Immuno-Biological Labs (Minneapolis, MN) |
| S-APP β | WB | Immuno-Biological Labs |
| IBA-1 | WB,IHC | Novus (Centennial, CO) |
| NLRP-3 | WB | Novus |
| Anti-Goat labeled secondary, HRP | WB | R&D systems (Minneapolis, MN) |
| Actin (H-6) | WB | Santa Cruz (Santa Cruz, CA) |
| GFAP (N18) | IHC | Santa Cruz |
| MMP-9 (E-11) | WB | Santa Cruz |
| Tubulin (5F131) | WB | Santa Cruz |
| Procaspase-1 | WB | Santa Cruz |
| Cleaved Casp-1 (P20) | WB | Santa Cruz |
| Cleaved Casp-1 (P10) | WB | Santa Cruz |
| Procaspase-8 | WB | Santa Cruz |
| Cleaved Casp-8 (P18) | WB | Santa Cruz |
| CFL594-conjugated anti-rabbit IgG | | Santa Cruz |
| Anti-goat IgG-CFL 488 | IHC | Santa Cruz |
| Phospho-Tau (Thr231) | WB | Signalway antibody (College Park, MD) |
| Tau-Total (TAU-5) | WB | ThermoFisher (Waltham, MA) |
| Anti-Rabbit IgG (H+L) Secondary Antibody, HRP | WB | ThermoFisher |
| Anti-Mouse IgG (H+L) Secondary Antibody, HRP | WB | ThermoFishe |
| Antibody | Application | Source |
| BACE-1 | WB | Abcam (Cambridge, MA) |
| Alexa-fluor 488-labeled 6E10 | IHC | BioLegend (San Diego, CA) |

**Animals**

TgSwDI mice were purchased from Jackson Laboratories (Bar Harbor, ME). TgSwDI mice express human APP under control of Thy 1.2 neuronal promoter harboring double Swedish mutations and the Dutch and Iowa Aβ mutations leading to extensive Aβ deposition associated with neuroinflammation, astrogliosis and memory decline (Davis *et al.*, 2004). In the brains of TgSwDI mice, Aβ begins to accumulate at 2 to 3 months of age, and by 6 months the number of amyloid deposits increases significantly with pronounced astrogliosis and activated microglia (Davis *et al.*, 2004). Thus, for the purpose of this study, mice were used at the age of 6 months. All mice were housed in plastic cages under standard conditions including 12 h light/dark cycle, 22°C, 35% relative humidity, and *ad libitum* access to water and food. All animal experiments and procedures were approved by the University of Louisiana at Monroe Animal Care and Use Committee and according to the National Institutes of Health guidelines Principles of laboratory animal care (NIH publication No. 86-23, revised 1996).

**Animals' treatment**

Here, we used female mice for the experiments because they were readily available in the number needed to perform the study. TgSwDI mice were divided into two groups ($n$=7 mice/group): control group provided powdered diet (Teklad Laboratory diets, Harlan Laboratories, Madison, WI) enriched with refined olive oil (Great-Value™ classic Olive Oil diet; Walmart®, LA, USA). Refined olive oil contains negligible to null levels of phenolic compounds (Hornedo-ortega *et al.*, 2018). The EVOO group was fed with a powdered diet enriched with oleocanthal-rich EVOO. The brand used was "The Governor™" from Corfu Greece

(http://thegovernor.gr/index.php/our-products/the-governor-premium). According to the producer website, this oil contains 680 mg/kg oleocanthal as determined by a validated NMR method (Karkoula *et al.*, 2014), The amount of oleocanthal in both brands were confirmed by our lab in collaboration with Dr. Khalid El Sayed (ULM) by mass spectrometry and NMR ( Siddique *et al.*, 2019). Mice treatments with refined oil (control) and OC-rich EVOO (EVOO) started at 6 months of age and continued for 3 months. The mice were 9 months of age at the end of treatment. Control and EVOO-enriched diets were prepared by mixing oil with powdered diet to yield a dose of 0.714 g/kg/day. This dose represents the estimated dietary intake of olive oil in Greek population (50 g/day), and to mimic EVOO dose in Mediterranean diet followers (Tuck and Hayball, 2002). Oil-enriched diet was provided to mice in glass containers, which were replaced every other day to maintain freshness. Based on oleocanthal amount in "The Governor™", EVOO administered dose is estimated to contain 476 μg/kg/day oleocanthal. Animals body weights were recorded weekly through the treatment period, and health status and behavior were daily monitored. Mice fed with refined olive oil and EVOO demonstrated similar body weights ranging from 23.0±2.9 to 25.3±3.1 g, respectively. At the end of treatment and before euthanizing the mice to collect tissues, three mice from each group received an intravenous injection of 10 mg/kg FEPPA (N-acetyl-N-(2-[18F]fluoroethoxybenzyl)-2-phenoxy-5-pyridinamine; kindly provided by Dr. Pradeep Garg, Center for Molecular Imaging and Therapy, Biomedical Research Foundation, Shreveport, LA), a specific marker for activated microglia (Suridjan *et al.*, 2015). One hour later, mice were anesthetized with IP xylazine (20 mg/kg)/ketamine (125 mg/kg) mixture followed by decapitation and mice brains collection. The two hemispheres of each brain were divided and used for analysis; blood samples were also collected for HPLC analysis of plasma FEPPA levels. All samples were stored in -80$^{o}$C until analysis.

**Western Blot analysis**

Western blotting was performed as we reported previously ( Mohamed *et al.*, 2016). In brief, protein samples (25 µg) were loaded and resolved using 10% SDS-polyacrylamide gel at 200V for 1 h and transferred electrophoretically to PVDF membrane (Millipore) at 300 mA for 1.5 h at 4°C. Nonspecific binding was blocked by pre-incubation of the PVDF membrane in PBS solution containing 3% BSA with rocking for 1 h at room temperature followed by overnight incubation at 4°C with primary antibodies. Primary and secondary antibodies used for brain homogenate samples, are listed in Table 3. Proteins' blots were developed using a chemiluminescence detection kit (SuperSignal West Femto substrate; ThermoFisher). Bands were visualized using ChemiDoc™ MP Imaging System (Bio-Rad Hercules, CA, USA) and quantified by densitometric analysis of each protein normalized to the housekeeping protein used ( Actin or Tubulin) using Image Lab™ Software V.6.0 (Bio-Rad).

**Immunohistochemical analysis**

Immunohistochemical analysis was performed as we previously reported (Batarseh *et al.*, 2017). Brain sections (16 µm-thick) were prepared using Leica CM3050S Research Cryostat (Buffalo Grove, IL, USA). Sections were fixed by methanol for 10 min at -20°C. Next, sections were washed 5 times in PBS and blocked with PBS containing 10% donkey serum for 1 h at room temperature. Immunostaining was performed for brains hippocampi and cortices of TgSwDI mice. The entire cortex and hippocampus regions were included in the analysis. IgG extravasation from brain microvessels was assessed by dual immunohistochemical staining for collagen IV and mouse IgG using rabbit anti-collagen-IV and fluorescein-conjugated donkey anti-IgG (both at 1:200

dilution), respectively. To detect collagen IV, CFL594-conjugated donkey anti-rabbit IgG was used as the secondary antibody (Batarseh *et al.*, 2017). For total Aβ detection, TgSwDI brain sections were immunostained with Alexa-fluor 488 labeled 6E10 human-specific anti-Aβ antibody at 1:200 dilution. For detection of Aβ-plaque load, the brain tissue sections were stained with a freshly prepared and filtered 0.02% Thio-S solution in 70% ethanol for 30 min followed by incubation in 70% ethanol as described previously (Kruyer *et al.*, 2015). For reactive astrocytes, TgSwDI sections were probed with rabbit anti-GFAP polyclonal IgG at 1:100 dilution followed by anti-rabbit IgG-CFL594 secondary antibody. For reactive microglia, TgSwDI sections were probed with goat anti-Iba1 polyclonal IgG at 1:100 dilution followed by anti-goat IgG-CFL488 secondary antibody. For each treatment, image acquisition was performed in 10 tissue sections (separated by 150 μm) containing the hippocampus (total of 40 sections/mouse). Total Aβ load and Thio-S were captured and quantified at a total magnification of 4X; GFAP, Iba-1 and IgG extravasation images were captured at a total magnification of 20X. Fluorescence intensity quantification was performed using ImageJ® version 1.6.0 software (Research Services Branch, National Institute of Mental Health/National Institutes of Health, Bethesda, MD) after adjusting for threshold. Images were visualized using Nikon Eclipse Ti-S inverted fluorescence microscope (Melville, NY).

**Determination of oxidative stress and neuroinflammation markers**

Brain homogenates were centrifuged for 15 min at 20,800 *g* to separate the supernatants and were used to assay protein carbonyl, SOD, IL-1β and IL-10 levels following the manufacturers' instructions. All samples were performed in triplicates and corrected to protein amount using BCA assay. In addition, the quantification of FEPPA in brains and plasma samples

collected from the three mice received the injections was conducted by Shimadzu® HPLC system (Shimadzu, OR) consisting of the following: isocratic LC-20AB equipped with a SIL-20A HT autosampler and LC-20AB pump connected to a DGU-20A3 degasser. The separation method consists of an acetonitrile:water (45:50 v/v) mobile phase used for the separation of brain and blood samples and was delivered at 1.0 ml/min flow rate, Agilent eclipse XDB-C18 column (5µm, 4.6 x 150 mm ID; Agilent Technologies Inc., CA, USA), detector wavelength was set at 210 nm, and the injection volume was 20 µl. Each chromatographic run was completed in 10 min with FEPPA eluted at a retention time of 6 min. One hour later, FEPPA was detected in the brains but not in the in the plasma (Figure 18).

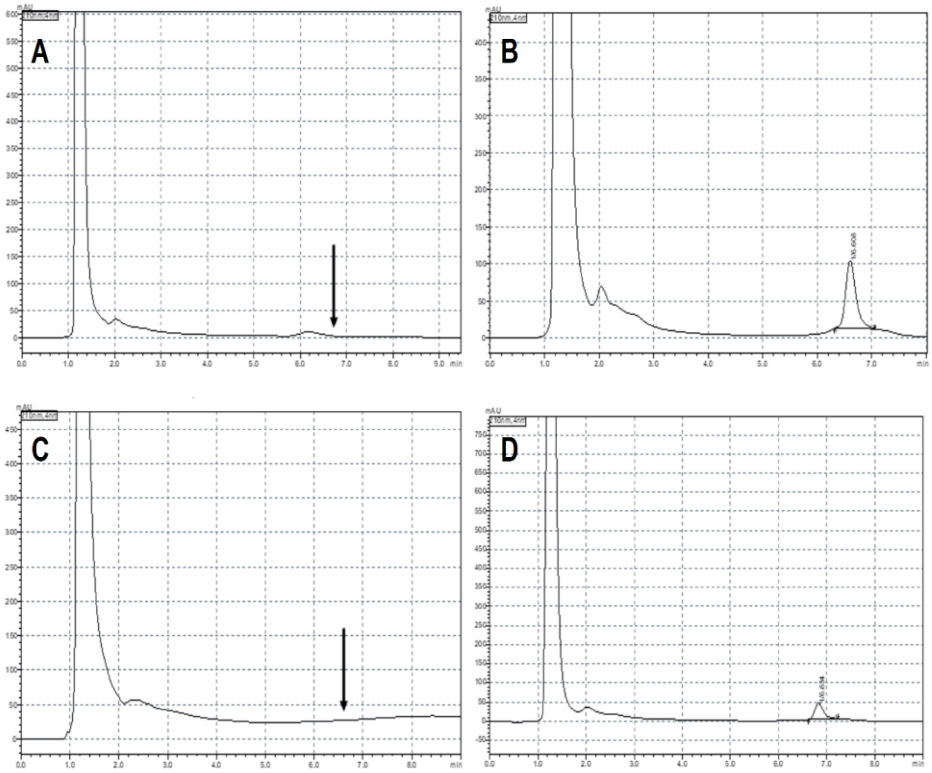


Figure 18. Representative chromatograms from plasma and brain samples of mice received 10 mg/kg FEPPA. Plasma and brain samples were collected one hour after FEPPA injection. (A)

Plasma and (B) brain samples of control mice received refined OO. (C) Plasma and (D) brain samples from EVOO treated mice. Arrows represent the retention time where FEPPA should appear in plasma samples.

### Statistical analysis

Data were expressed as mean ± SEM for n=7 mice/group. The experimental results were statistically analyzed for significant difference using Student's t-test for two groups. Values of $P<.05$ were considered statistically significant. Data analyses were performed using GraphPad Prism, version 6.0. In the figures, the fold change for control groups was calculated by dividing each control value on the average of all control mice values for a specific protein. Treatment values were then normalized to control (1.0).

## Results

### OC stability in EVOO

OC relative stability was measured over 2 months using the Shimadzu® HPLC system (Shimadzu, OR) consisting of the following: isocratic LC-20AB equipped with a SIL-20A HT autosampler and LC-20AB pump connected to a DGU-20A3 degasser. The separation method consists of an acetonitrile: water (35:65 v/v) mobile phase and was delivered at 1.0 ml/min flow rate, Agilent eclipse XDB-C18 column (5µm, 4.6 x 150 mm ID; Agilent Technologies Inc., CA, USA), detector wavelength was set at 230 nm and the injection volume was 10 µl. OC peak appears at 7 minutes. Sample preparation: the oil was mixed with acetonitrile in 5:1000 ratio (v/v), then samples was vortexed for 1 min and centrifuged at 10,000 rpm for 10 min. The supernatant was collected and 10 µl was injected onto the column.

Samples from both oils were analyzed and results are shown in Figure 19. Results indicated that OC in EVOO is relatively stable with less than 5% loss. Also, the results indicated OC-rich EVOO contains about 800 mg/kg OC.

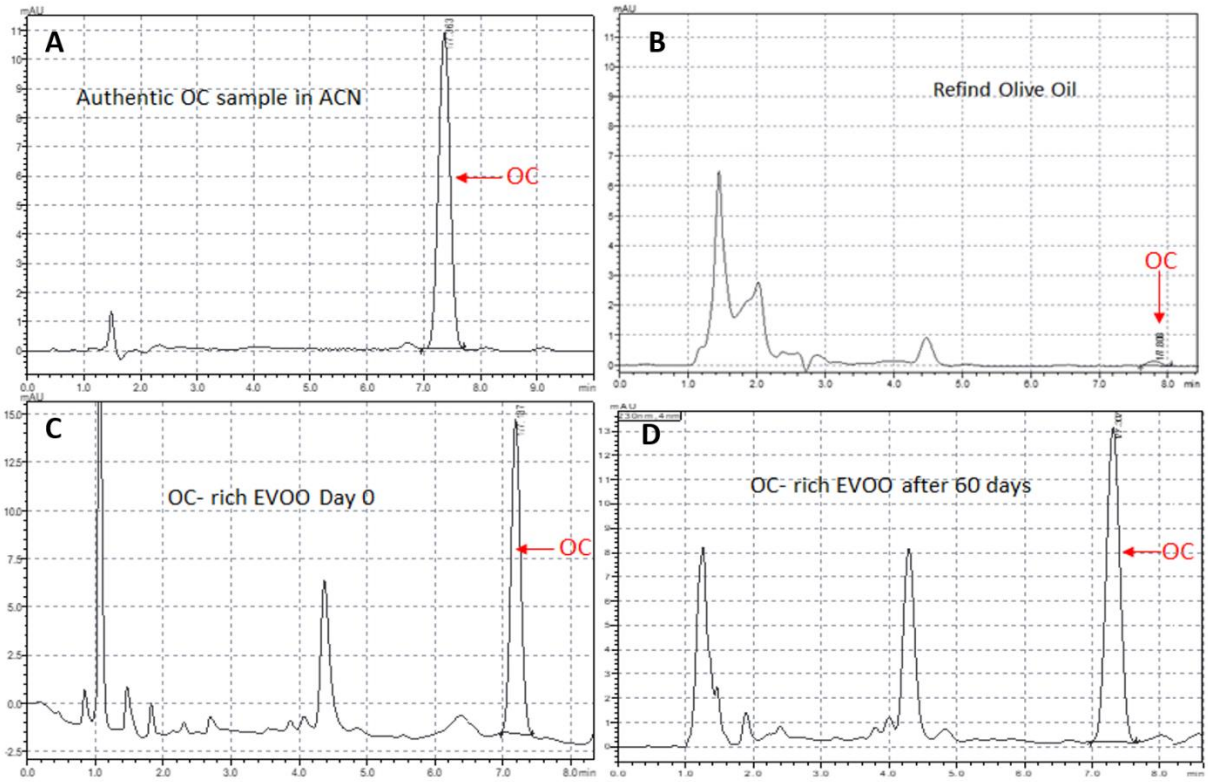


| | | | Day 0 | Day 60 |
|---|---|---|---|---|
| | Standard | Refined oil | OC-EVOO | OC-EVOO |
| Peak area | 157030 | 2060 | 182072 | 171756 |
| conc. mcg/ml | 40 | 0.36 | 48 | 46 |
| RT (min) | 7.3 | 7.23 | 7.28 | 7.3 |
| peak height | 10870 | 258 | 14987 | 13465 |

Figure 19. Representative chromatograms from HPLC analysis for OC relative stability. (A) Authentic OC dissolved in acetonitrile. (B) Sample from refined olive oil. (C) Sample of OC- rich EVOO on Day 0, and (D) Sample of OC- rich EVOO after 2 months. (E) Table showing the concentration (μM), peak area, retention time (RT) and peak height on day 0 and day 60, batch

number for refined oil is 609821 and for OC-EVOO is 1776-1831. No other lots were analyzed for stability or used in this study.

**OC-rich EVOO reduces total Aβ load and plaques in TgSwDI mice brains.**

The effect of OC-rich EVOO (hereafter EVOO) on mice brain Aβ load was evaluated. As shown in Figure 20, compared to OO treated (control) group, EVOO significantly reduced total 6E10-detected Aβ by 61 and 73% in brains cortex (Figure 20A,B,E) and hippocampus (Figure 20C,D,E).

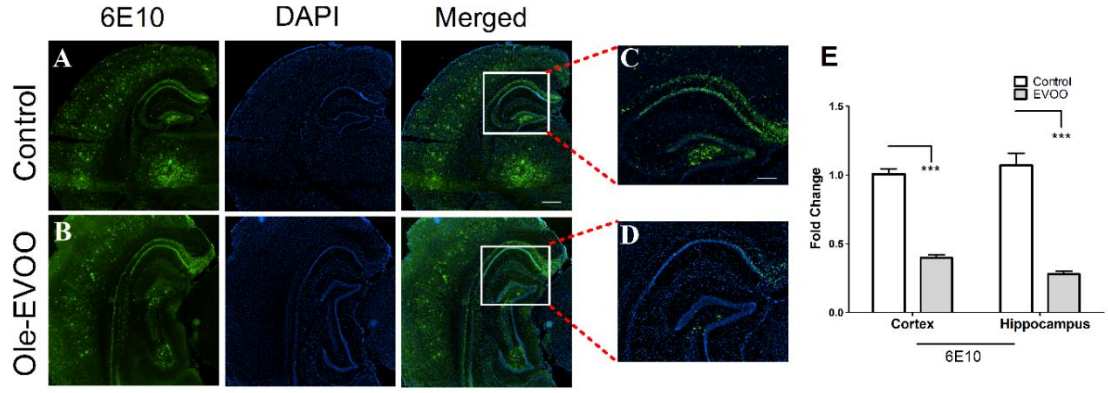


Figure 20. EVOO reduced Aβ (6E10) burden in TgSwDI mice brains. (A-E) Representative sections stained with 6E10 (green) antibody against Aβ to detect total Aβ load with their quantification for total Aβ deposition; DAPI (blue) to stain nuclei. Hippocampus is seen at higher magnification in the closed inserts. Data are presented as mean±SEM. Statistical analysis was determined by Student's t-test for n =7 mice/group. ***P<.001 versus control group (i.e. refined olive oil). Scale bar, 100 μm.

In addition, Thioflavin-S positive Aβ plaques staining showed similar pattern with an overall 47 and 79 % reduction in the cortex and hippocampus regions, respectively (Figure 21A-E).

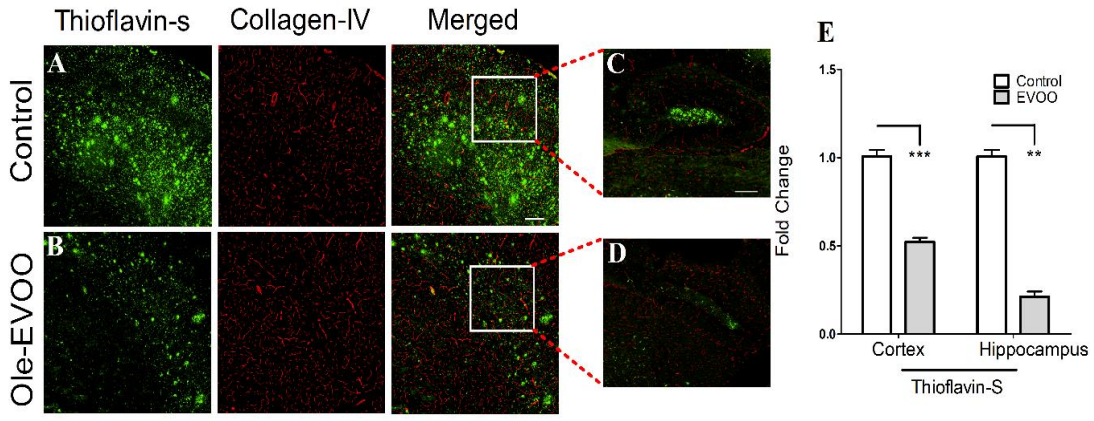


Figure 21. EVOO reduced Aβ plaques (Thio-S) burden in TgSwDI mice brains. (A-E) Representative stained with Thio-S (green) antibody to detect Aβ plaques load with their corresponding quantification of covered area with Aβ plaques; anti-collagen IV (red) to stain microvessels. Data are presented as mean±SEM. Statistical analysis was determined by Student's t-test for n =7 mice/group. ***P<.001 versus control group (i.e. refined olive oil). Scale bar, 100 μm.

**EVOO modulates APP processing, total tau and its phosphorylation expression.**

We then assessed EVOO effect on APP processing by western blot analysis. As shown in Figure 22, EVOO treatment significantly increased sAPPα levels by 1.4-fold and decreased sAPPβ and BACE1 expressions by ~30%. Interestingly, a significant 40% reduction in the level of total APP was also observed. In addition to APP processing, we sought to confirm the effect of EVOO consumption on the expression of tau and its phosphorylation in the brains of TgSwDI mice with advanced disease pathology at 9 months by western blot. While TgSwDI mice is not known to overexpress tau or to develop tau pathology, we evaluated the effect of EVOO consumption and autophagy regulators induction on endogenous tau protein levels. Recent body of evidence

supported the correlation between autophagy induction and tau-protein expression(Hernandez *et al.*, 2019) For example, Youshkawa et al., recently reported that the depletion of tau protein ameliorated the hyper-locomotor behavior in J20 transgenic mice, an APP model, which signifies the functional results of Aβ-tau interactions and correlations (Yoshikawa *et al.*, 2018). Findings from our studies showed EVOO significantly reduced total tau by 48% and tau phosphorylation at Threonine position 231 (p-Tau-Thr 231) by 38%, which is consistent with our previous findings with EVOO (Qosa *et al.*, 2015b), however, it could be necessary to evaluate the effect of treatments on mRNA levels of both APP and tau to explain observed reductions and confirm whether this effect is mediated by induced autophagy or affecting the genes that encode both proteins.

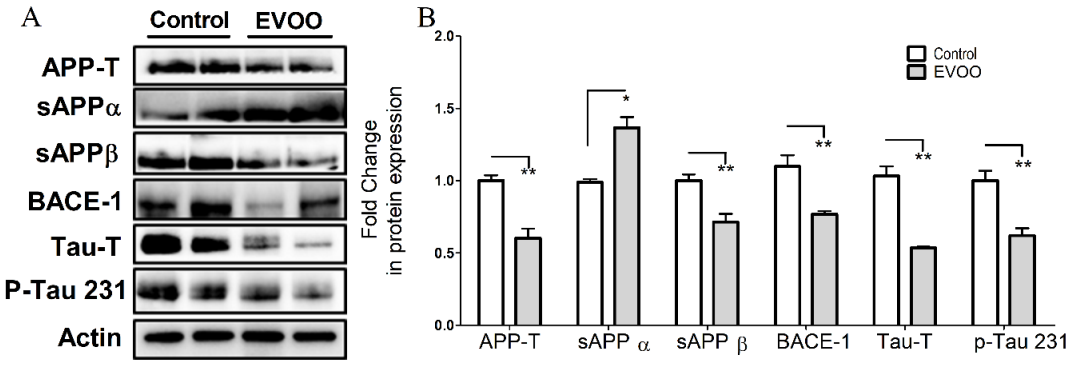


Figure 22. Effect of EVOO consumption on APP processing, total tau and tau phosphorylation at amino acid residue threonine 231 in TgSwDI mice brains. Representative blots (A), and densitometry analysis (B) showed a significant increase in sAPPα and reduction in APP-T (total APP), sAPPβ , BACE-1 enzyme, total-Tau and phosphorylated-Tau (Thr 231) levels in brain homogenates of mice consumed EVOO. Data are presented as mean±SEM. Statistical analysis

was determined by Student's t-test of n=7 mice/group. * P<.05, **P<.01 versus control group (i.e. refined olive oil).

**EVOO attenuates brain neuroinflammation.**

In the brain of TgSwDI, an increase in the number of GFAP-positive astrocytes and activated microglia that starts at the age of 6 months was reported (Miao *et al.*, 2005b). As shown in Figure 23A-D, EVOO significantly reduced astrocytes activation and ameliorated the astrocytes shape in mice cortexes and hippocampi when compared to the control group. Moreover, EVOO fed mice showed a significant reduction in brain levels of the microglial marker Iba-1 as analyzed by immunostaining (Figure 23E-H).

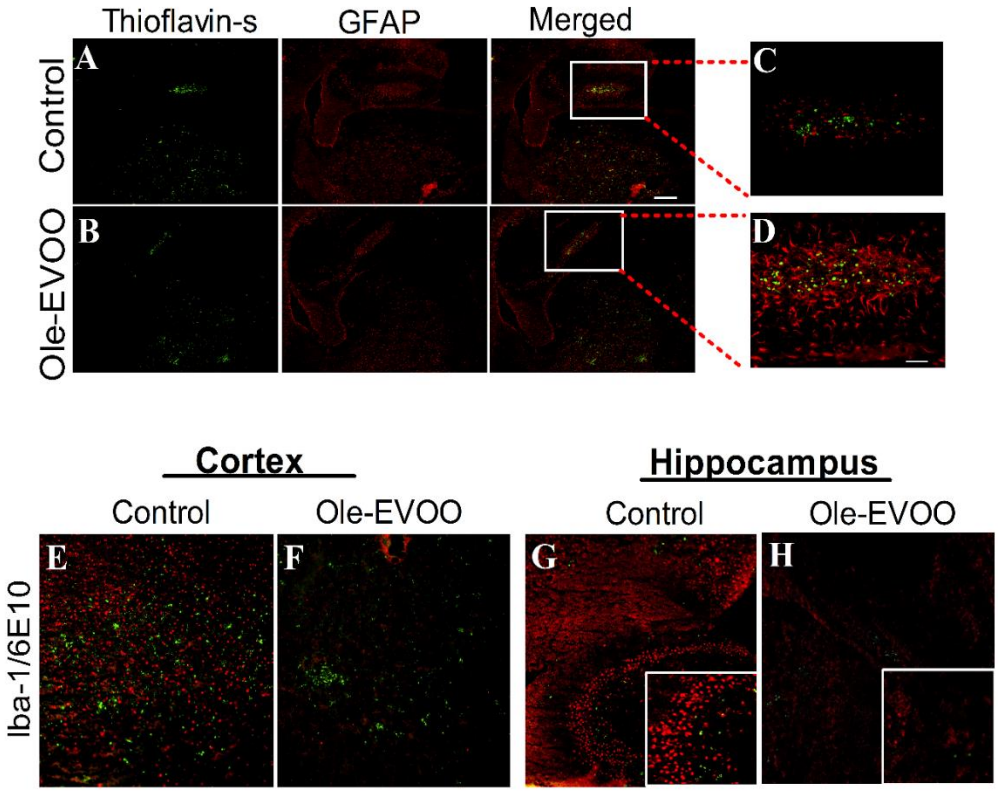


Figure 23. EVOO diet reduced astrocytes and microglial activation in TgSwDI mice brains. Astrocytes were assessed using GFAP expression and morphology. For microglial activation the

microglial marker Iba-1 intensity was used. (A-D) Representative brain sections from 9-month-old TgSwDI mice were co-labelled with GFAP antibody (red) to detect activated astrocytes and Thioflavin-S (green) to detect Aβ plaques. Hippocampus is seen at higher magnification. Activated astrocytes with long and thick branches noticed in control group that were significantly reduced by EVOO (seen at higher magnification in the closed inserts). (E-H) Representative cortex and hippocampal sections double stained with Iba1 (red) and 6E10 antibody (green) to detect activated microglia and total Aβ, respectively, in EVOO and control (i.e. refined olive oil) groups. Scale bar, 100 μm.

This reduction in neuroinflammation was further confirmed by immunoblotting demonstrated a 43% reduction in Iba-1 (Figure 24A,B). EVOO treatment was associated with reduced microglial activation that was associated with 40% reduction in FEPPA levels, a specific marker for activated microglia, as determined by HPLC (Figure 24C). In addition, western blot analysis of metalloproteinase-9 (MMP9) enzyme showed EVOO to significantly reduce MMP9 by 57% compared to control group (Figure 24A, B).

The transient receptor potential ankyrin 1 (TRPA1) is a membrane-linked cation channel that is widely expressed in neuronal and non-neuronal cells. TRPA1 is another important key mediator that has been pointed in several inflammatory processes, including inflammatory pain, allergy, and colitis, amongst others (Lee *et al.*, 2016b; Mendes *et al.*, 2016; Yin *et al.*, 2018). Here and as shown in (Figure 24 A,B), TRPA-1 expression was significantly reduced by EVOO treatment by 46% when compared to control group. IL-1β and IL-10 were analyzed by ELISA and as demonstrated in Figure 24 D&E, EVOO significantly reduced IL-1β brain levels by 75%, and increased IL-10 levels by 31%.

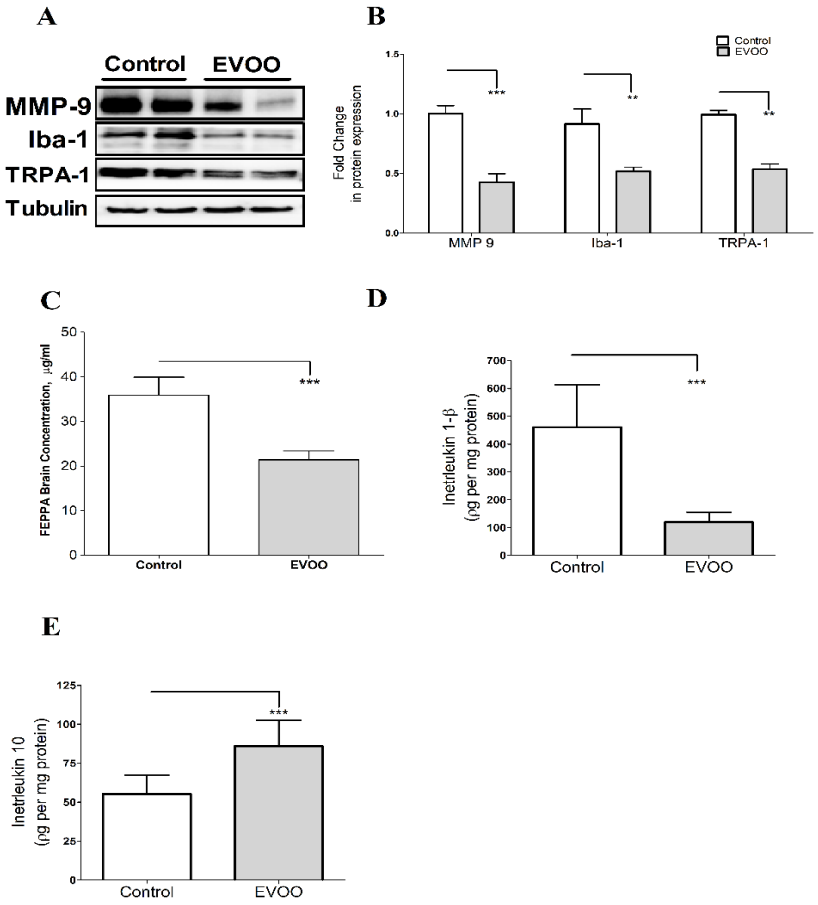


Figure 24. EVOO diet decreased neuroinflammation in TgSwDI mice brains. Neuroinflammation was evaluated by assessing astrocytes and microglial activation status monitored by astrocytes GFAP expression, the microglial marker Iba-1 expressions, TRPA-1 and MMP-9 expression, FEPAA microglial marker, IL-1β and IL-10 brain levels. (A-B) Representative blots and densitometry analysis of MMP9, Iba-1 and TRPA-1 in TgSwDI mice brains homogenates. (C) Results from HPLC analysis for the level of FEPPA, a specific marker for microglial activation in the brain homogenate of TgSwDI mice which was significantly reduced in EVOO diet group compared to control (n=3 mice/group). (D) Effect of EVOO on IL-1β levels in mice brain homogenates. (E) Effect of EVOO on IL-10 levels in mice brain homogenates. For B, D & E Data are presented as mean ± SEM for n=7 mice/group. For C, data are presented as mean ± SEM for

n=3 mice/group. Statistical analysis was determined by Student's t-test. **P<.01, and ***P<.001 versus control group (i.e. refined olive oil).

To correlate the anti-inflammatory effect of EVOO on the BBB integrity, immunoglobulin-G (IgG) extravasation was measured as an endogenous BBB permeability marker; EVOO consumption significantly decreased IgG extravasation by 75 and 31 % in both the cortex and the hippocampus regions, respectively, when compared to control diet (Figure 23A-C).

**EVOO diet reduces oxidative stress markers in TgSwDI mice brains.**

Carbonyl formation is an important detectable marker of protein oxidation, and protein carbonyls are significantly increased in AD (Allan Butterfield and Boyd-Kimball, 2018), therefore we evaluated the effect of EVOO on total protein carbonyl formation. EVOO consumption significantly reduced protein carbonyl levels by 64% (Figure 25D). EVOO consumption also significantly increased superoxide dismutase (SOD) formation by 79% compared to control group (Figure 25E).

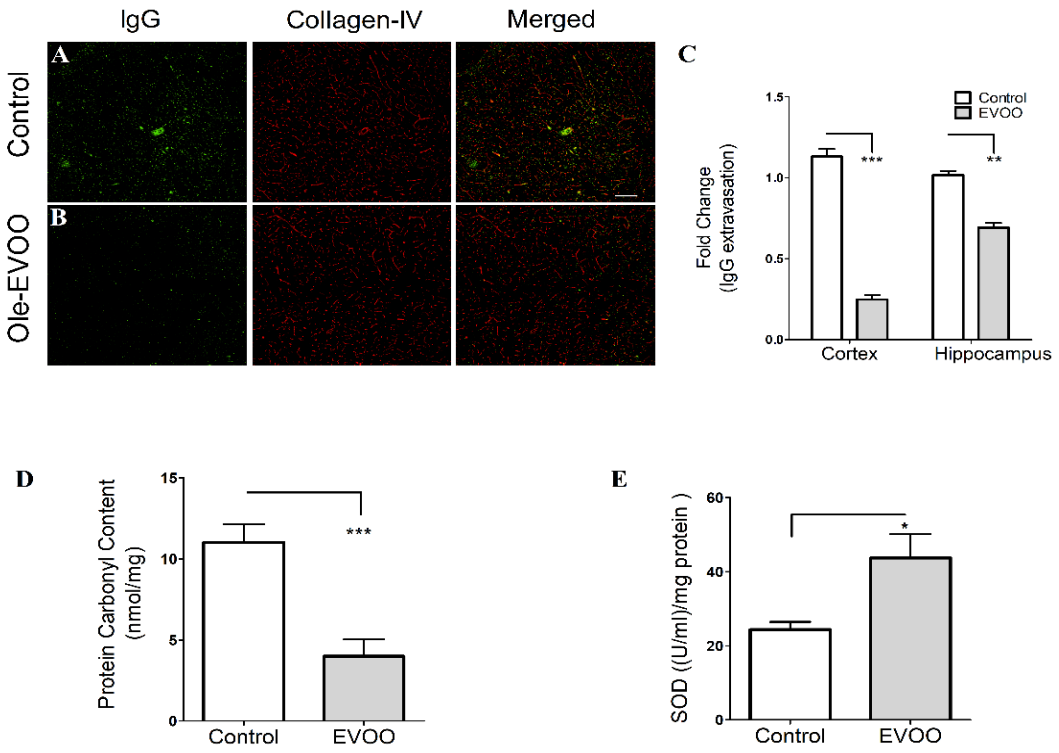


Figure 25. EVOO enhanced BBB tightness and antioxidant capacity in TgSwDI mice brains. (A-B) Representative sections immunostained with mouse IgG (green) and collagen (red) antibodies. (C) IgG optical density in mice cortexes and hippocampi were quantified for IgG extravasation. Scale bar, 100 μm. (D) Effect of EVOO on protein carbonyl levels in mice brains. (E) Effect of EVOO on SOD levels in mice brains. Data are presented as mean±SEM (n=7 mice/group). Statistical analysis was determined by Student's t-test. *P<.05, **P<.01 and ***P<.001 versus control group (i.e. refined olive oil).

**EVOO diet reduces Il-1ß production through the NLRP3 pathway in TgSwDI mice brains.**

IL-1β upstream inflammasome activation and production pathway was evaluated. Findings revealed EVOO significantly reduced NLRP3 protein expression by 41%, which was also associated with a significant reduction in the expression levels of procaspase-1, cleaved caspase-1 p20 and p10 by 31, 45 and 28%, respectively. Besides, this effect was also associated with a significant reduction in procaspase-8 by 56% and cleaved caspase-8 p18 by 60% when compared to the control diet (Figure 26).

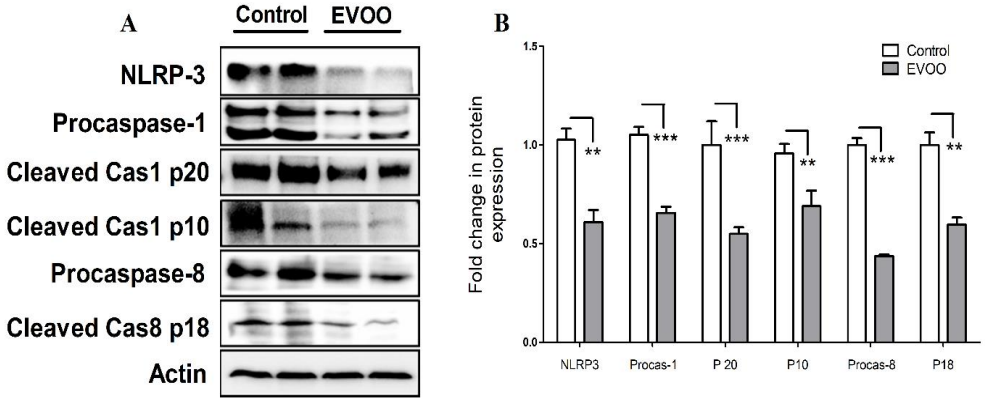


Figure 26. EVOO reduced inflammasomes formation by modulating NLRP-3/caspase1 and 8 pathways. (A) Representative blots, and (B) densitometry analysis showed a significant reduction in the expression of NLRP3, procaspase-1, cleaved caspase p20 & p10 (Cle- Casp1 p20 & 10), procaspase-8 and cleaved caspase-8 p18 (Cle- Cas8 p18) in brain homogenates of mice consumed EVOO compared to control group. Data are presented as mean±SEM of n=7 mice in each group. Statistical analysis was determined by Student's t-test. **P<.01, and ***P<.001 versus the control group (i.e. refined olive oil).

**EVOO diet induces autophagy markers in TgSwDI mice brains.**

Recent studies established that autophagy induction plays a key role in the regulation of BACE1 turnover and APP processing (Feng *et al.*, 2017) and that autophagy process is downregulated with aging (Plaza-Zabala *et al.*, 2017). Several autophagy markers affecting either the initiation or the maturation of autophagosomes and autophagic flux were analyzed in this study. As shown in Figure 27, EVOO significantly induced major autophagosome initiation proteins AMPK (2.2-fold) and ULK1 (2.4-fold) expressions and their phosphorylation (30-60%). While the increase in beclin-1 levels did not reach a significant level, a significant increase in ATG7 and ATG3 proteins level by 2.4 and 1.7-fold, respectively, was observed without significantly altering ATG-12/5 level (Figure 27). In addition, the microtubule-associated protein light chain 3 conversion (LC3-I) and the ubiquitin-binding protein p62 were significantly reduced by 22 and 37%, respectively, which was associated with a 1.6-fold increase in the level of LC3-II (Figure 27). On the other hand, EVOO consumption has no significant effect on the mTOR pathway or its downstream proteins P70S6K and 4EBP1 (Figure 28). A graphical scheme summarizing the observed effect of OC-EVOO on autophagy markers induction is described in Scheme 3.

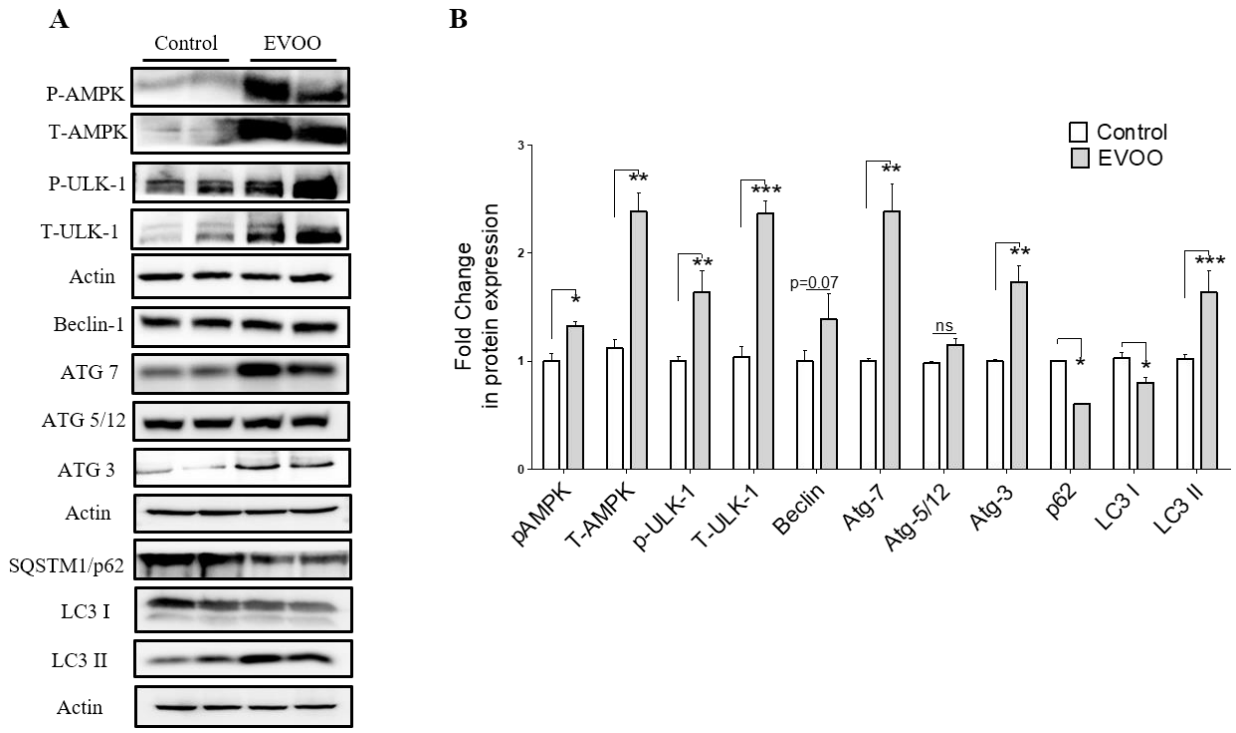


Figure 27. EVOO induced autophagy markers through AMPK pathway activation. (A) Representative blots, and (B) densitometry analysis of AMPK, phosphorylated-AMPK (pAMPK), ULK1, phosphorylated-ULK1 (pULK1), beclin, ATG 7, ATG 5/12, ATG 3, SQSTM1/p62, LC3 I and LC3 II in brain homogenates of mice consumed EVOO compared to control group (n=7 mice in each group). Statistical analysis was determined by Student's t-test. ns = not significant, *P<.05, **P<.01, and ***P<.001 versus control group (i.e. refined olive oil).

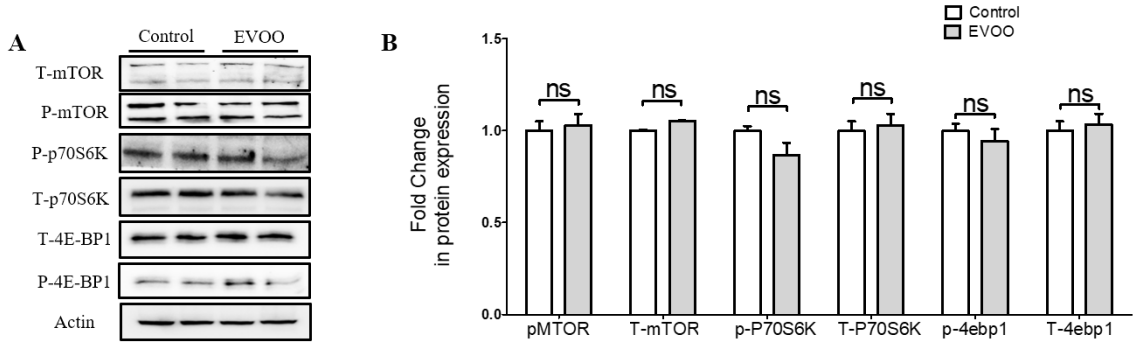


Figure 28. EVOO induction of autophagy markers was not mediated through the mTOR pathway. (A) Representative blots, and (B) densitometry analysis of mTOR, pMTOR, P70S6K, p-P70S6K, 4EBP1, and p-4EBP1 in brain homogenates of mice fed with EVOO and OO as a control group. Data are presented as mean±SEM of n=7 mice in each group. Statistical analysis was determined by Student's t-test. ns = not significant versus the control group (i.e. refined olive oil).

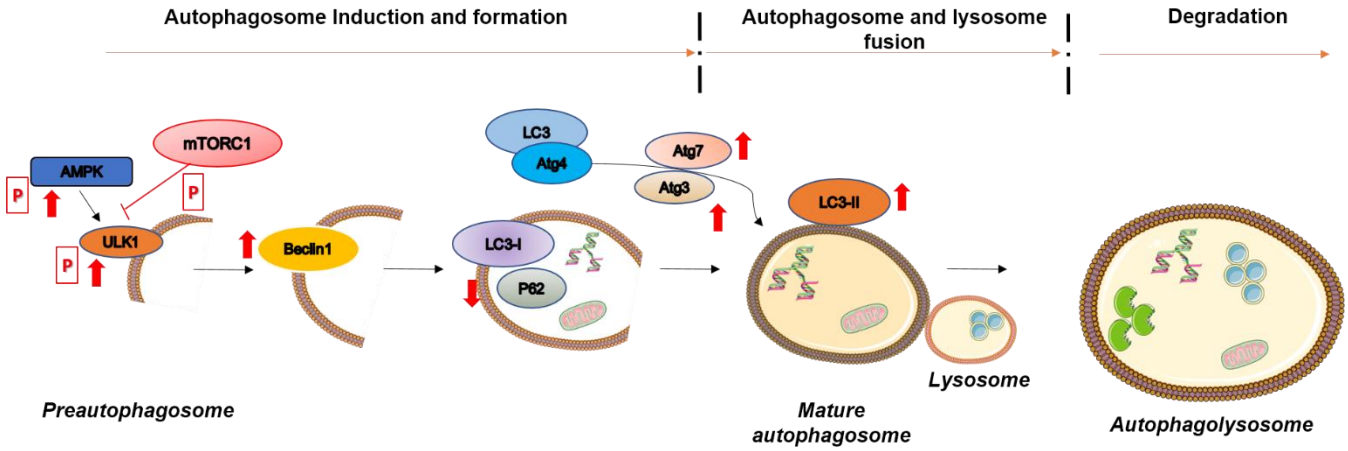


**Scheme 3.** Schematic summary describing the effect of OC-EVOO on several autophagy regulation markers, red arrows reflects the western blots results on the different steps of autophagy from Autophagosome induction to autophagolysosome degradation. P, indicates the phosphorylation of AMPK, ULK and mTORC1.

**Effect of EVOO diet on synaptic markers.**

As shown in Figure 29, Western blot findings demonstrated EVOO was partially associated with increase in the expression of three major synaptic markers PSD-95, synapsin-1 and SNAP-25 by 2.3-, 1.3- and 1.7-fold, respectively, compared to OO enriched-diet (control group).

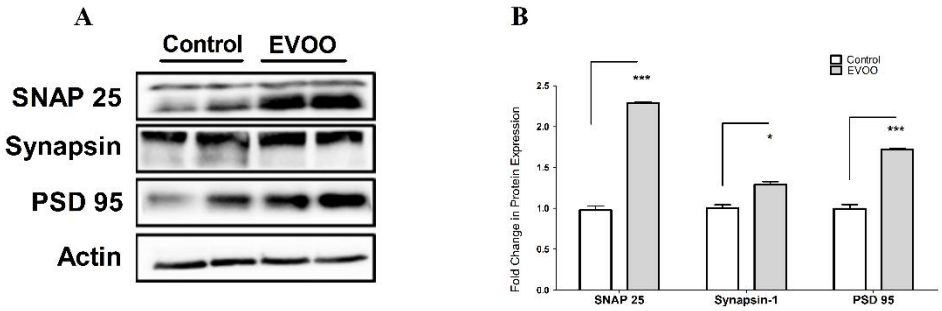


Figure 29. EVOO partially increased synaptic markers expression in TgSwDI mice. (A) Representative blots, and (B) densitometry analysis of the synaptic markers SNAP-25, Synapsin-1 and PSD-95 in brain homogenates of mice consumed EVOO compared to control group. Statistical analysis was determined by Student's t-test (n=7 mice/group). *P<.05, ***P<.001 versus control group (i.e. refined olive oil).

**Discussion**

In this work, we evaluated the effect of 3 months consumption of OC-rich EVOO, added to diet, on Aβ-related pathology in TgSwDI mice at an older age with advanced pathology compared to our previous studies using younger TgSwDI mice (Qosa *et al.*, 2015b), and evaluated potential mechanisms by which OC-rich EVOO exerts the observed beneficial effect. Neuroinflammation, and autophagy dysregulation have been linked to aging and AD (Plaza-Zabala *et al.*, 2017; Valero *et al.*, 2017; Hamano *et al.*, 2018), thus their simultaneous targeting could provide an effective approach for healthy aging, reduce risk of AD, and/or halt AD progression. In this study, oleocanthal daily dose was estimated based on its content in the Governor brand that was confirmed in our lab. However, oleocanthal level when added to the diet or the exact amount of

the diet consumed by each mouse daily were not determined. While adding treatment to diet could create variability, the results demonstrated acceptable variability as determined by the small error bars. Findings of this study demonstrated for the first time, to the best of our knowledge, that long-term dietary supplementation with OC-rich EVOO significantly reduced inflammasome activation through NLPR3 inhibition and increased autophagy markers through AMPK-ULK1 pathway activation. This effect was concomitant to reduced Aβ-load and associated synaptotoxicity, improved BBB function, and reduced neuroinflammation and oxidative stress biomarkers in TgSwDI mice with extensive disease pathology. These findings are consistent with our previous studies when EVOO was used in TgSwDI mice at a younger age and before Aβ deposition (Qosa *et al.*, 2015b, a).

NLRP3 inflammasome activation in microglia and astrocytes has been involved in several chronic inflammatory diseases and in AD (Heneka *et al.*, 2013; Houtman *et al.*, 2019). Aβ-induced activation of NLRP3 inflammasome stimulates AD progression by accelerating chronic inflammatory responses (Heneka *et al.*, 2013), which are partly involved in restricting glial function, and mediating synaptic dysfunction and cognitive impairment (Heneka *et al.*, 2013). Therefore, blocking NLRP3 inflammasome activity could effectively interfere with the progression of AD (Heneka *et al.*, 2013; Houtman *et al.*, 2019). NLRP3 inflammasome converts pro-IL-1 to mature and functional IL-1β. In the brains of EVOO-treated mice, the brain levels of IL-1β were significantly lower than IL-1β levels in mice consumed refined olive oil, which was associated with a significant decrease in the expression of two major caspases responsible for the increased formation of IL-1β , namely caspase-1 (Kaushal *et al.*, 2015) and caspase-8 (Gurung and Kanneganti, 2015) . In addition, NLRP3-inflammasome inhibition by EVOO was associated with a significant reduction in astrogliosis, measured by GFAP, and microglial activation,

measured by Iba1 and FEPPA was also observed. FEPPA is a specific ligand for translocator protein (TSPO). FEPPA is used as a biomarker for glial activation and neuroinflammation by imaging with positron emission tomography (Suridjan *et al.*, 2015). TSPO is a heterooliomeric complex protein; it is situated in the outer mitochondrial membrane of microglia; its expression increases in response to neuroinflammation and thus considered as a biomarker of activated microglia (Bradburn *et al.*, 2019). Our results from FEPPA study demonstrated EVOO significantly reduced TSPO, which suggests reduced inflammation. A recent study reported a strong positive correlation between NLRP3 inflammasome activation and TSPO upregulation, which is implicated in mitochondrial dysfunction (Scaini *et al.*, 2018), suggesting an additional therapeutic target for EVOO.

Moreover, calcium signaling has been identified as an essential mediator pathway in NLRP3 inflammasome activation where increased intracellular calcium levels were associated with inflammasome activation (Lee *et al.*, 2012). In the brain, the TRPA1 receptor is expressed in primary sensory neurons and in non-neuronal cells mainly in astrocytes (Anand *et al.*, 2008; Shigetomi *et al.*, 2011). TRPA1 plays a major role in inflammation and tissue damage and is recognized as a gatekeeper of inflammation (Bautista *et al.*, 2013). It acts as a sensor for detecting several toxic signals such as reactive oxygen species, inflammatory cytokines and Aβ, which upon their detection, TRPA1 is activated. In AD, it has been shown that in the brains of APP/PS1 mice, Aβ-mediated chronic inflammation caused TRPA1 activation, which triggered calcium influx and inflammation in astrocytes (Lee *et al.*, 2016a). Our results demonstrated EVOO significantly reduced TRPA1expression, which is one of the molecular targets of OC (Peyrot des Gachons *et al.*, 2011), suggesting another mechanism by which EVOO was able to reduce brain inflammation following chronic administration. While further studies are necessary to understand the link

between TRPA1 activation and NLRP3 inflammasome activation, a very recent study reported that cigarette smoke-induced TRPA1 was able to activate NLRP3 inflammasome and ROS in the alveolar epithelial cells A549 that was calcium-mediated (Wang *et al.*, 2019). These results suggest the anti-inflammatory effect of OC-rich EVOO could directly inhibited NLRP3 inflammasome activation and/or indirectly mediated by TRPA1 down-regulation that could trigger NLRP3 inflammasome inactivation and reduced IL-1β production. Collectively, our findings support the TRPA1 and NLRP3-IL-1β axis as targets for the overall beneficial effect of EVOO.

Chronic inflammasome activation and neuroinflammation associated with prolonged accumulation of Aβ and tau hyper-phosphorylation could damage autophagy (Álvarez-Arellano *et al.*, 2018). Autophagy dysregulation has been demonstrated in brains of AD patients, which could impair effective elimination of aggregates and damaged mitochondria leading to their accumulation associated with toxicity and oxidative stress (Álvarez-Arellano *et al.*, 2018). In this study, the 3-months consumption of EVOO significantly increased several autophagy markers that regulate autophagy induction and maturation in the brains of TgSwDI mice compared to the control group. Our findings confirm an earlier observation for EVOO effect on inducing autophagy markers where its chronic administration significantly increased the steady-state levels of ATG5 and ATG7, established biomarkers of autophagy activation, in the brains of 3x-Tg mice (Lauretti *et al.*, 2017). To expand on the potential mechanism by which EVOO induced autophagy markers, AMPK and mTOR pathways were evaluated. Based on the results, EVOO induced autophagy through AMPK pathway activation, but not through mTOR pathway inhibition. Besides acting as a positive regulator of autophagy, through phosphorylating ULK1, AMPK has multiple functions including general regulation of cellular metabolism, regulation of NLRP3 inflammasome throughout aging, and mitochondrial homeostasis (Corona Velazquez and Jackson, 2018). In

addition, several recent studies have shown autophagy induction by AMPK can reduce the levels of Aβ load in AD (Park *et al.*, 2016), α-synuclein in Parkinson's disease (Curry *et al.*, 2018) and ameliorates Huntington's disease pathology and prevents neurodegeneration (Peixoto *et al.*, 2017). A recent study examined the postmortem brains of AD patients showed the possible relation between autophagy and the upregulation of NLRP3 in response to Aβ aggregation (Ahmed *et al.*, 2017). An abnormal accumulation of the autophagy markers SQSTM1/p62 and LC3 was observed in these brains, where both of these markers were co-localized with Aβ deposits and hyper-phosphorylated tau (Ahmed *et al.*, 2017). Increased autophagy has been found to ameliorate the pathology of various diseases by promoting the clearance of aggregated and hyper-phosphorylated proteins in the cytoplasm (Álvarez-Arellano *et al.*, 2018). Our immunostaining analysis demonstrated fewer Aβ plaques and total Aβ load in the brains of TgSwDI mice consumed EVOO compared to the control mice. This significant reduction in Aβ levels could be related to autophagy induction through the AMPK pathway.

Besides autophagy, another significant outcome that most likely caused by neuroinflammation inhibition (Botteri *et al.*, 2018) is the reduced levels of BACE1 in EVOO mice brains, which could also contribute to the reduced levels of sAPPβ and thus brain Aβ load. The levels of sAPPα, on the other hand, were significantly increased; sAPPα possesses neurotrophic and neuroprotective activities (Mattson *et al.*, 2002b). Decreased brain Aβ deposits could have contributed to the increased production of IL-10, consistent with previous reports (Peyrot des Gachons *et al.*, 2011), and reduced MMP9 and oxidative stress. Within this scenario, interestingly, the 3-months consumption of EVOO significantly reduced full-APP and tau levels in mice brains homogenates suggesting the re-establishment of proper processing of both proteins. While further studies are necessary to explain this observation, available studies in mouse models have already

shown that autophagy-lysosomal degradation of APP and Aβ (Nixon, 2007), and tau and hyper-phosphorylated tau (Chesser *et al.*, 2013) reduce AD.

Several studies linked BBB disruption (Muszynski *et al.*, 2017), Aβ toxicity (Minter *et al.*, 2016), tau aggregation (Stancu *et al.*, 2019), and memory impairment to neuroinflammation. Thus, reduced neuroinflammation associated with reduced Aβ-related pathology and oxidative stress by EVOO could explain, at least in part, the enhanced BBB integrity and function to limit brain access of unwanted molecules as demonstrated by reduced IgG extravasation, a finding that is consistent with our previous reports (Batarseh and Kaddoumi, 2018a). These positive effects resulted in improved performance of EVOO treated mice compared to the control group as determined by Morris Water Maze test (See appendix 2, Figure 2S). The effect of OC rich-EVOO could be better explained if we included age matched non transgenic mice to clarify whether the observed effect is due to BBB enhanced integrity or indirectly that was mediated by reduced brain Aβ levels and related pathology. Furthermore, an additional group that receives plain diet without oil enrichment could be necessary to differentiate the phenolic fraction effect from that of the non-phenolic fraction.

Collectively, this study is a continuation of previous studies by our lab (Qosa *et al.*, 2015b; Batarseh and Kaddoumi, 2018a). However, the new addition in the current work is assessing the effect of EVOO in a later stage of the disease compared to our 2 previous studies that assessed EVOO for prevention. In addition, in this study we evaluated the potential mechanism(s) by which EVOO could exert its effect.

Conflict of interest

My major adviser Dr. Amal Kaddoumi is a Chief Scientific Officer without compensation in the Shreveport, Louisiana-based Oleolive, LLC.

# Chapter 5

## Conclusions

The BBB is a highly selective permeable barrier formed by a monolayer of vascular ECs that line the brain microvasculature and acts as a vital regulator for the exchange of molecules between the blood and the brain (Yamazaki and Kanekiyo, 2017). An extremely important function of the BBB is to regulate and restrict the entrance of blood-derived components such as plasma proteins, neurotoxins and proinflammatory factors, immunoglobulins, fibrinogen, bacterial breakdown products, thrombin, hemoglobin, and ions, into the brain , in addition to the removal of brain borne noxious molecules to the blood (Zlokovic, 2011).

Recent clinical and experimental studies have supported the hypothesis that BBB breakdown as one of the earliest events in the pathogenesis of AD (Zlokovic, 2011), that has been linked to reductions in cerebral blood flow (Erickson and Banks, 2013). Moreover, recent clinical imaging and biomarker studies showed an early BBB disruption and vascular breakdown in AD is found before the onset of cognitive impairment and/or other neurodegeneration (Montagne *et al.*, 2016b). Several AD reports also indicated the crucial correlation between disrupted BBB integrity and functional activity triggering the imbalance in the levels of the two major AD hallmark proteins, amyloid beta (Aβ) and tau protein, which subsequently leads to Aβ accumulation and tau hyperphosphorylation observed in AD (Montagne *et al.*, 2016a; Zenaro *et al.*, 2017), both hallmarks are associated with a further disruption of cerebrovascular function (Miao *et al.*, 2005b;

Blair *et al.,* 2015). This concept has been framed as the "two-hit" hypothesis of AD offering potential targets for intervention (Zhu *et al.,* 2004).

Despite these advances, clinically relevant approaches for the prevention of BBB disruption in AD are not available. Recently, we have developed and validated an HTS assay that was utilized to find hit compounds, which have the potential to increase the BBB tightness (Qosa *et al.*, 2016). This assay was used in the current work to evaluate the ability of selected FDA drugs, identified from the screen, to enhance integrity of an *in-vitro* BBB model with CAA features. In this project, findings demonstrated granisetron enhanced the BBB integrity in both aged and AD mice. This effect was associated with an overall reduction in amyloid-β load and neuroinflammation in TgSwDI mice brains. Supported by proteomics analysis of mice brains, granisetron significantly reduced amyloid-β induced calcium influx *in-vitro*, and modulated calcium dyshomeostasis by restoring the CaMKII/CREB pathway in TgSwDI mice brain.

In our study, the anti-AD effect of granisetron was observed at a dose of 3 mg/kg administered daily for 28 days, a regimen that is higher and longer than prescribed for humans (Spartinou *et al.,* 2017). While mice treatment for 28 days with 3 mg/kg daily dose didn't demonstrate visible side effects. In humans, oral granisetron is administered in 1 to 2 mg dose up to one week, or subcutaneously for extended release in 10 mg dose. Within this regimen, in most human studies, granisetron has had minimal effect on heart rate, blood pressure or ECG (Kim *et al.*, 2015), however, pending further studies, precautions have recently been issued of possible QT prolongation especially in patients with cardiac diseases (Brygger and Herrstedt, 2014). The consequences of translating the chronic administration of such dose to humans are unknown that necessitate further evaluation and without a doubt, testing granisetron in AD mouse models at doses that correspond to human dose or less, in parallel with toxicity studies, are necessary.

However, as a proof-of-concept study with the tested dosage regimen, granisetron demonstrated a therapeutic potential against AD that prompts further evaluations. While further studies are essential to test the effect of long-term administration of granisetron in dose-dependent studies, our findings suggest the repurposing of granisetron as a possible candidate drug for AD, and also could be beneficial for other neurological diseases associated with BBB disruption.

In a different approach, in our next project, we evaluated the effect of OC- EVOO on AD pathology at an advanced stage of the disease compared to our previous study with younger TgSwDI mice (Qosa *et al.*, 2015b) and investigated the potential mechanism(s) by which OC and EVOO exert the positive effect.

Overall findings demonstrated OC-rich EVOO diet was associated with reduced AD pathology, mainly Aβ-related, and was also associated with a reduction in neuroinflammation which could be linked to the inhibition of NLRP3 inflammasome and inducing several autophagy markers through activation of AMPK/ULK1 pathway.

The translational value of our findings lies in the observation that OC-rich EVOO added to the diet can have a significant effect on the overall progression of AD. Our studies provide mechanistic support to the beneficial effect of this component of the MedD, and most importantly the biological rationale to the novel hypothesis that OC-rich EVOO could be considered as a viable medical food for preventing or halting AD. In conclusion, our findings in this study suggest the beneficial effect of OC-rich EVOO to protect, halt and/or stop the progression of AD even when given at advanced stage of the disease.

## Appendix

**Appendix 1**: List of all hit compounds.

| Library | Vendor Reagent ID | Compound Names |
|---|---|---|
| NIH Clinical Collection 1 - 2013 | SAM001246733 | ACARBOSE |
| NINDS Custom Collection 2 | 1500101 | Acetaminophen |
| NIH Clinical Collection 2 - 2013 | SAM002589967 | Acyclovir |
| NINDS Custom Collection 2 | 1500807 | Adenine |
| NINDS Custom Collection 2 | 1500801 | Allantoin |
| NINDS Custom Collection 2 | 1500110 | Amantadine hydrochloride |
| NIH Clinical Collection 2 - 2013 | SAM002699903 | AMCINONIDE |
| NIH Clinical Collection 1 - 2013 | SAM001246699 | Amfebutamone |
| NIH Clinical Collection 2 - 2013 | SAM002589964 | Aminoglutethimide |
| NINDS Custom Collection 2 | 1500115 | Aminoglutethimide |
| NINDS Custom Collection 2 | 1500116 | Aminosalicylate sodium |
| NIH Clinical Collection 1 - 2013 | SAM001246639 | Amisulpride |
| NINDS Custom Collection 2 | 1500117 | Amitriptyline hydrochloride |
| NIH Clinical Collection 1 - 2013 | SAM001246705 | Amlodipine |
| NINDS Custom Collection 2 | 1500119 | Amodiaquine dihydrochloride |
| NINDS Custom Collection 2 | 1500123 | Ampicillin sodium |
| NINDS Custom Collection 2 | 1500124 | Amprolium |
| NINDS Custom Collection 2 | 1500126 | Antazoline phosphate |
| NINDS Custom Collection 2 | 1500127 | Anthralin |
| NINDS Custom Collection 2 | 1502103 | Anthraquinone |
| NINDS Custom Collection 2 | 1500128 | Antipyrine |
| NINDS Custom Collection 2 | 1500129 | Apomorphine hydrochloride |
| NIH Clinical Collection 1 - 2013 | SAM001246750 | ARIPIPRAZOLE |

| | | |
|---|---|---|
| NINDS Custom Collection 2 | 1502230 | Ascorbic acid |
| NINDS Custom Collection 2 | 1500130 | Aspirin |
| NINDS Custom Collection 2 | 1503722 | Atorvastatin calcium |
| NINDS Custom Collection 2 | 1504210 | Atovaquone |
| NINDS Custom Collection 2 | 1500131 | Atropine sulfate |
| NINDS Custom Collection 2 | 1500133 | Azathioprine |
| NINDS Custom Collection 2 | 1501172 | Azobenzene |
| NINDS Custom Collection 2 | 1500134 | Bacitracin |
| NINDS Custom Collection 2 | 1500135 | Baclofen |
| NINDS Custom Collection 2 | 1504002 | Baicalein |
| NIH Clinical Collection 1 - 2013 | SAM001246804 | BALSALAZIDE |
| NIH Clinical Collection 2 - 2013 | SAM002699895 | Beclomethasone dipropionate |
| NINDS Custom Collection 2 | 1500136 | Beclomethasone dipropionate |
| NIH Clinical Collection 1 - 2013 | SAM001246968 | Benzeneacetonitrile |
| NINDS Custom Collection 2 | 1500465 | Benzyl penicillin potassium |
| NINDS Custom Collection 2 | 1503106 | Bepridil hydrochloride |
| NIH Clinical Collection 2 - 2013 | SAM002589959 | Betamethasone |
| NINDS Custom Collection 2 | 1500144 | Betamethasone |
| NINDS Custom Collection 2 | 1500145 | Betamethasone valerate |
| NINDS Custom Collection 2 | 1503234 | Beta-propiolactone |
| NINDS Custom Collection 2 | 1500146 | Bethanechol chloride |
| NINDS Custom Collection 2 | 1500147 | Bisacodyl |
| NIH Clinical Collection 1 - 2013 | SAM001246618 | BISOPROLOL FUMARATE |
| NINDS Custom Collection 2 | 1500148 | Bithionol |
| NINDS Custom Collection 2 | 1500151 | Bromocriptine mesylate |
| NINDS Custom Collection 2 | 1500623 | Broxyquinoline |
| NINDS Custom Collection 2 | 1500822 | Brucine |

| | | |
|---|---|---|
| NINDS Custom Collection 2 | 1500813 | Budesonide |
| NINDS Custom Collection 2 | 1500152 | Busulfan |
| NINDS Custom Collection 2 | 1500155 | Caffeine |
| NIH Clinical Collection 1 - 2013 | SAM001246772 | CALCITRIOL |
| NINDS Custom Collection 2 | 1500828 | Canrenoic acid, potassium salt |
| NIH Clinical Collection 1 - 2013 | SAM001246692 | CARMOFUR |
| NIH Clinical Collection 1 - 2013 | SAM001247065 | CCPA |
| NIH Clinical Collection 1 - 2013 | SAM001246643 | CEFATRIZINE PROPYLENE GLYCOL |
| NINDS Custom Collection 2 | 1500164 | Cefazolin sodium |
| NIH Clinical Collection 1 - 2013 | SAM001246816 | CEFIXIME TRIHYDRATE |
| NINDS Custom Collection 2 | 1500165 | Cefotaxime sodium |
| NIH Clinical Collection 1 - 2013 | SAM001246674 | CEFPODOXIME PROXETIL |
| NIH Clinical Collection 2 - 2013 | SAM002589995 | Celecoxib |
| NINDS Custom Collection 2 | 1500836 | Cephalosporin c sodium |
| NINDS Custom Collection 2 | 1500166 | Cephalothin sodium |
| NINDS Custom Collection 2 | 1500167 | Cephapirin sodium |
| NINDS Custom Collection 2 | 1500168 | Cephradine |
| NIH Clinical Collection 1 - 2013 | SAM001246695 | CETRAXATE HCl |
| NIH Clinical Collection 1 - 2013 | SAM001247066 | CGS 12066B |
| NINDS Custom Collection 2 | 1500837 | Chenodiol |
| NIH Clinical Collection 2 - 2013 | SAM002548963 | Chloramphenicol |
| NINDS Custom Collection 2 | 1500174 | Chloramphenicol |
| NINDS Custom Collection 2 | 1500177 | Chlorhexidine |
| NINDS Custom Collection 2 | 1503341 | Chloroacetoxyquinoline |
| NINDS Custom Collection 2 | 1500180 | Chlorothiazide |
| NINDS Custom Collection 2 | 1500709 | Chrysin |
| NIH Clinical Collection 1 - 2013 | SAM001246552 | Cilastatin sodium |

| | | |
|---|---|---|
| NINDS Custom Collection 2 | 1500839 | Cinchonidine |
| NINDS Custom Collection 2 | 1500841 | Cinchonine |
| NIH Clinical Collection 1 - 2013 | SAM001246748 | CLARITHROMYCIN |
| NINDS Custom Collection 2 | 1500200 | Clotrimazole |
| NINDS Custom Collection 2 | 1500201 | Cloxacillin sodium |
| NINDS Custom Collection 2 | 1500202 | Cloxyquin |
| NINDS Custom Collection 2 | 1503804 | Colforsin |
| NINDS Custom Collection 2 | 1500206 | Colistimethate sodium |
| NIH Clinical Collection 1 - 2013 | Cohen-A1 | Compound A1 |
| NINDS Custom Collection 2 | 1500861 | Coralyne chloride |
| NINDS Custom Collection 2 | 1400208 | Coumarin |
| NINDS Custom Collection 2 | 1503207 | Cyclobenzaprine hydrochloride |
| NINDS Custom Collection 2 | 1500220 | Danazol |
| NINDS Custom Collection 2 | 1500222 | Dapsone |
| NIH Clinical Collection 2 - 2013 | SAM002264599 | D-CYCLOSERINE |
| NINDS Custom Collection 2 | 1500224 | Deferoxamine mesylate |
| NINDS Custom Collection 2 | 1500226 | Demeclocycline hydrochloride |
| NIH Clinical Collection 2 - 2013 | SAM002699893 | DEPO-MEDROL |
| NINDS Custom Collection 2 | 1500227 | Desipramine hydrochloride |
| NIH Clinical Collection 2 - 2013 | SAM002548948 | Dexamethasone |
| NINDS Custom Collection 2 | 1500230 | Dexamethasone |
| NINDS Custom Collection 2 | 1500232 | Dexamethasone sodium phosphate |
| NIH Clinical Collection 1 - 2013 | SAM001246556 | DEXBROMPHENIRAMINE MALEATE |
| NIH Clinical Collection 1 - 2013 | SAM001246557 | DEXCHLORPHENIRAMINE MALEATE |
| NINDS Custom Collection 2 | 1500514 | Dexpropranolol hydrochloride |
| NINDS Custom Collection 2 | 1500235 | Dibenzothiophene |
| NINDS Custom Collection 2 | 1500236 | Dibucaine hydrochloride |

| | | |
|---|---|---|
| NINDS Custom Collection 2 | 1500237 | Diclofenac sodium |
| NIH Clinical Collection 2 - 2013 | SAM002589990 | DICLOXACILLIN SODIUM |
| NINDS Custom Collection 2 | 1500239 | Dicumarol |
| NINDS Custom Collection 2 | 1500240 | Dicyclomine hydrochloride |
| NINDS Custom Collection 2 | 1500241 | Dienestrol |
| NINDS Custom Collection 2 | 1500242 | Diethylcarbamazine citrate |
| NINDS Custom Collection 2 | 1500244 | Diethylstilbestrol |
| NINDS Custom Collection 2 | 1500245 | Diflunisal |
| NINDS Custom Collection 2 | 1500246 | Digitoxin |
| NINDS Custom Collection 2 | 1500248 | Dihydroergotamine mesylate |
| NINDS Custom Collection 2 | 1500249 | Dihydrostreptomycin sulfate |
| NINDS Custom Collection 2 | 1500253 | Dimethadione |
| NINDS Custom Collection 2 | 1503219 | Diosmin |
| NINDS Custom Collection 2 | 1500258 | Diphenylpyraline hydrochloride |
| NINDS Custom Collection 2 | 1500259 | Dipyridamole |
| NINDS Custom Collection 2 | 1500261 | Disopyramide phosphate |
| NINDS Custom Collection 2 | 1503212 | Dobutamine hydrochloride |
| NIH Clinical Collection 1 - 2013 | SAM001246627 | Donepezil |
| NINDS Custom Collection 2 | 1500263 | Dopamine hydrochloride |
| NINDS Custom Collection 2 | 1500267 | Doxylamine succinate |
| NIH Clinical Collection 1 - 2013 | SAM001246523 | duloxetine hydrochloride |
| NINDS Custom Collection 2 | 1500269 | Dyphylline |
| NIH Clinical Collection 1 - 2013 | SAM001246856 | ENROFLOXACIN |
| NINDS Custom Collection 2 | 1503221 | Ethisterone |
| NIH Clinical Collection 1 - 2013 | SAM001247008 | ETHYNYLESTRADIOL |
| NIH Clinical Collection 1 - 2013 | SAM001247005 | Felbamate |
| NIH Clinical Collection 2 - 2013 | SAM002589971 | Felodipine |

| | | |
|---|---|---|
| NINDS Custom Collection 2 | 1501021 | Fenspiride hydrochloride |
| NIH Clinical Collection 1 - 2013 | SAM001246541 | FINASTERIDE |
| NIH Clinical Collection 2 - 2013 | SAM002589966 | FluniSOLIDe |
| NINDS Custom Collection 2 | 1501187 | Flunisolide |
| NINDS Custom Collection 2 | 1500303 | Fluocinonide |
| NIH Clinical Collection 2 - 2013 | SAM002700174 | Fluorometholone |
| NINDS Custom Collection 2 | 1504173 | Fluoxetine |
| NIH Clinical Collection 1 - 2013 | SAM001246583 | FLUTICASONE PROPIONATE |
| NIH Clinical Collection 1 - 2013 | SAM001247060 | Glycine, N-[2-[(acetylthio)methyl]-1-oxo-3-phenylpropyl]-,phenylmethyl ester [CAS] |
| NIH Clinical Collection 1 - 2013 | SAM001246784 | GOSERELIN ACETATE |
| NINDS Custom Collection 2 | 200046 | Griseofulvin |
| NIH Clinical Collection 1 - 2013 | SAM001247088 | Guanidine |
| NINDS Custom Collection 2 | 1503237 | Halcinonide |
| NIH Clinical Collection 1 - 2013 | SAM001246822 | HOMOHARRINGTONINE |
| NIH Clinical Collection 1 - 2013 | SAM001247089 | HTMT |
| NINDS Custom Collection 2 | 1500338 | Hydrocortisone acetate |
| NINDS Custom Collection 2 | 1503273 | Hydrocortisone butyrate |
| NIH Clinical Collection 2 - 2013 | SAM002564213 | HYDROCORTISONE HEMISUCCINATE |
| NINDS Custom Collection 2 | 1500339 | Hydrocortisone hemisuccinate |
| NIH Clinical Collection 1 - 2013 | SAM001246560 | ICARIIN |
| NIH Clinical Collection 1 - 2013 | SAM001246980 | Ifenprodil |
| NIH Clinical Collection 1 - 2013 | SAM001246982 | Indomethacin |
| NINDS Custom Collection 2 | 1503923 | Iopanic acid |
| NIH Clinical Collection 1 - 2013 | SAM001246584 | ISRADIPINE |
| NINDS Custom Collection 2 | 1505038 | Kasugamycin hydrochloride |
| NIH Clinical Collection 1 - 2013 | SAM001246731 | KITASAMYCIN |

| | | |
|---|---|---|
| NIH Clinical Collection 2 - 2013 | SAM002589994 | LAMIVUDINE |
| NINDS Custom Collection 2 | 1503927 | Lefunomide |
| NIH Clinical Collection 1 - 2013 | SAM001246758 | LEVOFLOXACIN |
| NIH Clinical Collection 1 - 2013 | SAM001246624 | LINEZOLID |
| NINDS Custom Collection 2 | 1504269 | Lithium citrate |
| NIH Clinical Collection 1 - 2013 | SAM001247050 | LOBELINE HYDROCHLORIDE |
| NIH Clinical Collection 1 - 2013 | SAM001247049 | L-Ornithine, N5-[imino(methylamino)methyl]-[CAS] |
| NIH Clinical Collection 1 - 2013 | SAM001246687 | MECILLINAM |
| NIH Clinical Collection 2 - 2013 | SAM002564220 | Medroxyprogesterone 17-acetate |
| NIH Clinical Collection 2 - 2013 | SAM002699894 | Mefloquine hydrochloride |
| NIH Clinical Collection 2 - 2013 | SAM002699890 | Memantine hydrochloride |
| NINDS Custom Collection 2 | 1501140 | Mephenesin |
| NINDS Custom Collection 2 | 1502014 | Mesna |
| NINDS Custom Collection 2 | 211175 | Metacetamol |
| NINDS Custom Collection 2 | 1500396 | Methimazole |
| NINDS Custom Collection 2 | 1500397 | Methocarbamol |
| NINDS Custom Collection 2 | 1500398 | Methotrexate(+/-) |
| NINDS Custom Collection 2 | 1500399 | Methoxamine hydrochloride |
| NINDS Custom Collection 2 | 1500401 | Methscopolamine bromide |
| NINDS Custom Collection 2 | 1500403 | Methyldopa |
| NIH Clinical Collection 2 - 2013 | SAM002589984 | METHYLPREDNISOLONE |
| NINDS Custom Collection 2 | 1500406 | Methylprednisolone |
| NINDS Custom Collection 2 | 1500408 | Methylthiouracil |
| NIH Clinical Collection 1 - 2013 | SAM001246585 | Midazolam Hydrochloride |
| NINDS Custom Collection 2 | 1500415 | Minoxidil |
| NINDS Custom Collection 2 | 330082 | Mitotane |

| | | |
|---|---|---|
| NIH Clinical Collection 2 - 2013 | SAM002548933 | Moban |
| NINDS Custom Collection 2 | 1500418 | Moxalactam disodium |
| NIH Clinical Collection 1 - 2013 | SAM001246654 | Moxifloxacin hydrochloride |
| NIH Clinical Collection 1 - 2013 | SAM001246764 | MOXONIDINE HCl |
| NINDS Custom Collection 2 | 1500420 | Nafcillin sodium |
| NIH Clinical Collection 1 - 2013 | SAM001247063 | Nalbuphine |
| NINDS Custom Collection 2 | 1500422 | Naloxone hydrochloride |
| NIH Clinical Collection 1 - 2013 | SAM001247004 | Naltrindole |
| NINDS Custom Collection 2 | 1500424 | Naphazoline hydrochloride |
| NIH Clinical Collection 1 - 2013 | SAM001246874 | NAPROXEN SODIUM |
| NINDS Custom Collection 2 | 1500425 | Naproxen(+) |
| NINDS Custom Collection 2 | 1500428 | Neostigmine bromide |
| NINDS Custom Collection 2 | 1500430 | Niacin |
| NINDS Custom Collection 2 | 1502015 | Niflumic acid |
| NINDS Custom Collection 2 | 1500639 | Octopamine hydrochloride |
| NIH Clinical Collection 1 - 2013 | SAM001246769 | OLIGOMYCIN C |
| NIH Clinical Collection 1 - 2013 | SAM001246634 | OLMESARTAN MEDOXOMIL |
| NIH Clinical Collection 1 - 2013 | SAM001246802 | OLOPATADINE HYDROCHLORIDE |
| NIH Clinical Collection 2 - 2013 | SAM002589958 | Ondansetron |
| NIH Clinical Collection 1 - 2013 | SAM001246728 | ORMETOPRIM |
| NIH Clinical Collection 1 - 2013 | SAM001246724 | OXICONAZOLE NITRATE |
| NINDS Custom Collection 2 | 1500456 | Oxyquinoline hemisulfate |
| NINDS Custom Collection 2 | 1500457 | Oxytetracycline |
| NIH Clinical Collection 1 - 2013 | SAM001246791 | Palonosetron hydrochloride |
| NINDS Custom Collection 2 | 1500459 | Papaverine hydrochloride |
| NINDS Custom Collection 2 | 1500460 | Parachlorophenol |
| NINDS Custom Collection 2 | 1500464 | Penicillamine |

| | | |
|---|---|---|
| NINDS Custom Collection 2 | 1500467 | Penicillin v potassium |
| NINDS Custom Collection 2 | 1502101 | Perillic acid (-) |
| NINDS Custom Collection 2 | 1500472 | Phenacemide |
| NIH Clinical Collection 2 - 2013 | SAM002589985 | Phenelzine |
| NIH Clinical Collection 1 - 2013 | SAM001246992 | Physostigmine |
| NIH Clinical Collection 1 - 2013 | SAM001246762 | PIDOTIMOD |
| NIH Clinical Collection 1 - 2013 | SAM001246907 | Pinacidil monohydrate |
| NINDS Custom Collection 2 | 1500489 | Piperacillin sodium |
| NIH Clinical Collection 1 - 2013 | SAM001246995 | Prazosin |
| NINDS Custom Collection 2 | 1500497 | Prednisolone acetate |
| NIH Clinical Collection 2 - 2013 | SAM002589935 | Priscoline |
| NINDS Custom Collection 2 | 1505270 | Propranolol hydrochloride (+/-) |
| NINDS Custom Collection 2 | 1500516 | Pseudoephedrine hydrochloride |
| NINDS Custom Collection 2 | 1500260 | Pyrithione zinc |
| NINDS Custom Collection 2 | 1500759 | Quinalizarin |
| NIH Clinical Collection 2 - 2013 | SAM002589972 | QUINAPRIL HYDROCHLORIDE |
| NINDS Custom Collection 2 | 1502102 | Quinolinic acid |
| NINDS Custom Collection 2 | 1500525 | Racephedrine hydrochloride |
| NIH Clinical Collection 1 - 2013 | SAM001246796 | RALTITREXED |
| NIH Clinical Collection 2 - 2013 | SAM002699899 | RAMIPRIL |
| NIH Clinical Collection 1 - 2013 | SAM001246889 | Reichsteins substance S |
| NINDS Custom Collection 2 | 1500527 | Resorcinol |
| NIH Clinical Collection 2 - 2013 | SAM002589953 | RIFAPENTINE |
| NIH Clinical Collection 1 - 2013 | SAM001246615 | RIZATRIPTAN BENZOATE |
| NINDS Custom Collection 2 | 1504263 | Rosiglitazone |
| NINDS Custom Collection 2 | 1502094 | Rosmarinic acid |
| NINDS Custom Collection 2 | 1503276 | Roxithromycin |

| | | |
|---|---|---|
| NIH Clinical Collection 1 - 2013 | SAM001246726 | rufloxacin monohydrochloride |
| NINDS Custom Collection 2 | 1500532 | Salicylamide |
| NINDS Custom Collection 2 | 1503602 | Salinomycin, sodium |
| NIH Clinical Collection 1 - 2013 | SAM001246678 | SECOISOLARICIRESINOL |
| NIH Clinical Collection 2 - 2013 | SAM002700175 | Sertraline |
| NINDS Custom Collection 2 | 1500860 | S-isocorydine (+) |
| NINDS Custom Collection 2 | 1500225 | Sodium dehydrocholate |
| NIH Clinical Collection 1 - 2013 | SAM001247042 | Stiripentol |
| NINDS Custom Collection 2 | 100291 | Strophanthidin |
| NINDS Custom Collection 2 | 1501148 | Sulconazole nitrate |
| NINDS Custom Collection 2 | 1501144 | Sulfadimethoxine |
| NINDS Custom Collection 2 | 1501155 | Sulfameter |
| NINDS Custom Collection 2 | 1500548 | Sulfamethazine |
| NINDS Custom Collection 2 | 1500549 | Sulfamethizole |
| NIH Clinical Collection 1 - 2013 | SAM001246896 | SYNEPHRINE |
| NIH Clinical Collection 1 - 2013 | SAM001246778 | TAXIFOLIN-(+) |
| NIH Clinical Collection 1 - 2013 | SAM001246606 | TEGASEROD MALEATE |
| NIH Clinical Collection 2 - 2013 | SAM002589997 | THIOTHIXENE |
| NINDS Custom Collection 2 | 1503135 | Thonzylamine hydrochloride |
| NINDS Custom Collection 2 | 1500774 | Thyroxine |
| NIH Clinical Collection 1 - 2013 | SAM001246625 | TIAGABINE HCl |
| NIH Clinical Collection 1 - 2013 | SAM001246558 | Ticlopidine Hydrochloride |
| NINDS Custom Collection 2 | 1503094 | Tioxolone |
| NIH Clinical Collection 1 - 2013 | SAM001246759 | TOCAINIDE |
| NIH Clinical Collection 1 - 2013 | SAM001246691 | TOLTERODINE TARTRATE |
| NIH Clinical Collection 1 - 2013 | SAM001246852 | TREMULACIN |
| NINDS Custom Collection 2 | 1500585 | Triacetin |

| | | |
|---|---|---|
| NINDS Custom Collection 2 | 1500587 | Triamcinolone acetonide |
| NIH Clinical Collection 1 - 2013 | SAM001246747 | TRIMEBUTINE MALEATE |
| NINDS Custom Collection 2 | 1500270 | Trisodium ethylenediamine tetracetate |
| NINDS Custom Collection 2 | 1502203 | Troleandomycin |
| NIH Clinical Collection 1 - 2013 | SAM001246576 | Tropisetron hydrochloride |
| NINDS Custom Collection 2 | 1503922 | Tryptamine |
| NINDS Custom Collection 2 | 1500601 | Tuaminoheptane sulfate |
| NINDS Custom Collection 2 | 1500607 | Vancomycin hydrochloride |
| NIH Clinical Collection 1 - 2013 | SAM001246573 | VARDENAFIL CITRATE |
| NIH Clinical Collection 1 - 2013 | SAM001246572 | Venlafaxine hydrochloride |
| NIH Clinical Collection 2 - 2013 | SAM002589925 | Westcort |
| NIH Clinical Collection 1 - 2013 | SAM001246912 | XANTHINOL NICOTINATE |
| NIH Clinical Collection 1 - 2013 | SAM001246738 | ZILEUTON |
| NIH Clinical Collection 2 - 2013 | SAM002564250 | |
| NIH Clinical Collection 2 - 2013 | SAM002564208 | |
| NIH Clinical Collection 2 - 2013 | SAM002264605 | |
| NIH Clinical Collection 2 - 2013 | SAM002589945 | |
| NIH Clinical Collection 2 - 2013 | SAM002589968 | |
| NIH Clinical Collection 2 - 2013 | SAM002699901 | (+/-)-NOREPINEPHRINE HYDROCHLORIDE |
| NIH Clinical Collection 1 - 2013 | SAM001246706 | . |
| NIH Clinical Collection 1 - 2013 | SAM001246697 | . |
| NIH Clinical Collection 1 - 2013 | SAM001246737 | . |
| NIH Clinical Collection 1 - 2013 | SAM001246673 | . |
| NIH Clinical Collection 1 - 2013 | SAM001246722 | . |
| NIH Clinical Collection 1 - 2013 | SAM001246753 | . |
| NIH Clinical Collection 1 - 2013 | SAM001246746 | . |

| | | |
|---|---|---|
| NIH Clinical Collection 1 - 2013 | SAM001246882 | . |
| NIH Clinical Collection 1 - 2013 | SAM001246893 | . |
| NIH Clinical Collection 1 - 2013 | SAM001246563 | . |
| NIH Clinical Collection 1 - 2013 | SAM001246892 | . |
| NIH Clinical Collection 1 - 2013 | SAM001246887 | . |
| NIH Clinical Collection 1 - 2013 | SAM001246531 | . |
| NIH Clinical Collection 1 - 2013 | SAM001246885 | . |
| NIH Clinical Collection 1 - 2013 | SAM001246909 | . |
| NIH Clinical Collection 1 - 2013 | SAM001246818 | . |
| NIH Clinical Collection 1 - 2013 | SAM001246867 | . |
| NIH Clinical Collection 1 - 2013 | SAM001246602 | . |
| NIH Clinical Collection 1 - 2013 | SAM001246880 | . |
| NIH Clinical Collection 1 - 2013 | SAM001246716 | 1-(2-Methyl-5-nitro-imidazol-1-yl)-propan-2-ol |
| NIH Clinical Collection 1 - 2013 | SAM001246646 | 19774-82-4 |
| NIH Clinical Collection 1 - 2013 | SAM001247073 | 1H-Imidazol-2-amine, N-(2,6-dichlorophenyl)-4,5-dihydro- [CAS] |
| NIH Clinical Collection 1 - 2013 | SAM001246779 | 2',3'-DIDEOXYCYTIDINE |
| NIH Clinical Collection 1 - 2013 | SAM001247045 | 25332-39-2 |
| NIH Clinical Collection 1 - 2013 | SAM001247015 | 3-HYDROXY-1,2-DIMETHYL-4(1H)-PYRIDONE |
| NIH Clinical Collection 1 - 2013 | SAM001246894 | 3-PYRIDINEMETHANOL |
| NIH Clinical Collection 2 - 2013 | SAM002589996 | 4-(AMINOMETHYL)BENZENESULFONAMIDE ACETATE |
| NIH Clinical Collection 1 - 2013 | SAM001247016 | 4-Thiazolidinecarboxylic acid, 2-oxo-, (R)- [CAS] |
| NIH Clinical Collection 2 - 2013 | SAM002699898 | 51333-22-3 |

| | | |
|---|---|---|
| NIH Clinical Collection 1 - 2013 | SAM001246775 | 60628-96-8 |
| NIH Clinical Collection 2 - 2013 | SAM002564258 | 6ALPHA-METHYL-11BETA-HYDROXYPROGESTERONE |
| NIH Clinical Collection 2 - 2013 | SAM002564237 | 76-25-5 |
| NIH Clinical Collection 1 - 2013 | SAM001246855 | 92-84-2 |
| Sigma Lopac 1028 | NA | Pirenzepine dihydrochloride |
| Sigma Lopac 1028 | NA | (±)-cis-Piperidine-2,3-dicarboxylic acid |
| Sigma Lopac 1028 | NA | SC-57461A |
| Sigma Lopac 1028 | NA | Daidzein |
| Sigma Lopac 1028 | NA | Dicyclomine hydrochloride |
| Sigma Lopac 1028 | NA | DBO-83 |
| Sigma Lopac 1028 | NA | Pindolol |
| Sigma Lopac 1028 | NA | Parthenolide |
| Sigma Lopac 1028 | NA | PD-156707 |
| Sigma Lopac 1028 | NA | TMB-8 hydrochloride |
| Sigma Lopac 1028 | NA | S-(p-Azidophenacyl)glutathione |
| Sigma Lopac 1028 | NA | N6-Methyladenosine |
| Sigma Lopac 1028 | NA | SB 202190 |
| Sigma Lopac 1028 | NA | Benzamidine hydrochloride |
| Sigma Lopac 1028 | NA | Ro 20-1724 |
| Sigma Lopac 1028 | NA | BRL 50481 |
| Sigma Lopac 1028 | NA | Arecaidine propargyl ester hydrobromide |
| Sigma Lopac 1028 | NA | 8-(p-Sulfophenyl)theophylline |
| Sigma Lopac 1028 | NA | (±)-AMT hydrochloride |

| | | |
|---|---|---|
| Sigma Lopac 1028 | NA | Beclomethasone |
| Sigma Lopac 1028 | NA | 8-(p-Sulfophenyl)theophylline |

## Appendix 2

### Morris Water Maze (MWM) test

The water maze consisted of a circular 120 cm (diameter) and 60 cm (height) white plastic pool and a white plastic platform of 11 cm diameter; the pool was filled with water at 25°C. The pool was surrounded by solid, gray sectioned curtains with high contrast (yellow and orange) differently shaped cues on all curtains surrounding the pool. On day one and two, a visible test was performed using clear water in the tank and a platform with an attached flag was placed 1 cm above the water. The platform was placed in the Southwest (SW) quadrant, and the mice were released from the Northeast (NE) quadrant for each of the 3 trials per day. Each mouse was giving 60 seconds to find the platform, and an additional 30-60 seconds where the mouse was placed on top of the platform, after which the mouse immediately underwent training in another trial such that there was no inter-trial-interval.

On days 3-6, a hidden platform test was performed where the water was made opaque using a non-toxic white paint, and the platform was immersed 1 cm below the water surface after removing the flag. The platform and cues were in the same place as described during the visible test. During the hidden test days, each mouse underwent 12 trials per day in which the mice were released from the NE quadrant for trials 1-3, from the Northwest (NW) quadrant for trials 4-6, from the Southeast (SE) quadrant for trials 7-9, and from the SW quadrant where the platform was located in trials 10-12. Each mouse was given 60 seconds to find the platform, and an additional 30-60 seconds where the mouse was placed on top of the platform, after which the mouse immediately underwent training in another trial such that there was no inter-trial-interval. The data collected from the visible and the hidden tests where analyzed using SMART 3.0 video tracking

software (Panlab Harvard Apparatus; Holliston, MA), and the distance to platform was selected as the primary measure.

Because the platform was in the same location for both visible and hidden platform training and the release sequence was the same each day, we cannot conclude that any differences were due to hippocampal-dependent spatial learning. Likewise, because a probe trail in which the platform is removed from the pool was not conducted, we cannot conclude that mice exhibited hippocampal-dependent memory deficits.

For MWM, a repeated measures ANOVA (RMANOVA) was performed with as a between-subjects variable of Group (Tg vs. Tg*Tx) and a within-subjects variable of Trial or Day.

GRS Visible – While both groups improved with training in the visible platform test (effect of Trial: $F(5,4)=12.5$, $p=.01$), there were no differences between the groups, suggesting no motoric or visual deficits.

GRS Hidden – For the hidden platform task, both groups improved with additional training (effect of Day: $F(3,6)=33$, $p=.0004$) with the Tg*Tx group performing better overall (effect of Group: $F(1,8)=13$, $p=.0066$).

EVOO Visible – For visible platform training, there were no differences between the groups, suggesting no motoric or visual deficits (*p*s >.05).

EVOO Hidden – For the hidden platform task, both groups improved with additional training (effect of Day: $F(3,6)=12$, $p=.0059$) with the Tg*Tx group performing better overall (effect of Group: $F(1,8)=14$, $p=.0055$).

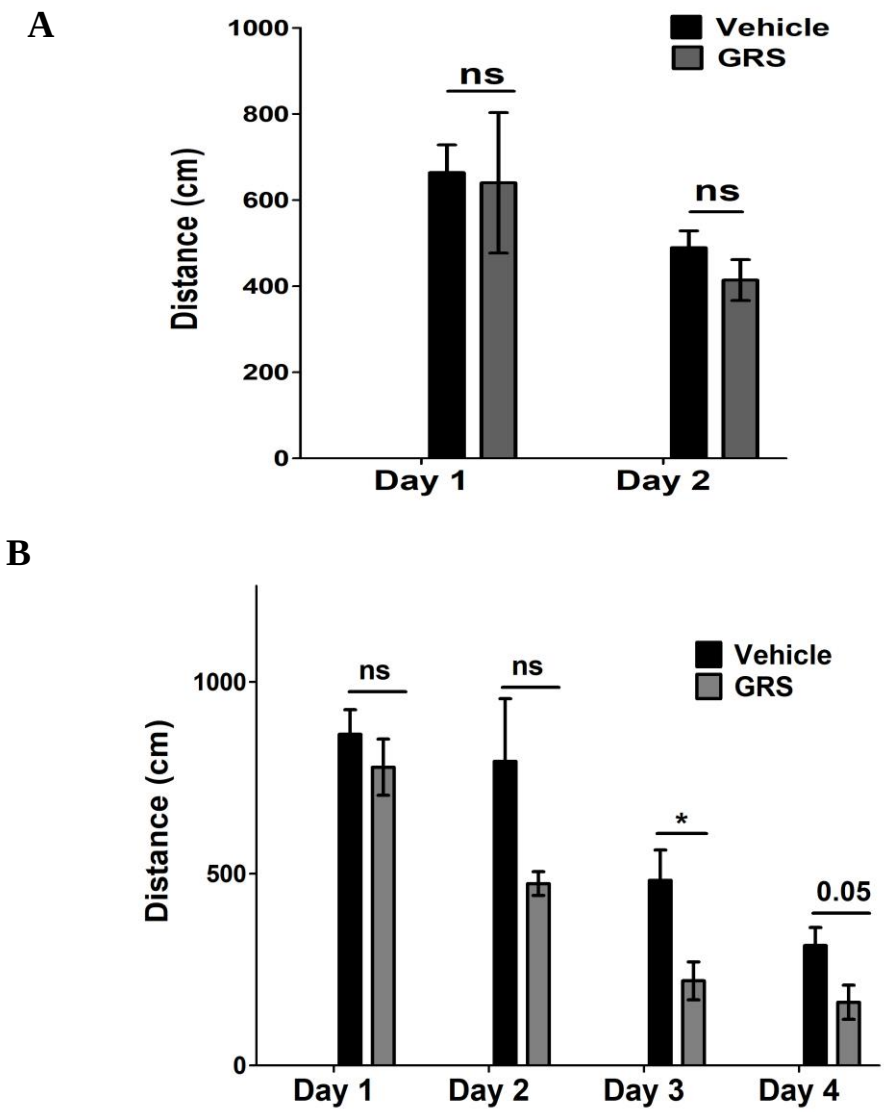


Figure 1S. MWM test for vehicle vs granisetron (GRS) in TgSWDI mice (n=5 mice/group). (A) Visible test showed no significant difference was observed between the two groups, however both groups, regardless of treatment, improved with additional training trials. (B) Hidden platform task showed a significant different between the groups and GRS group demonstrated improvement in performance compared to control group.

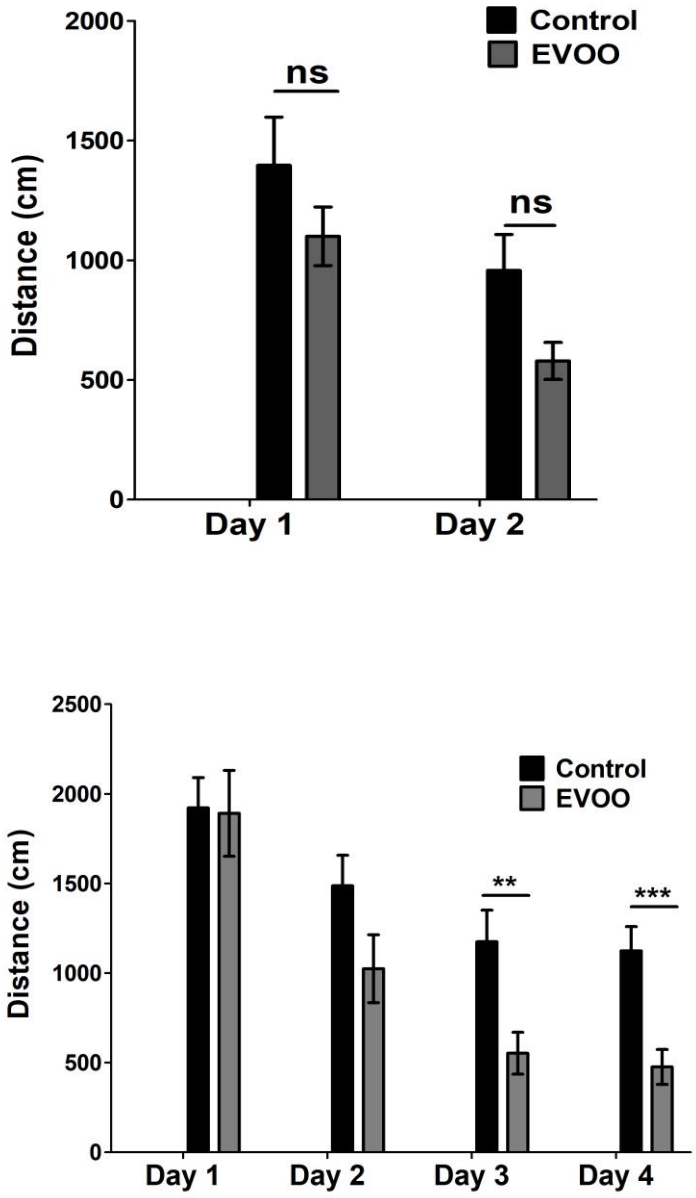


Figure 2S. MWM test for control vs EVOO in TgSWDI mice (n=5 mice/group). (A) Visible test showed no significant difference was observed between the two groups. (B) Hidden platform task showed a significant different between the groups, and EVOO group demonstrated improvement in performance compared to control group.

**List of References**

Abdelmonem R, Attia A. Development of novel bioadhesive granisetron hydrochloride spanlastic gel and insert for brain targeting and study their effects on rats. Drug Deliv. 2018; 0: 70–77.

Abuznait AH, Qosa H, Busnena BA, El Sayed KA, Kaddoumi A. Olive-oil-derived oleocanthal enhances β-amyloid clearance as a potential neuroprotective mechanism against Alzheimer's disease: In vitro and in vivo studies. ACS Chem. Neurosci. 2013; 4: 973–982.

Ahmed ME, Iyer S, Thangavel R, Kempuraj D, Selvakumar GP, Raikwar SP, et al. Co-Localization of Glia Maturation Factor with NLRP3 Inflammasome and Autophagosome Markers in Human Alzheimer's Disease Brain. J. Alzheimer's Dis. 2017; 60: 1143–1160.

Aithal S, Geetha S, Swetha ES, Balaji V, Chethan Kumar S. Evaluation of antidepressant activity of granisetron in albino mice. Int. J. Pharm. Sci. Rev. Res. 2014; 27: 345–348.

Allan Butterfield D, Boyd-Kimball D. Oxidative Stress, Amyloid-β Peptide, and Altered Key Molecular Pathways in the Pathogenesis and Progression of Alzheimer's Disease. J. Alzheimer's Dis. 2018; 62: 1345–1367.

Allen I V. THE EFFECT OF BACTERIAL PYROGEN ON THE BLOOD-BRAIN BARRIER FOR TRYPAN BLUE. J. Pathol. Bacteriol. 1965; 89: 481–494.

Álvarez-Arellano L, Pedraza-Escalona M, Blanco-Ayala T, Camacho-Concha N, Cortés-Mendoza J, Pérez-Martínez L, et al. Autophagy impairment by caspase-1-dependent inflammation mediates memory loss in response to β-Amyloid peptide accumulation. J. Neurosci. Res. 2018; 96: 234–246.

Alzheimer's Association. 2018 Alzheimer's Disease Facts and Figures. Alzheimers Dement 2018; 14: 367–429.

Alzheimer's Disease International. World Alzheimer Report 2018 - The state of the art of dementia research: New frontiers. 2018a: 1–48.

Alzheimer's Disease International. World Alzheimer Report 2018 - The state of the art of dementia research: New frontiers. 2018b: 1–48.

Anand U, Otto WR, Facer P, Zebda N, Selmer I, Gunthorpe MJ, et al. TRPA1 receptor localisation in the human peripheral nervous system and functional studies in cultured human and rat sensory neurons. Neurosci. Lett. 2008; 438: 221–227.

Appleby B, Cummings J. Discovering New Treatments for Alzheimer's Disease by Repurposing Approved Medications. Curr. Top. Med. Chem. 2013; 13: 2306–2327.

Appleby BS, Nacopoulos D, Milano N, Zhong K, Cummings JL. A review: Treatment of Alzheimer's disease discovered in repurposed agents. Dement. Geriatr. Cogn. Disord. 2013; 35: 1–22.

Bachy A, Heaulme M, Giudice A, Michaud JC, Lefevre IA, Souilhac J, et al. SR 57227A: a potent and selective agonist at central and peripheral 5-HT3 receptors in vitro and in vivo. Eur. J. Pharmacol. 1993; 237: 299–309.

Ban JY, Seong YH. Blockade of 5-HT3 receptor with MDL72222 and Y25130 reduces ??-amyloid protein (25-35)-induced neurotoxicity in cultured rat cortical neurons. Eur. J. Pharmacol. 2005; 520: 12–21.

Banks WA, Gray AM, Erickson MA, Salameh TS, Damodarasamy M, Sheibani N, et al. Lipopolysaccharide-induced blood-brain barrier disruption: Roles of cyclooxygenase, oxidative stress, neuroinflammation, and elements of the neurovascular unit. J. Neuroinflammation 2015; 12: 1–15.

Batarseh YS, Bharate SS, Kumar V, Kumar A, Vishwakarma RA, Bharate SB, et al. Crocus

sativus Extract Tightens the Blood-Brain Barrier, Reduces Amyloid β Load and Related Toxicity in 5XFAD Mice. ACS Chem. Neurosci. 2017; 8: 1756–1766.

Batarseh YS, Kaddoumi A. Oleocanthal-rich extra-virgin olive oil enhances donepezil effect by reducing amyloid-β load and related toxicity in a mouse model of Alzheimer's disease. J. Nutr. Biochem. 2018a; 55: 113–123.

Batarseh YS, Kaddoumi A. Oleocanthal-rich extra-virgin olive oil enhances donepezil effect by reducing amyloid-β load and related toxicity in a mouse model of Alzheimer's disease. J. Nutr. Biochem. 2018b; 55: 113–123.

Bautista DM, Pellegrino M, Tsunozaki M. TRPA1: A gatekeeper for inflammation. Annu. Rev. Physiol. 2013; 75: 181–200.

Bianchi C, Siniscalchi A, Beani L. 5-HT1A agonists increase and 5-HT3 agonists decrease acetylcholine efflux from the cerebral cortex of freely-moving guinea-pigs. Br. J. Pharmacol. 1990; 101: 448–452.

Blair LJ, Frauen HD, Zhang B, Nordhues BA, Bijan S, Lin YC, et al. Tau depletion prevents progressive blood-brain barrier damage in a mouse model of tauopathy. Acta Neuropathol. Commun. 2015; 3: 8.

Boast C, Bartolomeo AC, Morris H, Moyer JA. 5HT antagonists attenuate MK801-impaired radial arm maze performance in rats. Neurobiol. Learn. Mem. 1999; 71: 259–271.

Boland B, Kumar A, Lee S, Platt FM, Wegiel J, Yu WH, et al. Autophagy induction and autophagosome clearance in neurons: relationship to autophagic pathology in Alzheimer's disease. J. Neurosci. 2008; 28: 6926–6937.

Botteri G, Salvadó L, Gumà A, Lee Hamilton D, Meakin PJ, Montagut G, et al. The BACE1 product sAPPβ induces ER stress and inflammation and impairs insulin signaling.

Metabolism 2018; 85: 59–75.

Bowman G, Kaye J, Moore M, Waichunas D, Carlson N, Quinn J. Blood–brain barrier impairment in Alzheimer disease. Neurology 2007; 68: 1809–1814.

Bowman GL, Dayon L, Kirkland R, Wojcik J, Peyratout G, Severin IC, et al. Blood-brain barrier breakdown, neuroinflammation, and cognitive decline in older adults. Alzheimer's Dement. 2018; 14: 1640–1650.

Bradburn S, Murgatroyd C, Ray N. Neuroinflammation in mild cognitive impairment and Alzheimer's disease: A meta-analysis. Ageing Res. Rev. 2019; 50: 1–8.

Brown RC, Davis TP. Calcium modulation of adherens and tight junction function: A potential mechanism for blood-brain barrier disruption after stroke. Stroke 2002; 33: 1706–1711.

Brygger L, Herrstedt J. 5-Hydroxytryptamine3 receptor antagonists and cardiac side effects. Expert Opin. Drug Saf. 2014; 13: 1407–1422.

Bufton KE, Steward LJ, Barber PC, Barnes NM. Distribution and characterization of the [3H]granisetron-labelled 5-HT3 receptor in the human forebrain. Neuropharmacology 1993; 32: 1325–1331.

Bussiere R, Lacampagne A, Reiken S, Liu X, Scheuerman V, Zalk R, et al. Amyloid β production is regulated by β2-adrenergic signaling-mediated post-translational modifications of the ryanodine receptor. J. Biol. Chem. 2017; 292: 10153–10168.

Callahan PM, Bertrand D, Bertrand S, Plagenhoef MR, Terry A V. Tropisetron sensitizes α7 containing nicotinic receptors to low levels of acetylcholine in vitro and improves memory-related task performance in young and aged animals. Neuropharmacology 2017; 117: 422–433.

Carty N, Nash KR, Brownlow M, Cruite D, Wilcock D, Selenica M-LB, et al. Intracranial

Injection of AAV Expressing NEP but Not IDE Reduces Amyloid Pathology in APP+PS1 Transgenic Mice. PLoS One 2013; 8: e59626.

Cass SP. Alzheimer's Disease and Exercise: A Literature Review. Curr. Sports Med. Rep. 2017; 16: 19–22.

Chaturvedula A, Joshi DP, Anderson C, Morris R, Sembrowich WL, Banga AK. Dermal, subdermal, and systemic concentrations of granisetron by iontophoretic delivery. Pharm. Res. 2005; 22: 1313–1319.

Chein-Tsai H, Cheih-fu C, Tung-Hu T. PHARMACOKINETICS OF GRANISETRON IN RAT BLOOD AND BRAIN BY MICRODIALYSIS. 1999; 3205: 1921–1931.

Chen R, Chen X, Wang H, Zhong W, Oh ES, Park MS, et al. Pharmacokinetics and safety of transdermal and oral granisetron in healthy Chinese subjects: An open-label, randomized, crossover study. Int. J. Clin. Pharmacol. Ther. 2019; 57: 24–31.

Chesser AS, Pritchard SM, Johnson GVW. Tau clearance mechanisms and their possible role in the pathogenesis of Alzheimer disease. Front. Neurol. 2013; 4: 122.

Chishti MA, Yang DS, Janus C, Phinney AL, Horne P, Pearson J, et al. Early-onset amyloid deposition and cognitive deficits in transgenic mice expressing a double mutant form of amyloid precursor protein 695. J. Biol. Chem. 2001; 276: 21562–21570.

Chugh Y, Saha N, Sankaranarayanan A, Sharma PL. Memory enhancing effects of granisetron (BRL 43694) in a passive avoidance task. Eur. J. Pharmacol. 1991; 203: 121–123.

Cirrito JR, Deane R, Fagan AM, Spinner ML, Parsadanian M, Finn MB, et al. P-glycoprotein deficiency at the blood-brain barrier increases amyloid-beta deposition in an Alzheimer disease mouse model. J. Clin. Invest. 2005; 115: 3285–90.

Coleman HN, Greenfield WW, Stratton SL, Vaughn R, Kieber A, Moerman-Herzog AM, et al.

Human papillomavirus type 16 viral load is decreased following a therapeutic vaccination. Cancer Immunol. Immunother. 2016; 65: 563—573.

Corbett A, Williams G, Ballard C. Drug repositioning: An opportunity to develop novel treatments for Alzheimer's disease. Pharmaceuticals 2013; 6: 1304–1321.

Cordero JG, García-escudero R, Avila J, Gargini R. Review Article Benefit of Oleuropein Aglycone for Alzheimer ' s Disease by Promoting Autophagy. 2018; 2018

Corona G, Spencer J, Dessì M. Extra virgin olive oil phenolics: Absorption, metabolism, and biological activities in the GI tract. Toxicol. Ind. Health 2009; 25: 285–293.

Corona Velazquez AF, Jackson WT. So many roads: the multi-faceted regulation of autophagy induction. Mol. Cell. Biol. 2018: 1–14.

Curry DW, Stutz B, Andrews ZB, Elsworth JD. Targeting AMPK Signaling as a Neuroprotective Strategy in Parkinson's Disease. J. Parkinsons. Dis. 2018; 8: 161–181.

Davis J, Xu F, Deane R, Romanov G, Previti M Lou, Zeigler K, et al. Early-onset and Robust Cerebral Microvascular Accumulation of Amyloid β-Protein in Transgenic Mice Expressing Low Levels of a Vasculotropic Dutch/Iowa Mutant Form of Amyloid β-Protein Precursor. J. Biol. Chem. 2004; 279: 20296–20306.

Deretic V, Levine B. Autophagy balances inflammation in innate immunity. Autophagy 2018; 14: 243–251.

Derkach V, Surprenant A, North RA. 5-HT3 receptors are membrane ion channels. Nature 1989; 339: 706–709.

Disterhoft JF, Moyer JR, Thompson LT. The calcium rationale in aging and Alzheimer's disease. Evidence from an animal model of normal aging. Ann. N. Y. Acad. Sci. 1994; 747: 382–406.

Di Domenico F, Barone E, Perluigi M, Butterfield DA. The Triangle of Death in Alzheimer's Disease Brain: The Aberrant Cross-Talk Among Energy Metabolism, Mammalian Target of Rapamycin Signaling, and Protein Homeostasis Revealed by Redox Proteomics. Antioxid. Redox Signal. 2017; 26: 364–387.

Dong Y, Li X, Cheng J, Hou L. Drug Development for Alzheimer's Disease: Microglia Induced Neuroinflammation as a Target? Int. J. Mol. Sci. 2019; 20: 558.

Eckman PL, KING WM, BRUNSON JG. Studies on the blood brain barrier. I. Effects produced by a single injection of gramnegative endotoxin on the permeability of the cerebral vessels. Am. J. Pathol. 1958; 34: 631–643.

Egawa G, Nakamizo S, Natsuaki Y, Doi H, Miyachi Y, Kabashima K. Intravital analysis of vascular permeability in mice using two-photon microscopy. Sci. Rep. 2013; 3: 1–6.

Egorova PA, Bezprozvanny IB. Inositol 1,4,5-trisphosphate receptors and neurodegenerative disorders. FEBS J. 2018: 1–19.

Elahy M, Jackaman C, Mamo JCL, Lam V, Dhaliwal SS, Giles C, et al. Blood-brain barrier dysfunction developed during normal aging is associated with inflammation and loss of tight junctions but not with leukocyte recruitment. Immun. Ageing 2015; 12: 1–9.

Elfakhri KH, Duong Q-V, Langley C, Depaula A, Mousa YM, Lebeouf T, et al. Characterization of Hit Compounds Identified from High-throughput Screening for their Effect on Bloodâ€"brain Barrier Integrity and Amyloid-Î² Clearance: In Vitro and In Vivo Studies [Internet]. Neuroscience 2018Available from: https://ac.els-cdn.com/S0306452218302197/1-s2.0-S0306452218302197-main.pdf?_tid=5fc6b767-d68d-4c9c-ae4f-49c6072b7b2e&acdnat=1522852463_012a73d67028c3fe08ec86b13ba5a03d

Erdö F, Denes L, De Lange E. Age-associated physiological and pathological changes at the

blood-brain barrier: A review. J. Cereb. Blood Flow Metab. 2017; 37: 4–24.

Erickson MA, Banks WA. Blood-brain barrier dysfunction as a cause and consequence of Alzheimer's disease. J. Cereb. Blood Flow Metab. 2013; 33: 1500–1513.

Erickson MA, Banks WA. Age-Associated Changes in the Immune System and Blood(-)Brain Barrier Functions. Int. J. Mol. Sci. 2019; 20

Erickson MA, Dohi K, Banks WA. Neuroinflammation: A common pathway in CNS diseases as mediated at the blood-brain barrier. Neuroimmunomodulation 2012; 19: 121–130.

Fakhfouri G, Mousavizadeh K, Mehr SE, Dehpour AR, Zirak MR, Ghia JE, et al. From Chemotherapy-Induced Emesis to Neuroprotection: Therapeutic Opportunities for 5-HT3 Receptor Antagonists. Mol. Neurobiol. 2015; 52: 1670–1679.

Fakhfouri G, Rahimian R, Daneshmand A, Bahremand A, Rasouli MR, Dehpour AR, et al. Granisetron ameliorates acetic acid-induced colitis in rats. Hum. Exp. Toxicol. 2010; 29: 321–328.

Feng T, Tammineni P, Agrawal C, Jeong YY, Cai Q. Autophagy-mediated regulation of BACE1 protein trafficking and degradation. J. Biol. Chem. 2017; 292: 1679–1690.

Franceschi C, BONAFÈ M, VALENSIN S, OLIVIERI F, DE LUCA M, OTTAVIANI E, et al. Inflamm-aging: An Evolutionary Perspective on Immunosenescence. Ann. N. Y. Acad. Sci. 2006; 908: 244–254.

Gage GJ, Kipke DR, Shain W. Whole Animal Perfusion Fixation for Rodents. J. Vis. Exp. 2012: 1–9.

Games D, Adams D, Alessandrini R, Barbour R, Berthelette P, Blackwell C, et al. Alzheimer-type neuropathology in transgenic mice overexpressing V717F beta-amyloid precursor protein. Nature 1995; 373: 523–527.

Gardener H, Caunca MR. Mediterranean Diet in Preventing Neurodegenerative Diseases. Curr. Nutr. Rep. 2018; 7: 10–20.

Gibson G, Cotman C, Lynch G, Blass J. Calcium Hypothesis of Alzheimer's disease and brain aging: A framework for integrating new evidence into a comprehensive theory of pathogenesis. Alzheimer's Dement. 2017; 13: 178-182.e17.

De Giusti VC, Caldiz CI, Ennis IE, Pérez NG, Cingolani HE, Aiello EA. Mitochondrial reactive oxygen species (ROS) as signaling molecules of intracellular pathways triggered by the cardiac renin-angiotensin II-aldosterone system (RAAS). Front. Physiol. 2013; 4 MAY: 1–9.

Goadsby PJ, Kurth T, Pressman A. HHS Public Access. 2016; 35: 1252–1260.

Gold M, El Khoury J. beta-amyloid, microglia, and the inflammasome in Alzheimer's disease. Semin. Immunopathol. 2015; 37: 607–611.

González-Reyes RE, Nava-Mesa MO, Vargas-Sánchez K, Ariza-Salamanca D, Mora-Muñoz L. Involvement of Astrocytes in Alzheimer's Disease from a Neuroinflammatory and Oxidative Stress Perspective. Front. Mol. Neurosci. 2017; 10: 427.

Gorlé N, Van Cauwenberghe C, Libert C, Vandenbroucke RE. The effect of aging on brain barriers and the consequences for Alzheimer's disease development. Mamm. Genome 2016; 27: 407–420.

Grabowski TJ, Cho HS, Vonsattel JP, Rebeck GW, Greenberg SM. Novel amyloid precursor protein mutation in an Iowa family with dementia and severe cerebral amyloid angiopathy. Ann. Neurol. 2001; 49: 697–705.

Grolla AA, Sim JA, Lim D, Rodriguez JJ, Genazzani AA, Verkhratsky A. Amyloid-b and Alzheimer's disease type pathology differentially affects the calcium signalling toolkit in

astrocytes from different brain regions. Cell Death Dis. 2013; 4: e623-7.

Gu Z, Liu W, Yan Z. ??-amyloid impairs AMPA receptor trafficking and function by reducing Ca2+/calmodulin-dependent protein kinase II synaptic distribution. J. Biol. Chem. 2009; 284: 10639–10649.

Guerreiro R, Bras J. The age factor in Alzheimer's disease. Genome Med. 2015; 7: 106.

Gunn AP, Wong XBX, Johanssen XT, Griffith XJC, Masters CL, Bush AI, et al. Amyloid-Peptide A-3pE-42 Induces Lipid Peroxidation, Membrane Permeabilization, and Calcium Influx in Neurons. J. Biol. Chem. 2016; 291: 6134–6145.

Gurpide A, Sadaba B, Martin-Algarra S, Azanza JR, Lopez-Picazo JM, Campanero MA, et al. Randomized Crossover Pharmacokinetic Evaluation of Subcutaneous Versus Intravenous Granisetron in Cancer Patients Treated with Platinum-Based Chemotherapy. Oncologist 2007; 12: 1151–1155.

Gurung P, Kanneganti TD. Novel Roles for Caspase-8 in IL-1β and Inflammasome Regulation. Am. J. Pathol. 2015; 185: 17–25.

van de Haar HJ, Jansen JFA, van Osch MJP, van Buchem MA, Muller M, Wong SM, et al. Neurovascular unit impairment in early Alzheimer's disease measured with magnetic resonance imaging. Neurobiol. Aging 2016; 45: 190–196.

Hamano T, Hayashi K, Shirafuji N, Nakamoto Y. The Implications of Autophagy in Alzheimer's Disease. Curr. Alzheimer Res. 2018; 15: 1283–1296.

Hardingham GE, Arnold FJ, Bading H. Nuclear calcium signaling controls CREB-mediated gene expression triggered by synaptic activity. Nat. Neurosci. 2001; 4: 261–267.

Harris H, Rubinsztein DC. Control of autophagy as a therapy for neurodegenerative disease. Nat. Rev. Neurol. 2011; 8: 108–117.

Hayflick L. The future of ageing. Nature 2000; 408: 267–269.

Heneka MT, Kummer MP, Stutz A, Delekate A, Saecker A, Griep A, et al. NIH Public Access. 2013; 493: 674–678.

Hernandez I, Luna G, Rauch JN, Reis SA, Giroux M, Karch CM, et al. A farnesyltransferase inhibitor activates lysosomes and reduces tau pathology in  mice with tauopathy. Sci. Transl. Med. 2019; 11

Homma K, Kitamura Y, Ogawa H, Oka K. Serotonin induces the increase in intracellular Ca2+ that enhances neurite outgrowth in PC12 cells via activation of 5-HT3 receptors and voltage-gated calcium channels. J. Neurosci. Res. 2006; 84: 316–325.

Honda M, Uchida K, Tanabe M, Ono H. Fluvoxamine, a selective serotonin reuptake inhibitor, exerts its antiallodynic effects on neuropathic pain in mice via 5-HT2A/2C receptors. Neuropharmacology 2006; 51: 866–872.

Hornedo-ortega R, Cerezo AB, Pablos RM De, Krisa S. Phenolic Compounds Characteristic of the Mediterranean Diet in Mitigating Microglia-Mediated Neuroinflammation. 2018; 12: 1–20.

Houtman J, Freitag K, Gimber N, Schmoranzer J, Heppner FL, Jendrach M. Beclin1-driven autophagy modulates the inflammatory response of microglia via NLRP3. EMBO J. 2019: e99430.

Howell J, Smeets J, Henk-J Drenth, Gill D. Pharmacokinetics of a granisetron transdermal system for the treatment of chemotherapy-induced nausea and vomiting. J. Oncol. Pharm. Pract. 2009; 15: 223–231.

Hsiao K, Chapman P, Nilsen S, Eckman C, Harigaya Y, Younkin S, et al. Correlative memory deficits, Abeta elevation, and amyloid plaques in transgenic mice. Science 1996; 274: 99–

102.

Hutchinson TE, Zhong W, Chebolu S, Wilson SM, Darmani NA. L-type calcium channels contribute to 5-HT3-receptor-evoked CaMKIIalpha and ERK activation and induction of emesis in the least shrew (Cryptotis parva). Eur. J. Pharmacol. 2015; 755: 110–118.

Iadecola C. The Pathobiology of Vascular Dementia. Neuron 2013; 80: 844–866.

Javadi-Paydar M, Zakeri M, Norouzi A, Rastegar H, Mirazi N, Dehpour AR. Involvement of nitric oxide in granisetron improving effect on scopolamine-induced memory impairment in mice. Brain Res. 2012; 1429: 61–71.

Jawhar S, Trawicka A, Jenneckens C, Bayer TA, Wirths O. Motor deficits, neuron loss, and reduced anxiety coinciding with axonal degeneration and intraneuronal Abeta aggregation in the 5XFAD mouse model of Alzheimer's disease. Neurobiol. Aging 2012; 33: 196.e29–40.

Kamba T, Lamb B. A model challenge Developing better models of Alzheimer's disease could be key to stemming the continued clinical failure of treatments. Nature 2018: 6–8.

Kang HM, Sohn I, Jung J, Jeong JW, Park C. Age-related changes in pial arterial structure and blood flow in mice. Neurobiol. Aging 2016; 37: 161–170.

Karkoula E, Skantzari A, Melliou E, Magiatis P. Quantitative Measurement of Major Secoiridoid Derivatives in Olive Oil Using qNMR. Proof of the Artificial Formation of Aldehydic Oleuropein and Ligstroside Aglycon Isomers. J. Agric. Food Chem. 2014; 62: 600–607.

Kashiwamura Y, Sano Y, Abe M, Shimizu F, Haruki H, Maeda T, et al. Hydrocortisone enhances the function of the blood-nerve barrier through the up-regulation of claudin-5. Neurochem. Res. 2011; 36: 849–855.

Kassner A, Merali Z. Assessment of Blood–Brain Barrier Disruption in Stroke. Stroke 2015; 46: 3310–3315.

Kaushal V, Dye R, Pakavathkumar P, Foveau B, Flores J, Hyman B, et al. Neuronal NLRP1 inflammasome activation of Caspase-1 coordinately regulates inflammatory interleukin-1-beta production and axonal degeneration-associated Caspase-6 activation. Cell Death Differ. 2015; 22: 1676–1686.

Keaney J, Campbell M. The dynamic blood-brain barrier. FEBS J. 2015; 282: 4067–4079.

Keys A. Mediterranean diet and public health: personal reflections. Am. J. Clin. Nutr. 1995; 61: 1321S-1323S.

Khachaturian ZS. Calcium Hypothesis of Alzheimer's Disease and Brain Aginga. Ann. N. Y. Acad. Sci. 2006; 747: 1–11.

Khodaie-Ardakani MR, Seddighi S, Modabbernia A, Rezaei F, Salehi B, Ashrafi M, et al. Granisetron as an add-on to risperidone for treatment of negative symptoms in patients with stable schizophrenia: Randomized double-blind placebo-controlled study. J. Psychiatr. Res. 2013; 47: 472–478.

Kim JE, Hong YS, Lee J-L, Kim K-P, Park SJ, Sym SJ, et al. A randomized study of the efficacy and safety of transdermal granisetron in the control of nausea and vomiting induced by moderately emetogenic chemotherapy in Korean patients. Support. care cancer Off. J. Multinatl. Assoc. Support. Care Cancer 2015; 23: 1769–1777.

Kinney JW, Bemiller SM, Murtishaw AS, Leisgang AM, Salazar AM, Lamb BT. Inflammation as a central mechanism in Alzheimer's disease. Alzheimer's Dement. (New York, N. Y.) 2018; 4: 575–590.

Kook S-Y, Hong HS, Moon M, Ha CM, Chang S, Mook-Jung I. A 1-42-RAGE Interaction Disrupts Tight Junctions of the Blood-Brain Barrier Via Ca2+-Calcineurin Signaling. J. Neurosci. 2012; 32: 8845–8854.

Korabecny J, Zemek F, Soukup O, Spilovska K, Musilek K, Jun D, et al. Pharmacotherapy of alzheimer's disease: Current state and future perspectives. 2015.

Kore RA, Edmondson JL, Jenkins S V, Jamshidi-Parsian A, Dings RPM, Reyna NS, et al. Hypoxia-derived exosomes induce putative altered pathways in biosynthesis and ion regulatory channels in glioblastoma cells. Biochem. Biophys. reports 2018; 14: 104–113.

Kruyer A, Soplop N, Strickland S, Norris EH. Chronic hypertension leads to neurodegeneration in the TgSwDI mouse model of Alzheimer's disease. Hypertension 2015; 66: 175–182.

LaFerla FM. Calcium dyshomeostasis and intracellular signalling in alzheimer's disease. Nat. Rev. Neurosci. 2002; 3: 862–872.

Lane CA, Hardy J, Schott JM. Alzheimer's disease. Eur. J. Neurol. 2018; 25: 59–70.

Lauretti E, Iuliano L, Praticò D. Extra-virgin olive oil ameliorates cognition and neuropathology of the 3xTg mice: role of autophagy. Ann. Clin. Transl. Neurol. 2017; 4: 564–574.

Lee G-S, Subramanian N, Kim AI, Aksentijevich I, Goldbach-Mansky R, Sacks DB, et al. The calcium-sensing receptor regulates the NLRP3 inflammasome through Ca2+ and cAMP. Nature 2012; 492: 123–127.

Lee K-I, Lee H-T, Lin H-C, Tsay H-J, Tsai F-C, Shyue S-K, et al. Role of transient receptor potential ankyrin 1 channels in Alzheimer's disease. J. Neuroinflammation 2016a; 13: 92.

Lee K, Lee H, Lin H, Tsay H, Tsai F, Shyue S, et al. Role of transient receptor potential ankyrin 1 channels in Alzheimer ' s disease. J. Neuroinflammation 2016b: 1–16.

Lencel P, Magne D. Inflammaging: The driving force in osteoporosis? Med. Hypotheses 2011; 76: 317–321.

Levy E, Carman MD, Fernandez-Madrid IJ, Power MD, Lieberburg I, van Duinen SG, et al. Mutation of the Alzheimer's disease amyloid gene in hereditary cerebral hemorrhage,

Dutch type. Science (80-. ). 1990; 248: 1124 LP – 1126.

Li L, Zhang X, Le W. Autophagy dysfunction in Alzheimer's disease. Neurodegener. Dis. 2010; 7: 265–271.

Li Q, Chen L, Liu X, Li X, Cao Y, Bai Y, et al. Pterostilbene inhibits amyloid-β-induced neuroinflammation in a microglia cell line by inactivating the NLRP3/caspase-1 inflammasome pathway. J. Cell. Biochem. 2018; 119: 7053–7062.

Liang Z, Liu F, Grundke-Iqbal I, Iqbal K, Gong C-X. Down-regulation of cAMP-dependent protein kinase by over-activated calpain in Alzheimer disease brain. J. Neurochem. 2007; 103: 2462–2470.

Liu CY, Jacobs RE, Sagare AP, Halliday MR, Zhao Z, Zlokovic BV, et al. Blood-Brain Barrier Breakdown in the Aging Human Hippocampus. Neuron 2015; 85: 296–302.

Louneva N, Cohen JW, Han LY, Talbot K, Wilson RS, Bennett DA, et al. Caspase-3 is enriched in postsynaptic densities and increased in Alzheimer's disease. Am. J. Pathol. 2008; 173: 1488–1495.

Maleki-Dizaji N, Eteraf-Oskouei T, Fakhrjou A, Maljaie SH, Garjani A. The effects of 5HT3receptor antagonist granisetron on inflammatory parameters and angiogenesis in the air-pouch model of inflammation. Int. Immunopharmacol. 2010; 10: 1010–1016.

Marambaud P, Dreses-Werringloer U, Vingtdeux V. Calcium signaling in neurodegeneration. Mol. Neurodegener. 2009; 4: 1–15.

Maricq A V, Peterson AS, Brake AJ, Myers RM, Julius D. Primary structure and functional expression of the 5HT3 receptor, a serotonin-gated ion channel. Science 1991; 254: 432–437.

Marques F, Sousa JC, Sousa N, Palha JA. Blood – brain-barriers in aging and in Alzheimer ' s

disease. 2013: 1–9.

Matalis A, Patent A, Rao R, John V. cognition in a murine Alzheimer ' s model. 2015: 25–44.

Mattson MP, Chan SL, Duan W. Modification of Brain Aging and Neurodegenerative Disorders by Genes, Diet, and Behavior. Physiol. Rev. 2002a; 82: 637–672.

Mattson MP, Chan SL, Duan W. Modification of brain aging and neurodegenerative disorders by genes, diet, and behavior. Physiol. Rev. 2002b; 82: 637–672.

Mattson MP, Cheng B, Davis D, Bryant K, Lieberburg I, Rydel RE. beta-Amyloid peptides destabilize calcium homeostasis and render human cortical neurons vulnerable to excitotoxicity. J. Neurosci. 1992; 12: 376–389.

Medyouf H, Alcalde H, Berthier C, Guillemin MC, dos Santos NR, Janin A, et al. Targeting calcineurin activation as a therapeutic strategy for T-cell acute lymphoblastic leukemia. Nat. Med. 2007; 13: 736–741.

Mendes SJF, Sousa FIAB, Pereira DMS, Ferro TAF, Pereira ICP, Silva BLR, et al. International Immunopharmacology Cinnamaldehyde modulates LPS-induced systemic in fl ammatory response syndrome through TRPA1-dependent and independent mechanisms. Int. Immunopharmacol. 2016; 34: 60–70.

Miao J, Xu F, Davis J, Otte-Holler I, Verbeek MM, Van Nostrand WE. Cerebral microvascular amyloid beta protein deposition induces vascular degeneration and neuroinflammation in transgenic mice expressing human vasculotropic mutant amyloid beta precursor protein. Am. J. Pathol. 2005a; 167: 505–515.

Miao J, Xu F, Davis J, Otte-Höller I, Verbeek MM, Van Nostrand WE. Cerebral microvascular amyloid β protein deposition induces vascular degeneration and neuroinflammation in transgenic mice expressing human vasculotropic mutant amyloid β precursor protein. Am. J.

Pathol. 2005b; 167: 505–515.

Minter MR, Taylor JM, Crack PJ. The contribution of neuroinflammation to amyloid toxicity in Alzheimer's disease. J. Neurochem. 2016; 136: 457–474.

Mohamed LA, Kaddoumi A, Keller J. Role of P-glycoprotein in mediating rivastigmine effect on amyloid-β brain load and related pathology in Alzheimer's disease mouse model. 2016; 1862: 778–787.

Mohamed LA, Qosa H, Kaddoumi A. Age-Related Decline in Brain and Hepatic Clearance of Amyloid- Beta is Rectified by the Cholinesterase Inhibitors Donepezil and Rivastigmine in Rats. ACS Chem. Neurosci. 2015; 6: 725–736.

Montagne A, Barnes SR, Sweeney MD, Halliday MR, Abhay P, Zhao Z, et al. Blood-Brain Barrier Breakdown in the Aging Human Hippocampus. Neuron 2016a; 85: 296–302.

Montagne A, Barnes SR, Sweeney MD, Halliday MR, Sagare AP, Zhao Z, et al. Blood-Brain barrier breakdown in the aging human hippocampus. Neuron 2015; 85: 296–302.

Montagne A, Nation DA, Pa J, Sweeney MD, Toga AW, Zlokovic B V. Brain imaging of neurovascular dysfunction in Alzheimer's disease. Acta Neuropathol. 2016b; 131: 687–707.

Montagne A, Zhao Z, Zlokovic B V. Alzheimer's disease : A matter of blood – brain barrier dysfunction ? The Journal of Experimental Medicine. J. Exp. Med. 2017; 214: 3151–3169.

Mucke L, Masliah E, Yu GQ, Mallory M, Rockenstein EM, Tatsuno G, et al. High-level neuronal expression of abeta 1-42 in wild-type human amyloid protein precursor transgenic mice: synaptotoxicity without plaque formation. J. Neurosci. 2000; 20: 4050–4058.

Mulkey RM, Endo S, Shenolikar S, Malenka RC. Involvement of a calcineurin/inhibitor-1 phosphatase cascade in hippocampal long-term depression. Nature 1994; 369: 486–488.

Mullan M, Crawford F, Axelman K, Houlden H, Lilius L, Winblad B, et al. A pathogenic

mutation for probable Alzheimer's disease in the APP gene at the N-terminus of beta-amyloid. Nat. Genet. 1992; 1: 345–347.

Muszynski P, Kulczynska-Przybik A, Borawska R, Litman-Zawadzka A, Slowik A, Klimkowicz-Mrowiec A, et al. The Relationship between Markers of Inflammation and Degeneration in the Central Nervous System and the Blood-Brain Barrier Impairment in Alzheimer's Disease. J. Alzheimers. Dis. 2017; 59: 903–912.

Nahata MC, Morosco RS, Hipple TF. Stability of granisetron hydrochloride in two oral suspensions. Am. J. Heal. Pharm. 1998; 55: 2511–2513.

Nation DA, Sweeney MD, Montagne A, Sagare AP, D'Orazio LM, Pachicano M, et al. Blood–brain barrier breakdown is an early biomarker of human cognitive dysfunction [Internet]. Nat. Med. 2019; 25Available from: http://dx.doi.org/10.1038/s41591-018-0297-y

Nayak S V., Rondé P, Spier AD, Lummis SCR, Nichols RA. Calcium changes induced by presynaptic 5-hydroxytryptamine-3 serotonin receptors on isolated terminals from various regions of the rat brain. Neuroscience 1999; 91: 107–117.

Nelson AR, Sweeney MD, Sagare AP, Zlokovic B V. Neurovascular dysfunction and neurodegeneration in dementia and Alzheimer's disease. Biochim. Biophys. Acta - Mol. Basis Dis. 2016; 1862: 887–900.

Nixon RA. Autophagy, amyloidogenesis and Alzheimer disease. J. Cell Sci. 2007; 120: 4081–4091.

Northrop N. HHS Public Access. 2018: 1–24.

Oddo S, Caccamo A, Shepherd JD, Murphy MP, Golde TE, Kayed R, et al. Triple-transgenic model of Alzheimer's disease with plaques and tangles: intracellular Abeta and synaptic dysfunction. Neuron 2003; 39: 409–421.

Ohno M, Watanabe S. Differential effects of 5-HT3 receptor antagonism on working memory failure due to deficiency of hippocampal cholinergic and glutamatergic transmission in rats. Brain Res. 1997; 762: 211–215.

Oulès B, Prete D Del, Greco B, Zhang X, Sevalle J, Moreno S, et al. Ryanodine receptors blockade reduces Amyloid-beta load and memory impairmnet of Tg2576 mouse model of Alzheimer's disease. J. Neurosci. 2013; 32: 11820–11834.

Palop J, Jones B, Kekonius L, Chin J, Yu G-Q, Raber J, et al. Neuronal depletion of calcium-dependent proteins in the dentate gyrus is tightly linked to Alzheimer's disease-related cognitive deficits. 2003.

Park SY, Lee HR, Lee WS, Shin HK, Kim HY, Hong KW, et al. Cilostazol Modulates Autophagic Degradation of beta-Amyloid Peptide via SIRT1-Coupled LKB1/AMPKalpha Signaling in Neuronal Cells. PLoS One 2016; 11: e0160620.

Peixoto CA, Oliveira WH de, Araujo SM da R, Nunes AKS. AMPK activation: Role in the signaling pathways of neuroinflammation and neurodegeneration. Exp. Neurol. 2017; 298: 31–41.

Peyrot des Gachons C, Uchida K, Bryant B, Shima A, Sperry JB, Dankulich-Nagrudny L, et al. Unusual pungency from extra-virgin olive oil is attributable to restricted spatial expression of the receptor of oleocanthal. J. Neurosci. 2011; 31: 999–1009.

Pierrot N, Santos SF, Feyt C, Morel M, Brion J-P, Octave J-N. Calcium-mediated transient phosphorylation of tau and amyloid precursor protein followed by intraneuronal amyloid-beta accumulation. J. Biol. Chem. 2006; 281: 39907–39914.

Pitozzi V, Jacomelli M, Zaid M, Luceri C, Bigagli E, Lodovici M, et al. Effects of dietary extra-virgin olive oil on behaviour and brain biochemical parameters in ageing rats. Br. J. Nutr.

2010; 103: 1674–1683.

Plaza-Zabala A, Sierra-Torre V, Sierra A. Autophagy and microglia: Novel partners in neurodegeneration and aging. Int. J. Mol. Sci. 2017; 18

Popescu BO, Toescu EC, Popescu LM, Bajenaru O, Muresanu DF, Schultzberg M, et al. Blood-brain barrier alterations in ageing and dementia. J. Neurol. Sci. 2009; 283: 99–106.

Popugaeva E, Pchitskaya E, Bezprozvanny I. DYSREGULATION OF INTRACELLULAR CALCIUM SIGNALING IN ALZHEIMER'S DISEASE. Antioxid. Redox Signal. 2018: ars.2018.7506.

Qosa H, Abuasal BS, Romero IA, Weksler B, Couraud P-O, Keller JN, et al. Differences in amyloid-beta clearance across mouse and human blood-brain barrier models: kinetic analysis and mechanistic modeling. Neuropharmacology 2014a; 79: 668–678.

Qosa H, Abuznait AH, Hill RA, Kaddoumi A. Enhanced brain amyloid-beta clearance by rifampicin and caffeine as a possible protective mechanism against Alzheimer's disease. J. Alzheimers. Dis. 2012; 31: 151–165.

Qosa H, Batarseh YS, Mohyeldin MM, El Sayed KA, Keller JN, Kaddoumi A. Oleocanthal Enhances Amyloid-β Clearance from the Brains of TgSwDI Mice and in Vitro across a Human Blood-Brain Barrier Model. ACS Chem. Neurosci. 2015a; 6: 1849–1859.

Qosa H, LeVine H 3rd, Keller JN, Kaddoumi A. Mixed oligomers and monomeric amyloid-beta disrupts endothelial cells integrity and reduces monomeric amyloid-beta transport across hCMEC/D3 cell line as an in vitro blood-brain barrier model. Biochim. Biophys. Acta 2014b; 1842: 1806–1815.

Qosa H, Mohamed LA, Batarseh YS, Alqahtani S, Ibrahim B, LeVine H, et al. Extra-virgin olive oil attenuates amyloid-β and tau pathologies in the brains of TgSwDI mice. J. Nutr.

Biochem. 2015b; 26: 1479–1490.

Qosa H, Mohamed LA, Al Rihani SB, Batarseh YS, Duong QV, Keller JN, et al. High-Throughput Screening for Identification of Blood-Brain Barrier Integrity Enhancers: A Drug Repurposing Opportunity to Rectify Vascular Amyloid Toxicity. J. Alzheimer's Dis. 2016; 53: 1499–1516.

Quercia RA, ZHANG J, FAN C, CHOW MSS. Stability of granisetron hydrochloride in an extemporaneously prepared oral liquid. Am. J. Heal. Pharm. 1997; 54: 1996–1998.

Querfurth HW, LaFerla FM. Alzheimer's disease. N. Engl. J. Med. 2010; 362: 329–344.

Radde R, Bolmont T, Kaeser SA, Coomaraswamy J, Lindau D, Stoltze L, et al. Abeta42-driven cerebral amyloidosis in transgenic mice reveals early and robust pathology. EMBO Rep. 2006; 7: 940–946.

Rahimian R, Daneshmand A, Mehr SE, Barzegar-Fallah A, Mohammadi-Rick S, Fakhfouri G, et al. Tropisetron ameliorates ischemic brain injury in an embolic model of stroke. Brain Res. 2011a; 1392: 101–109.

Rahimian R, Dehpour AR, Fakhfouri G, Khorramizadeh MR, Ghia J-E, Seyedabadi M, et al. Tropisetron upregulates cannabinoid CB1 receptors in cerebellar granule cells: possible involvement of calcineurin. Brain Res. 2011b; 1417: 1–8.

Rahimian R, Fakhfouri G, Ejtemaei Mehr S, Ghia J-E, Genazzani AA, Payandemehr B, et al. Tropisetron attenuates amyloid-beta-induced inflammatory and apoptotic responses in rats. Eur. J. Clin. Invest. 2013; 43: 1039–1051.

Ramirez MJ, Cenarruzabeitia E, Lasheras B, Del Rio J. Involvement of GABA systems in acetylcholine release induced by 5-HT3 receptor blockade in slices from rat entorhinal cortex. Brain Res. 1996; 712: 274–280.

Raza M, Deshpande LS, Blair RE, Carter DS, Sombati S, DeLorenzo RJ. Aging is associated with elevated intracellular calcium levels and altered calcium homeostatic mechanisms in hippocampal neurons. Neurosci. Lett. 2007; 418: 77–81.

Riazantseva MA, Mozhaeva GN, Kaznacheeva E V. [Calcium hypothesis of Alzheimer disease]. Usp. Fiziol. Nauk 2012; 43: 59–72.

Rigalli alfredo, Veronica DL. Experimental Surgical Models in the Laboratory Rat. CRC Press 2009

Ronde P, Nichols RA. 5-HT3 receptors induce rises in cytosolic and nuclear calcium in NG108-15 cells via calcium-induced calcium release. Cell Calcium 1997; 22: 357–365.

Rosa E, Fahnestock M. CREB expression mediates amyloid β-induced basal BDNF downregulation. Neurobiol. Aging 2018; 36: 2406–2413.

Rubinsztein DC, Mariño G, Kroemer G. Autophagy and aging. Cell 2011; 146: 682–695.

Sasaguri H, Nilsson P, Hashimoto S, Nagata K, Saito T, De Strooper B, et al. APP mouse models for Alzheimer's disease preclinical studies. EMBO J. 2017; 36: 2473–2487.

Scaini G, Barichello T, Fries GR, Kennon EA, Andrews T, Nix BR, et al. TSPO upregulation in bipolar disorder and concomitant downregulation of mitophagic proteins and NLRP3 inflammasome activation. Neuropsychopharmacology 2018

Seglen PO, Bohley P. Autophagy and other vacuolar protein degradation mechanisms. Experientia 1992; 48: 158–172.

Shibata M, Yamada S, Ram Kumar S, Calero M, Bading J, Frangione B, et al. Clearance of Alzheimer's amyloid-β1-40 peptide from brain by LDL receptor-related protein-1 at the blood-brain barrier. J. Clin. Invest. 2000; 106: 1489–1499.

Shigetomi E, Tong X, Kwan KY, Corey DP, Khakh BS. TRPA1 channels regulate astrocyte

resting calcium and inhibitory synapse efficacy through GAT-3. Nat. Neurosci. 2011; 15: 70–80.

Shimizu S. The Laboratory Mouse, Routes of Adminstration Chapter 32. 2004

Siddique AB, Ebrahim H, Mohyeldin M, Qusa M, Batarseh Y, Fayyad A, et al. Novel liquid-liquid extraction and self-emulsion methods for simplified isolation of extra-virgin olive oil phenolics with emphasis on (-)-oleocanthal and its oral anti-breast cancer activity. PLoS One 2019; 14: e0214798.

Son SM, Jung ES, Shin HJ, Byun J, Mook-Jung I. Abeta-induced formation of autophagosomes is mediated by RAGE-CaMKKbeta-AMPK signaling. Neurobiol. Aging 2012; 33: 1006.e11–23.

Spartinou A, Nyktari V, Papaioannou A. Granisetron: a review of pharmacokinetics and clinical experience in chemotherapy induced - nausea and vomiting. Expert Opin. Drug Metab. Toxicol. 2017; 13: 1289–1297.

Spilman P, Descamps O, Gorostiza O, Peters-Libeu C, Poksay KS, Matalis A, et al. The multi-functional drug tropisetron binds APP and normalizes cognition in a murine Alzheimer's model. Brain Res. 2014; 1551: 25–44.

Stancu I-C, Cremers N, Vanrusselt H, Couturier J, Vanoosthuyse A, Kessels S, et al. Aggregated Tau activates NLRP3–ASC inflammasome exacerbating exogenously seeded and non-exogenously seeded Tau pathology in vivo [Internet]. Acta Neuropathol. 2019Available from: https://doi.org/10.1007/s00401-018-01957-y

Sturchler-Pierrat C, Abramowski D, Duke M, Wiederhold KH, Mistl C, Rothacher S, et al. Two amyloid precursor protein transgenic mouse models with Alzheimer disease-like pathology. Proc. Natl. Acad. Sci. U. S. A. 1997; 94: 13287–13292.

Stutzmann GE. Calcium dysregulation, IP3 signaling, and Alzheimer's disease. Neuroscientist 2005; 11: 110–115.

Supnet C, Bezprozvanny I. The dysregulation of intracellular calcium in Alzheimer disease. Cell Calcium 2010; 47: 183–189.

Suridjan I, Pollock BG, Verhoeff NPLG, Voineskos AN, Chow T, Rusjan PM, et al. In-vivo imaging of grey and white matter neuroinflammation in Alzheimer's disease: A positron emission tomography study with a novel radioligand, ‘ 18 F'-FEPPA. Mol. Psychiatry 2015; 20: 1579–1587.

Sweeney MD, Sagare AP, Zlokovic B V. Blood-brain barrier breakdown in Alzheimer disease and other neurodegenerative disorders. Nat. Rev. Neurol. 2018a; 14: 133–150.

Sweeney MD, Sagare AP, Zlokovic B V. Blood-brain barrier breakdown in Alzheimer disease and other neurodegenerative disorders. Nat. Rev. Neurol. 2018b; 14: 133–150.

Sweeney MD, Zhao Z, Montagne A, Nelson AR, Zlokovic B V. Blood-Brain Barrier: From Physiology to Disease and Back. Physiol. Rev. 2019; 99: 21–78.

Takenouchi T, Munekata E. Serotonin increases cytoplasmic Ca2+ concentration in PC12h cells: effect of tachykinin peptides. Neurosci. Lett. 1998; 246: 141–144.

Tan MS, Yu JT, Jiang T, Zhu XC, Tan L. The NLRP3 inflammasome in alzheimer's disease. Mol. Neurobiol. 2013; 48: 875–882.

Teich AF, Nicholls RE, Puzzo D, Fiorito J, Purgatorio R, Fa' M, et al. Synaptic Therapy in Alzheimer's Disease: A CREB-centric Approach. Neurotherapeutics 2015; 12: 29–41.

Thibault O, Gant JC, Landfield PW. Expansion of the calcium hypothesis of brain aging and Alzheimer's disease: Minding the store. Aging Cell 2007; 6: 307–317.

Tuck KL, Hayball PJ. Major phenolic compounds in olive oil: metabolism and health effects. J.

Nutr. Biochem. 2002; 13: 636–644.

Uddin MS, Stachowiak A, Al Mamun A, Tzvetkov NT, Takeda S, Atanasov AG, et al. Autophagy and Alzheimer's disease: From molecular mechanisms to therapeutic implications. Front. Aging Neurosci. 2018; 10: 1–18.

Ujiie M, Dickstein DL, Carlow DA, Jefferies WA. Blood-brain barrier permeability precedes senile plaque formation in an Alzheimer disease model. Microcirculation 2003; 10: 463–470.

Uzuki BKS, Wata AI, Watsubo TI. Review The past , present , and future of disease-modifying therapies for Alzheimer ' s disease. 2017; 93: 757–771.

Valero J, Bernardino L, Cardoso FL, Silva AP, Fontes-Ribeiro C, Ambrosio AF, et al. Impact of Neuroinflammation on Hippocampal Neurogenesis: Relevance to Aging and Alzheimer's Disease. J. Alzheimers. Dis. 2017; 60: S161–S168.

Vitolo O V., Sant'Angelo A, Costanzo V, Battaglia F, Arancio O, Shelanski M. Amyloid - peptide inhibition of the PKA/CREB pathway and long-term potentiation: Reversibility by drugs that enhance cAMP signaling. Proc. Natl. Acad. Sci. 2002; 99: 13217–13221.

Walton MR, Dragunow M. Is CREB a key to neuronal survival? Trends Neurosci. 2018; 23: 48–53.

Wang M, Zhang Y, Xu M, Zhang H, Chen Y, Chung KF, et al. Roles of TRPA1 and TRPV1 in cigarette smoke -induced airway epithelial cell injury model. Free Radic. Biol. Med. 2019; 134: 229–238.

Weller J, Budson A. Current understanding of Alzheimer's disease diagnosis and treatment. F1000Research 2018; 7: 1161.

Wisniewski HM, VORBRODT AW, WEGIEL J. Amyloid Angiopathy and Blood–Brain Barrier

Changes in Alzheimer's Diseasea,b. Ann. N. Y. Acad. Sci. 1997; 826: 161–172.

Wisniewski T, Goñi F. Immunotherapeutic approaches for Alzheimer's disease. Neuron 2015; 85: 1162–1176.

Wu G, Irvine J, Luft C, Pressley D, Janzen CNH and B. Assay Development and High-Throughput Screening of Caspases in Microfluidic Format. Comb. Chem. High Throughput Screen. 2003; 6: 303–312.

Yamagata Y, Kobayashi S, Umeda T, Inoue A, Sakagami H, Fukaya M, et al. Kinase-Dead Knock-In Mouse Reveals an Essential Role of Kinase Activity of Ca2+/Calmodulin-Dependent Protein Kinase II in Dendritic Spine Enlargement, Long-Term Potentiation, and Learning. J. Neurosci. 2009; 29: 7607–7618.

Yamazaki Y, Kanekiyo T. Blood-brain barrier dysfunction and the pathogenesis of alzheimer's disease. Int. J. Mol. Sci. 2017; 18

Yan X, Liu J, Ye Z, Huang J, He F, Xiao W, et al. CaMKII-Mediated CREB Phosphorylation Is Involved in Ca(2+)-Induced BDNF mRNA Transcription and Neurite Outgrowth Promoted by Electrical Stimulation. PLoS One 2016; 11: e0162784.

Yang Z, Wu Y, Chen B, Zhang W, Zhang J, Huang C. Autophagy Protects the Blood-Brain Barrier Through Regulating the Dynamic of Claudin-5 in Short-Term Starvation. Front. Physiol. 2019; 10: 1–11.

Yarker YE, McTavish D. Granisetron. An update of its therapeutic use in nausea and vomiting induced by antineoplastic therapy. Drugs 1994; 48: 761–793.

Yarlagadda A, Kaushik S, Clayton AH. Blood brain barrier: the role of calcium homeostasis. Psychiatry (Edgmont). 2007; 4: 55–9.

Yin S, Wang P, Xing R, Zhao L, Li X, Zhang L. Transient Receptor Potential Ankyrin 1 (

TRPA1 ) Mediates Lipopolysaccharide ( LPS ) -Induced Inflammatory Responses in Primary Human Osteoarthritic Fibroblast-Like Synoviocytes. 2018; 1

Yin Y, Gao D, Wang Y, Wang Z-H, Wang X, Ye J, et al. Tau accumulation induces synaptic impairment and memory deficit by calcineurin-mediated inactivation of nuclear CaMKIV/CREB signaling. Proc. Natl. Acad. Sci. 2016; 113: E3773–E3781.

Yoshikawa M, Soeda Y, Michikawa M, Almeida OFX, Takashima A. Tau Depletion in APP Transgenic Mice Attenuates Task-Related Hyperactivation of the Hippocampus and Differentially Influences Locomotor Activity and Spatial Memory. Front. Neurosci. 2018; 12: 124.

Zenaro E, Piacentino G, Constantin G. The blood-brain barrier in Alzheimer's disease. Neurobiol. Dis. 2017; 107: 41–56.

Zhou F, van Laar T, Huang H, Zhang L. APP and APLP1 are degraded through autophagy in response to proteasome inhibition in neuronal cells. Protein Cell 2011; 2: 377–383.

Zhu X, Raina AK, Perry G, Smith MA. Alzheimer's disease: The two-hit hypothesis. Lancet Neurol. 2004; 3: 219–226.

Zlokovic B V. Neurovascular pathways to neurodegeneration in Alzheimer's disease and other disorders. Nat. Rev. Neurosci. 2011; 12: 723–738.

Zybailov BL, Glazko G V, Rahmatallah Y, Andreyev DS, McElroy T, Karaduta O, et al. Metaproteomics reveals potential mechanisms by which dietary resistant starch supplementation attenuates chronic kidney disease progression in rats. PLoS One 2019; 14: e0199274.